10 copies
11-8-67

MND-3607-173

SNAP 19 RADIATION MEASUREMENTS REPORT

MARTIN MARIETTA

DISCLAIMER

SNAP 19 RADIATION MEASUREMENTS REPORT

NOVEMBER 1967

MND-3607-173

CONTRACT AT(30-1)-3607

Approved by: John J. Jicha, Jr.
Clement Eicheldinger

Prepared by: H. B. Rosenthal
W. D. Owings
J. M. Hrubovcak

MARTIN MARIETTA CORPORATION
NUCLEAR DIVISION
BALTIMORE, MD. 21203

LEGAL NOTICE

This report was prepared as an account of Government sponsored work. Neither the United States, nor the Commission, nor any person acting on behalf of the Commission:

A. Makes any warranty or representation, expressed or implied, with respect to the accuracy, completeness, or usefulness of the information contained in this report, or that the use of any information, apparatus, method, or process disclosed in this report may not infringe privately owned rights, or

B. Assumes any liabilities with respect to the use of or for damages resulting from the use of any information apparatus, method, or process disclosed in this report.

As used in the above, "person acting on behalf of the Commission" includes any employee or contractor of the Commission, or employee of such contractor, to the extent that such employee or contractor of the Commission, or employee of such contractor prepares, disseminates, or provides access to, any information pursuant to his employment or contract with the Commission, or his employment with such contractor.

FOREWORD

This report is submitted by the Nuclear Division of the Martin Marietta Corporation, in support of United States Atomic Energy Commission contract AT(30-1)-3607. This volume and Appendix C (MND-3607-173-1) constitute the final report for Item 1 (e) of the experimental safety program for SNAP 19, dated January 1966.

For convenience, Appendix C which contains Confidential Restricted Data information has been placed in a separate volume.

Blank

CONTENTS

Blank

SUMMARY

The objective of the SNAP 19 Radiation Measurements Program was to determine the energy distribution and absolute magnitude of the neutron and gamma radiation emitted from SNAP 19 fuel capsules and assembled generator subsystems. A further objective was to apply the data obtained to determine the source of neutrons in the fuel capsule. The task included assembling and checking out instrumentation, evaluating the spectrometer system against a known neutron source, measuring SNAP 19 Subsystem S/N 4, providing analytical support for the measurements and determining the source of neutrons in the fuel capsule.

The stilbene neutron detecting system employed in the spectrometer measures the amplitude of light pulses produced by recoil protons resulting from neutron elastic scattering within the stilbene crystal. The light pulse data are reduced to neutron spectrum by means of a data reduction computer code. Since the stilbene crystal also responds to recoil electrons from Compton scattering of photons, a discriminating circuit was incorporated within the spectrometer to pass essentially only the neutron pulses.

The spectrometer consists of a scintillation counter employing a stilbene crystal detector, a preamplifier section, a discriminator section and a 256-channel analyzer. The preamplifier section of the system makes use of space charge effects in the photoamplifier tube to discriminate against gammas. Under this space charge saturation condition, the last dynode (which is driven negative by all pulses) remains negative for several microseconds in response to a pulse from a recoil electron resulting from an incident gamma. A recoil proton from an incident neutron will produce a pulse which goes positive in less than a microsecond. This positive-going pulse is shaped in the discriminator to provide a gating pulse which triggers the analyzer so that only neutron-produced pulses are counted by the amplifier.

The spectrometer was calibrated to establish the proper high voltage to be applied to the photomultiplier tube. To cover the energy range of about 0.5 to 12.5 Mev, two measurements at high voltage settings of 1535 and 1650 volts were required. The system was found to be sensitive to the count rate. Calibration showed that the gross count rate (neutron plus gamma) had to be restricted to the range between 1000 and 8000 counts/sec.

For routine calibration to establish reproducible data, the system was calibrated against the Compton recoil spectra from cesium-137, sodium-22 and manganese-54. This was accomplished by adjusting the gain of the linear amplifier so that the midpoint of the Compton edge always fell in the same channel for each of the gamma sources.

Measurements were made to evaluate the response of the spectrometer system. These measurements included: determination of appropriate range of gross count rate, evaluation of system reproducibility, determination of the effects of scattering on measurements, evaluation of the effects of crystal orientation with respect to the incident neutrons and determination of the ability of the system to spectral change through a hydrogenous shield material.

Absolute normalization of the system to determine absolute count rate from the measured spectral data was established. Calculational techniques were verified by comparing results for a fission source. The Martin Marietta Pu-Be source (M-740) was normalized by determining the neutron emission of the source using the activation of gold foils through various thicknesses of water and comparing with analytically determined thermal neutron flux. Measurements of the neutron spectrum from the Pu-Be source were made in air and through water. This normalization process verified that the stilbene system provides an accurate, reliable means of determining absolute dose rates as well as a relative neutron spectrum.

Neutron measurements were performed on SNAP 19 Subsystem S/N 4 at six spatial locations. The experimental and analytical dose rates at these locations are presented in the following table.

Comparison of Measured and Calculated Dose Rates

Dose Point	Distance from Subsystem Center (in.)	Measured (mrem/hr)	Calculated (mrem/hr)
	Axial		
1	13.8	662	826
2	15.8	411	512
	15° off midplane		
3	12.7	491	517
	Radial		
4	13.1	486	451
5	17.1	315	282
6	29.1	129	104

The gamma spectrum was measured on the SNAP 19 subsystem midplane, 29 inches from the subsystem axis. The measured spectrum compares favorably with the spectrum measured by Mound Research Corporation on System No. 6 capsules. Gamma dose rate data were not obtained.

The program demonstrated that neutron dose rate data obtained experimentally, analytically and using Health Physics techniques were in substantial agreement, and that the stilbene system provides an accurate, reliable means of determining relative neutron spectrum and absolute dose rates.

I. INTRODUCTION

The objective of the SNAP 19 Radiation Measurements Program, Subtask 10.1 of the SNAP 19 Experimental Safety Program, was to determine the energy distribution and absolute magnitude of the neutron and gamma radiation emitted from all SNAP 19 fuel capsules and assembled generator subsystems. A further objective was to apply the data obtained to determine the source of neutrons in the fuel capsule. The requirements for the program are defined in Ref. 1. Limitations imposed by the SNAP 19 program schedule confined the measurements to an evaluation of SNAP 19 Subsystem S/N 4 only. However, all background studies, preliminary measurements and data evaluation were pursued as defined in Ref. 1.

Efforts during the task included assembling the necessary instrumentation, checking out the measurement system and techniques against a neutron source of known strength and energy, measuring the neutron and gamma spectra and fluxes of the fueled subsystem, providing analytical support for the measurements, determining the source of neutrons in the fuel capsule, and proving analytical techniques for calculating potential shield requirements applicable to the subsystem integration process.

This report documents the background and the efforts pursued during this program. The report is divided into seven chapters, with general content as follows:

Chapter I	Introduction
Chapter II	Discusses the theory of neutron spectrum determination using a stilbene crystal detection system.
Chapter III	Describes the electronics, calibration and operation of the neutron spectrometer.
Chapter IV	Discusses preliminary measurements performed to evaluate system response; describes the method of obtaining absolute normalization; and discusses measurements made to establish the absolute normalization.
Chapter V	Describes the neutron spectrum and dose rate measurements and presents the data obtained.
Chapter VI	Discusses gamma measurement techniques, and gamma spectrum measurements and dose evaluation.
Chapter VII	Presents conclusions.

Analysis to determine the source of neutrons from a SNAP 19 fuel capsule is presented in Appendix C. This analysis is reported separately in a classified supplement (MND-3607-173-1) to this report.

BLANK

II. SPECTROMETER THEORY

The stilbene neutron detecting system is basically a device for measuring the amplitude of the light pulses produced by proton recoil resulting from neutron elastic scattering in a hydrogeneous system. The heart of the system is a stilbene crystal which provides the hydrogeneous medium. Extensive analysis and experimentation have been performed for such systems (see, for example, Refs. 2 through 9). This section presents a brief description of some of the aspects of the data reduction technique used to translate the scintillation count rate data to an energy-dependent neutron flux spectrum.

The relation between the observed pulse height spectrum and the neutron spectrum takes its simplest form if the crystal is of such proportions to minimize the probability of neutron second scattering and escape of recoil protons from the crystal. In the absence of these effects, the differential proton spectrum produced by an incident neutron spectrum is

$$\frac{dN_P}{dE_P} = N_h V \int_{E_P}^{\infty} \sigma(E_n) \frac{dN_n}{dE_n} \frac{dE_n}{E_n} \qquad \text{(II-1)}$$

where

E_n = neutron energy (Mev)

E_P = proton energy (Mev)

dN_P/dE_P = number of protons per unit proton energy (Mev^{-1})

dN_n/dE_n = number of neutrons per unit area per unit neutron energy interval incident on the crystal (cm^{-2} Mev^{-1})

σ = hydrogen scattering cross section (cm^2)

$N_h V$ = number of hydrogen atoms in the crystal (product of the hydrogen atom density per unit volume N_n (cm^{-3}) and the crystal volume V (cm^3)

The integration is necessary since, in neutron-proton scattering, a proton of energy, E_P, may be produced by any neutron whose energy is greater than E_P. An expression for the neutron spectrum is obtained by differentiating and solving Eq. II-1. Hence,

$$\frac{dN_n}{dE_n} = -\frac{E_n}{N_h V \sigma} \left[\frac{d^2 N_P}{dE_P^2}\right]_{E_n = E_P} \qquad \text{(II-2)}$$

The actual measurement is of the number of protons per unit pulse height, dN_P/dL (Mev^{-1}). In terms of this quantity, the neutron spectrum is

$$\frac{dN_n}{dE_n} = \frac{-E_n}{N_h V \sigma(E_n)} \left[\frac{dL}{dE_P} \frac{d}{dL} \left(\frac{dL}{dE_P} \frac{dN_P}{dL} \right) \right]_{E_n = E_P}$$

$$= \frac{-E_n}{N_h V \sigma(E_n)} \left[\left(\frac{dL}{dE_P} \right)^2 \frac{d^2 N_P}{dL^2} + \frac{dN_P}{dL} \frac{d^2 L}{dE_P} \right]_{E_n = E_P} \qquad \text{(II-3)}$$

Here, $L = f(E_P)$ is the response (nonlinear for stilbene) of the scintillation crystal to protons (Mev).

A computer program for the numerical solution of Eq. II-3 was obtained from Mound Research Corporation (MRC). This program, as-received, was coded for the IBM 1620. Modifications to this program were minimal; a subroutine for the correction of raw data for low energy channels was removed (this correction applied only to the MRC system) and modifications necessary to adapt the program to the Martin Marietta IBM 7094 or IBM 360 system were made. No changes were made in the theory and equations of the code. A description of this program and list of the FORTRAN IV source deck are given in Appendix A.

The data reduction technique is essentially the same as that used by McN. Wasson (Ref. 9). The normalization of this technique is such that calculated spectral values are of the correct magnitude. Thus, the stilbene system and the associated data reduction will yield not only the spectral shape but also the absolute magnitudes of the time-integrated differential flux over the applicable energy range. An assumption is made in the normalization that neutrons are incident only on the broad (flat) face of the cylindrical crystal. For this reason measurements are made with the stilbene crystal axis directed at the source. This is a reasonable approximation for relatively small sources. However, appreciable amounts of scattering material, such as test cell walls or structural material, could introduce a significant number of scattered neutrons which would perturb both the shape and magnitude of the spectral measurement.

The stilbene crystal also responds to recoil electrons from Compton scattering of photons. Included in the system are gamma discriminating circuits. The purpose of this device is to eliminate light pulses due to gammas from the recorded count. An assumption in the data reduction technique is that all recorded pulses are due to neutron scattering events.

Corrections are made for wall effect (protons which lose only part of their energy before escaping the crystal) and for neutron second scattering. Rigorous analysis of these effects is obviously very complex. Uncertainty related to these geometry-dependent corrections can be minimized by selection of the proper crystal size. A relationship has been derived which relates the minimum correction to the crystal thickness (Ref. 8) for a cylindrical crystal geometry in which the radius equals the thickness. This relationship is, however, energy-dependent. For measurement of mono-energetic neutron sources, a crystal size could be selected which would minimize uncertainty due to wall effect and second scattering. Optimum crystal sizes for a cylindrical crystal, as reported by Broek and Anderson (Ref. 8), are as follows:

Neutron Energy (Mev)	Optimum Crystal Thickness or Radius (cm)
1	0.14
2	0.28
5	0.78
10	1.8

For the measurement of continuous spectra, these considerations imply that crystal size should be chosen at the expected mid-range energy or at energies where error is to be minimized. The system employed in this program, and described in Chapter III, used a cylindrical crystal for which the radius, R, is equal to the thickness, τ, of 0.5 centimeter. This crystal appears to be a reasonable choice for measurement of continuous spectra over the range of 1 to 10 Mev.

The light response of stilbene to protons is nonlinear. Ideally, the response for a particular system could be measured utilizing a series of mono-energetic neutron sources which span the energy range over which spectral measurements are to be made to determine the response for each neutron energy. This procedure is far from practical, however, and limited experimental data have been used to construct the empirical form assumed for all analyses reported herein. The assumed relationship for the light pulse, L_P, (in Mev energy units) and the proton energy, E_P, (Mev) is

$$L_P = 0.192\ E_P^{1.342} \tag{II-4}$$

Greatest uncertainty in this relationship occurs for low energies.

Energy calibration of the detector systems is accomplished by using single line energy gamma sources. Crystal response to recoil electrons from gamma Compton scattering is linear. The energy at which the Compton edge occurs, E_C, (Mev) for a gamma line emission energy E_γ, is (Mev):

$$E_C = E_\gamma - \frac{0.51\ E_\gamma}{0.51 + 2\ E_\gamma} \tag{II-5}$$

Measurement of the energy spectrum from a gamma source provides the basis for assignment of energy to a channel by observing at which channel, H_C, the Compton edge occurs. Electron equivalent energy, L (Mev), for Channel H is then

$$L = aH + b \tag{II-6}$$

where the constants a and b are evaluated from Eq. (II-5) using two separate gamma energies, E_{γ_1} and E_{γ_2}. For two gamma source measurements of Compton edge energies, E_{C_1} and E_{C_2} occurring in channels H_{C_1} and H_{C_2}, the constants in Eq. (II-6) are evaluated to yield:

$$L = \frac{E_{C_2} - E_{C_1}}{H_{C_2} - H_{C_1}} (H - H_{C_1}) + E_{C_1} \tag{II-7}$$

The zero energy channel, H_b, is, according to Eq. (II-7),

$$H_b = -\left(\frac{H_{C_2} - H_{C_1}}{E_{C_2} - E_{C_1}}\right) E_{C_1} + H_{C_1} \tag{II-8}$$

Equation (II-7) in terms of H_b becomes

$$L = \left[\frac{H - H_b}{H_C - H_b}\right] E_{C_1} \tag{II-9}$$

H_b, referred to in Ref. 8 as a back bias, is a necessary input to the data reduction program (Appendix A).

The known electron energy equivalence (Eq II-9) and the proton-light response function (Eq II-4) are used to determine the relationship between neutron energy E_n (Mev) and channel number as

$$E_n = \left[\frac{L}{0.192}\right]^{\frac{1}{1.342}} = \left[\frac{1}{0.192}\ \frac{H - H_b}{H_C - H_b}\ E_{C_1}\right]^{\frac{1}{1.342}} \qquad \text{(II-10)}$$

Examination of the nonlinear dependence on channel number as expressed in Eq. (II-10) demonstrates the necessity of very accurate gamma calibration. Small uncertainties in determination of the Compton edge channel, H_C, and the electron zero energy channel, H_b, can cause great uncertainty in the calculated neutron energy, E_n. This is particularly true at high neutron energies. For this reason, the experimental procedure used with the Martin Marietta stilbene system calls for frequent gamma calibration with two gamma sources representing two different line energies.

The nonlinear energy dependence also necessitates two measurements at two different gamma settings to accurately determine a continuous spectrum which spans energies in the Mev range. For the Martin Marietta system, two different gamma energy settings are used. In terms of cesium-137 (E_C = 0.478 Mev), the system is adjusted for the following settings:

Setting	H_C Approximate Location of Cs-137 Compton Edge	Approximate Energy Range where Neutron Results are Valid (Mev)
1	110 to 120	1.0 to 3.0
2	15 to 20	>3.0

Two neutron measurements are then made for these two sections. The selection of the changeover energy of 3.0 Mev is somewhat arbitrary. This energy cutoff is only approximate and a judgment must be made as to which data are to be accepted. Normally, in the energy region where the results overlap, variation in the two sets of data is within 20% so that error in the overall measurement is relatively small.

III. SPECTROMETRY SYSTEM

A. ELECTRONIC EQUIPMENT

Measurements of neutron spectrum and absolute dose rate were made with the neutron spectrometer shown in Fig. III-1. The block diagram in Fig. III-2 shows that the spectrometer consists of a scintillation counter employing a stilbene crystal detector, a preamplifier section, a discriminator section and a 256-channel analyzer. The circuit employed in the preamplifier and discriminator sections is shown in Fig. III-3. This circuit is based on the electronic circuit described in Ref. 4.

Although organic scintillators have a very high efficiency for detection of fast neutrons, one limitation in their use as spectrometers in the past had been their high sensitivity to gammas and the resulting high gamma background (Ref. 8). The circuit in this system makes use of space charge effects in the photomultiplier tube to discriminate against the gammas. By maintaining the potential on Dynode 14 only a few volts below that on the anode, a space-charge saturation condition is set up. Under this condition, the last dynode is driven negative during the initial fast component part of all pulses. For a pulse from a recoil electron (due to an incident gamma), the last dynode will remain negative for several microseconds. A recoil proton (due to an incident neutron) will produce a pulse which goes positive in less than a microsecond. This positive-going pulse is shaped in the discriminator to provide a gating pulse. All pulses are picked off from Dynode 11, amplified and fed into the multichannel analyzer. The gating pulse triggers the analyzer so that only the pulses produced from incident neutrons are counted by the analyzer.

B. SPECTROMETER CALIBRATION

In the calibration of the neutron spectrometer, measurements were made to establish the proper high voltage to be applied to the photomultiplier tube and the appropriate potential difference between the anode and Dynode 14 for providing space-charge saturation. The effects of temperature on the electronic equipment were investigated. Daily routine calibration procedures were established.

Initially, the photomultiplier was operated at 1550 and 1700 volts with the voltage between the anode and last dynode adjusted so the positive excursions of the neutron pulses reached about 3.0 volts maximum to produce conditions of space-charge limitation of the current for the majority of pulses of interest. At 1550 volts, the neutron full-scale energy was 12.5 Mev, but resolution lower than about 1.5 Mev could not be achieved. At 1700 volts, the neutron full-scale energy was 3.5 Mev, and the lower limit was about 0.5 Mev. The neutron full-scale energy for each of the high-voltage settings could actually be varied by changing the electronic gain so that the midpoint of the drop off in the Compton recoil spectra from the gamma calibration sources falls into a different analyzer channel.

With the two high-voltage settings, a neutron energy range of about 0.5 to 12.5 Mev was achieved. These particular voltages, 1550 and 1700 volts, were chosen after measurements were made at several voltages to determine where optimum conditions for practical neutron detection with the maximum amount of gamma ray discrimination existed. During the period between the preliminary measurements with the spectrometry system and the measurements on the SNAP 19 No. 4 subsystem, the spectrometer was shut down for approximately six months. On startup it was found that a slight calibration change had taken place. As a result, all subsequent calibration measurements and measurements on the generator subsystem were made with high voltage settings of 1535 and 1650 volts. This permitted the system to cover the same energy range as achieved previously; that is, from about 0.5 to 12.5 Mev.

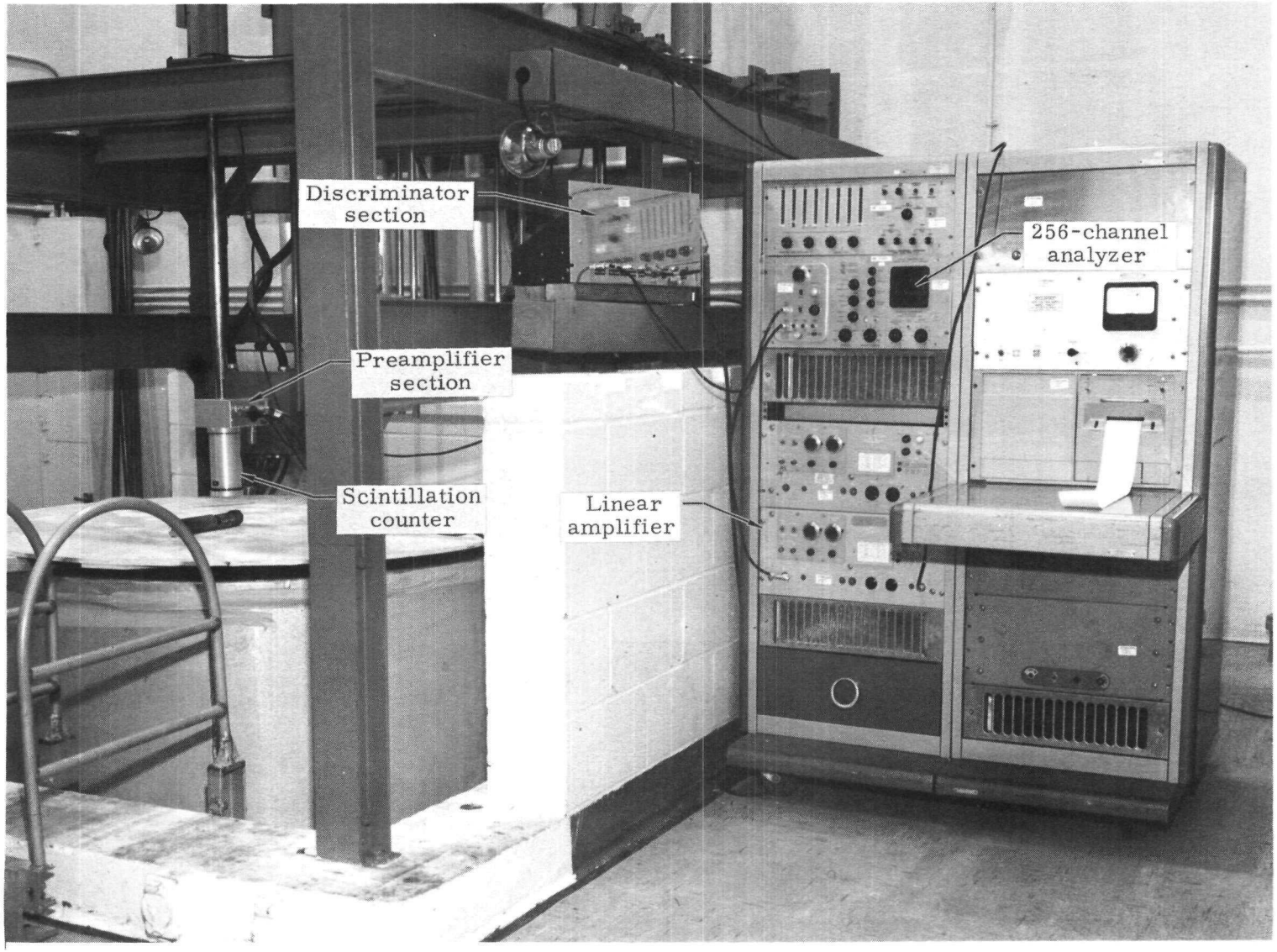

FIG. III-1. NEUTRON SPECTROMETER

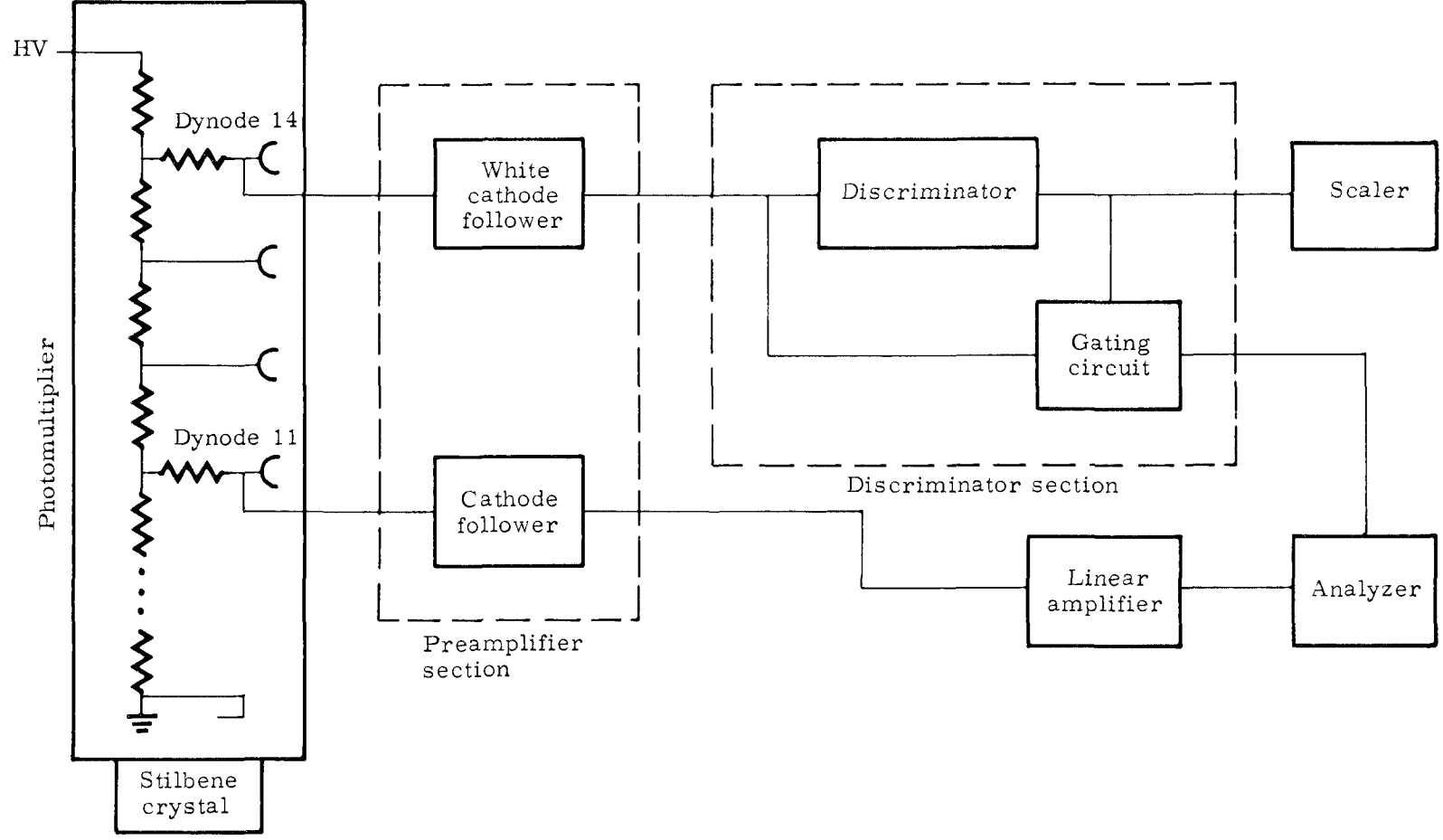

FIG. III-2. BLOCK DIAGRAM OF NEUTRON SPECTROMETER

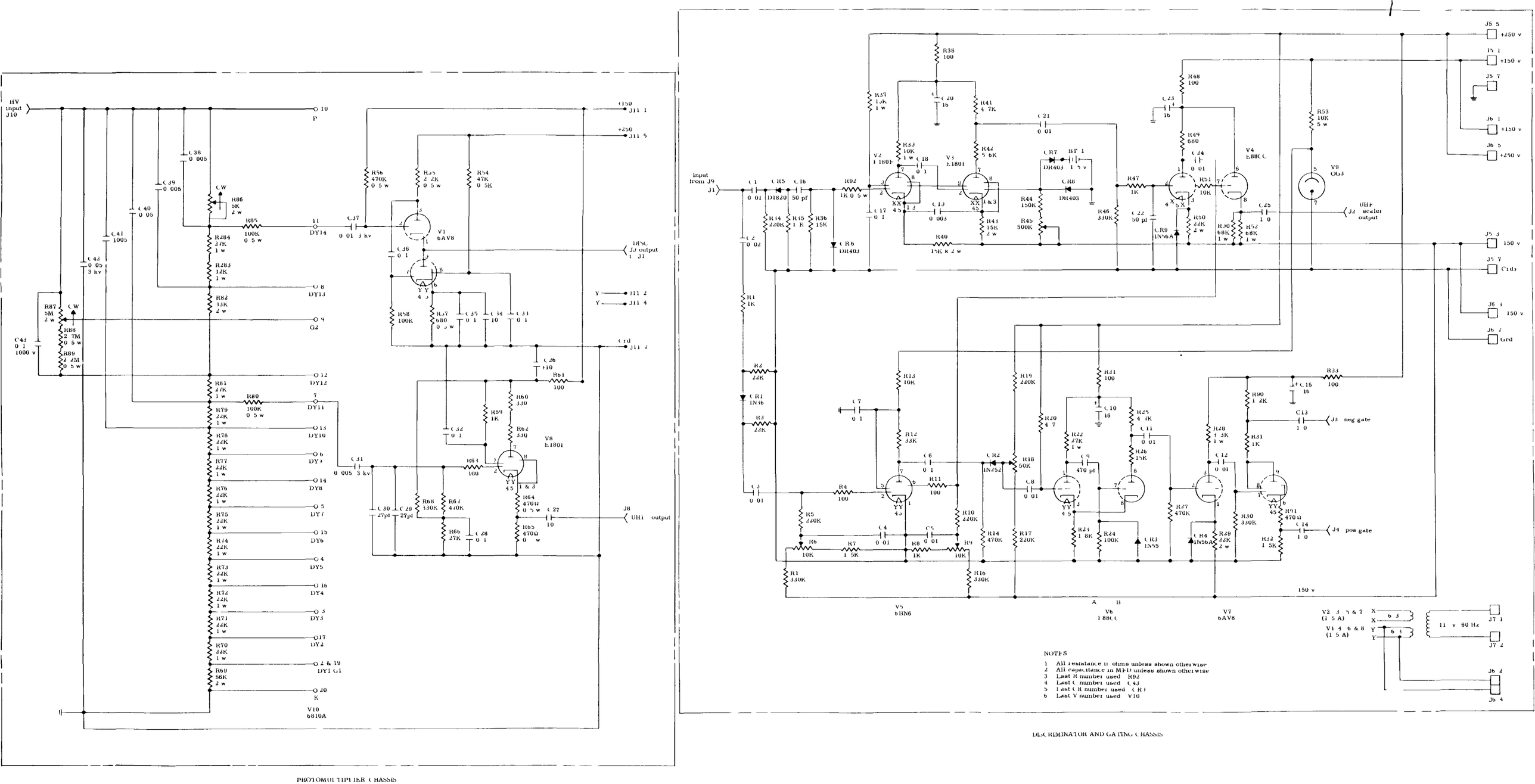

FIG. III-3. NEUTRON SPECTROMETER SCHEMATIC

The observed neutron spectrum is influenced by the total count rate to which the spectrometer is exposed. This combined neutron and gamma count rate is measured on the scaler shown in Fig. III-2. Based on the measurements described in Chapter IV-A, it was determined that at count rates above approximately 8000 counts/sec the spectrum became erratic. Based on this evaluation, measurements throughout the program were made with the system set up to limit the count rate to the range between 1000 and 8000 counts/sec.

The neutron spectrometer system was found to be extremely sensitive to temperature. There was no temperature problem as long as the spectrometer was operating in a room where the temperature was fixed, preferably below 70° F. The problem was caused by the address storage current in the computer of the multichannel analyzer. This current could be set to operate at a given temperature, but slight changes in temperature (greater than $\pm$ 5° F) caused it to vary. When the current varied, it caused the wrong number of counts to be randomly placed in different channels of the analyzer. Because of statistical variations in the output from the analyzer, it was not certain whether variations were real or false. Close control on the room temperature eliminated this uncertainty.

Output data from the spectrometer are in the form of integral spectra and are printed out on paper tape as relative number of counts per channel. These data (number of counts per channel) are actually the pulse height spectrum produced by the recoil protons originating in the stilbene crystal. Analysis of these data to yield the incident neutron energy distribution was performed using the techniques described in Chapter II.

C. CALIBRATION USING COMPTON EDGES

To establish the energy range of the neutron spectrometer at various photomultiplier high voltage settings, calibration was performed using the Compton recoil spectra of the gamma rays from cesium-137, sodium-22 and manganese-54. The response of the stilbene crystal to electrons is linear, but to protons it is nonlinear. The computer program has a neutron energy scale correction factor for this nonlinearity, but the program must have the neutron full-scale energy, E_{max}, as a reference. The neutron full-scale energy was determined (using the analyzer channel in which the midpoint of the dropoff in the Compton recoil spectrum from the gamma source is located) through the expression:

$$E_{max} = \left[\frac{255.5\ E_c}{0.192\ (H_c - H_b)} \right]^{0.7452} \qquad \text{(III-1)}$$

where

E_{max} = neutron full scale energy (Mev)

H_c = analyzer channel where the midpoint of the Compton edge is located

H_b = gamma zero energy channel

E_c = energy of the midpoint of the Compton edge (Mev)

For Cs-137, Na-22 and Mn-54, the values of E_c are 0.478, 0.341 and 0.64 Mev, respectively. This method is also used as the daily routine calibration check on the spectrometer to correct for drift or changes in gain of the electronic equipment.

BLANK

IV. DETERMINATION OF SPECTROMETER CHARACTERISTICS

A. INITIAL RESPONSE MEASUREMENTS

Several neutron experiments involving the stilbene detector system and the Martin Marietta plutonium-beryllium neutron source (M-740) were conducted.

The experiments were devised to demonstrate the characteristics of the Martin Marietta stilbene detector system and to verify that this system can duplicate results obtained from extensive prior experimentation and analysis of stilbene neutron spectroscopy. The purpose and description of each experiment is given in Table IV-1 along with a figure number reference showing the results. The neutron spectra shown in Figs. IV-1 through IV-11 were derived from the experimental data by use of the data reduction code obtained from Mound Research Corporation (Appendix A).

A spectral measurement involves two experimental measurements at different high voltages and instrument settings to obtain the low energy spectrum (less than 3.2 Mev) and the high energy spectrum (greater than 3.2 Mev). The selection of the 3.2 Mev cutoff was arbitrary but it appears to be a very reasonable choice. Actual measurements overlap as indicated by the data points on Figs. IV-1 through IV-11. In these figures, the symbol O is used for high energy measurements and the symbol Δ is used for low energy measurements. All spectral measurements have been normalized to approximately the same area under the curve. Linkage of the low and high energy spectra have been made by adjusting the absolute neutron flux from the low energy result to the absolute flux of the high energy measurements at the single energy point of 3.25 Mev. (This point is the approximate location of a maximum in the Pu-Be spectrum.) The adjustment factor varied from 0.91 to 1.12, corresponding to an uncertainty range of -9 to +12%. This uncertainty appears to be mainly due to the channel groupings selected for the reduction code analysis. Statistical uncertainty for these channel groupings was within $\pm$ 8% and $\pm$ 5% for the low and high energy measurements, respectively, with corresponding group widths of 12 and 8 channels. A somewhat more appropriate linking of high and low energy results would have been to match the peak in the vicinity of 3.2 Mev rather than to match at a single point. This procedure would, however, involve extensive re-analysis to adjust energy values of one or both low and high energy results.

A comparison of results for the various experiments was performed. The indicated results and conclusions follow.

1. Count Rate Determination

The results for fast neutrons (> 3.0 Mev) of the various count rates have been replotted on Fig. IV-12. Only very minor variations can be expected due to the manner of normalization and results do not lie within the computed statistical accuracy. However, with the exception of the results for the highest gross count rate of 8000 cps (the dotted line in Fig. IV-12) and the behavior about the peak near 10 Mev, all results are within $\pm$30% of a median spectrum which may be constructed by drawing a line through the midpoint of the band.

Two factors may significantly influence the results and account for most of the variation:

(1) The reported analysis was performed using a constant channel grouping of 8 channels. This channel grouping was chosen because the computed statistical uncertainty was small. Results obtained with larger groupings tend toward more consistent results. However, larger groupings also tend to smooth results and may result in omission of physically significant details of the spectrum.

TABLE IV-1

Neutron Experiment Description

Detector count rate

Purpose: To determine variation in spectral and total flux measurements at various count rates (and corresponding distances).

Description: Measurements of Pu-Be neutrons were made over a range spanning the anticipated count rates for the SNAP 19 capsules and generators. Gross count rates (neutron and gamma) for high energy measurements ranged from 100 to 8000 cps. Results are:

Gross Count Rate (cps)		
Neutrons		
> 3.2 Mev	< 3.2 Mev	Fig. No
100	--	IV-1
250	--	IV-2
1150	1600	IV-3
1700	2400	IV-4
3800	--	IV-5
8000	--	IV-6

Reproducibility

Purpose: To determine extent to which given measurement could be reproduced.

Description: Repeat measurement was made after time lapse of approximately a week, during which instruments were readjusted for high and low energy measurements several times. Instruments were reset at original settings and counting times were approximately same (within 10% of original counting time).

Measurement	Counting Time (min) (high)	(low)	Gross Count Rate (cps)	Fig. No.
Original	100	200	1700, 2400	IV-4
Repeat	90	210	1700, 2400	IV-7

Attenuation

Purpose: To determine ability of stilbene system to measure spectral change and magnitude of flux resulting from hydrogeneous shield material.

Description: For fixed source-detector separation distance of 6.5 in., 3 measurements were made with bare source, 3-in. slab of paraffin between source and detector, and two 3-in. slabs of paraffin. Slab dimensions were large (12 x 14 in.). Source and detector size and separation distance effectively simulated semi-infinite slab when placed perpendicular to source detector line.

Configuration	Fig. No.
Bare source	IV-7
3 in. paraffin	IV-8
6 in. paraffin	IV-9

Scattering

Purpose: To determine extent, if any, to which neutrons scattered from facility walls and support equipment influence measurements.

Description: Two measurements were made of neutrons through paraffin, one with slab 6 in. thick (see attenuation experiment) and one a 6-in. thick block shield. Block shield had lateral dimensions sufficiently small (2 x 4 in.) to attenuate only direct neutrons and neutrons reaching detector after relatively small angle scatter. Both measurements were made with fixed source-detector separation distance of 6.5 in.

Configuration	Fig. No.
Slab shield	IV-9
Block shield	IV-10

Crystal Orientation

Purpose: To determine reproducibility of spectral shape and differences in absolute count rate at differing stilbene crystal orientation with respect to source.

Description: Two measurements were made at fixed source detector separation of 6.3 in. Crystal orientations with respect to source detector line were alternately flat (top of cylindrical crystal directed toward source) and curved (curved cylindrical surface of crystal directed toward source). Nominal mode of measurement is flat orientation.

Crystal Orientation	Fig. No.
Flat	IV-7
Curved	IV-11

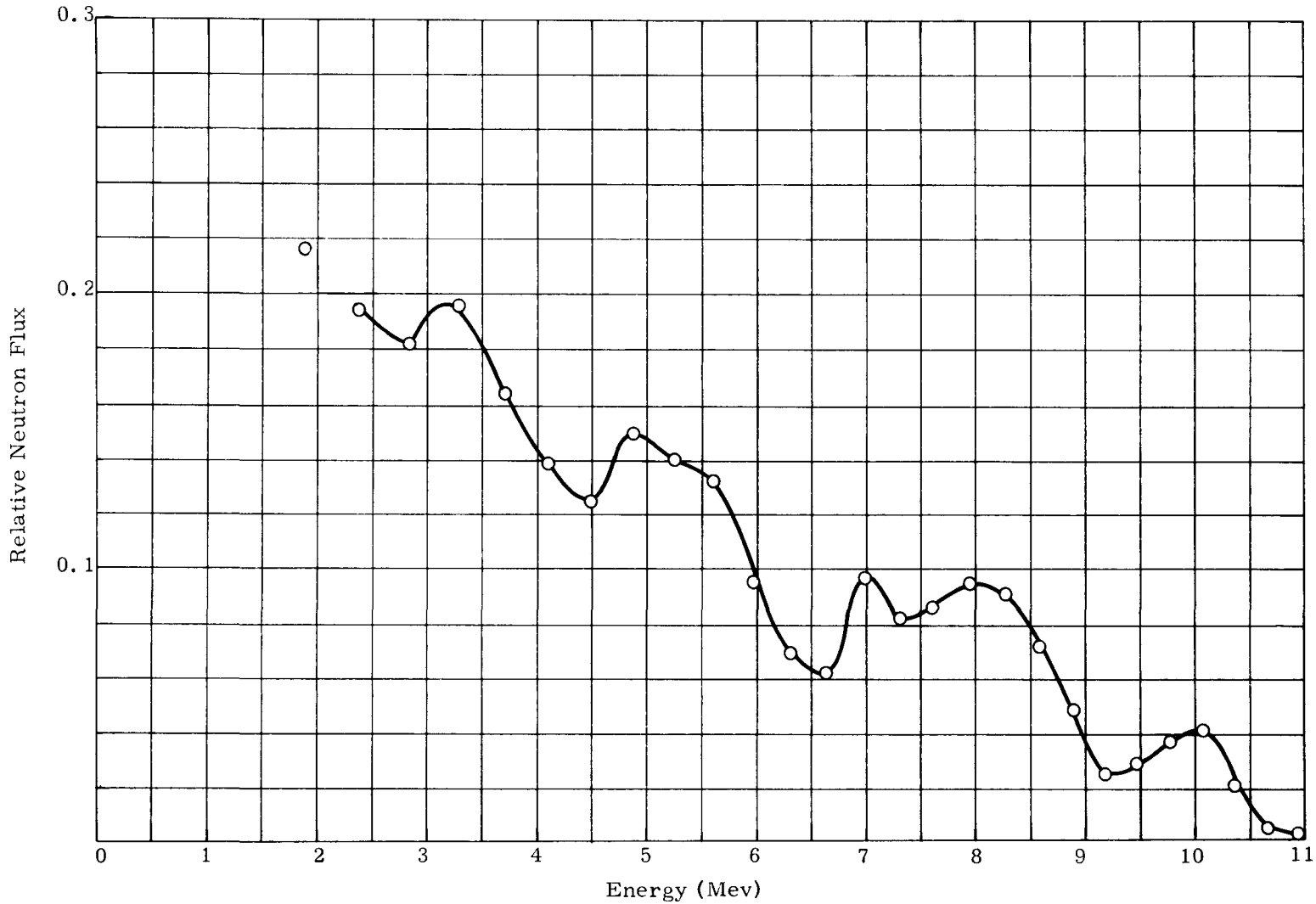

FIG. IV-1. BARE PuBe SOURCE GROSS COUNT RATE AT 100 CPS

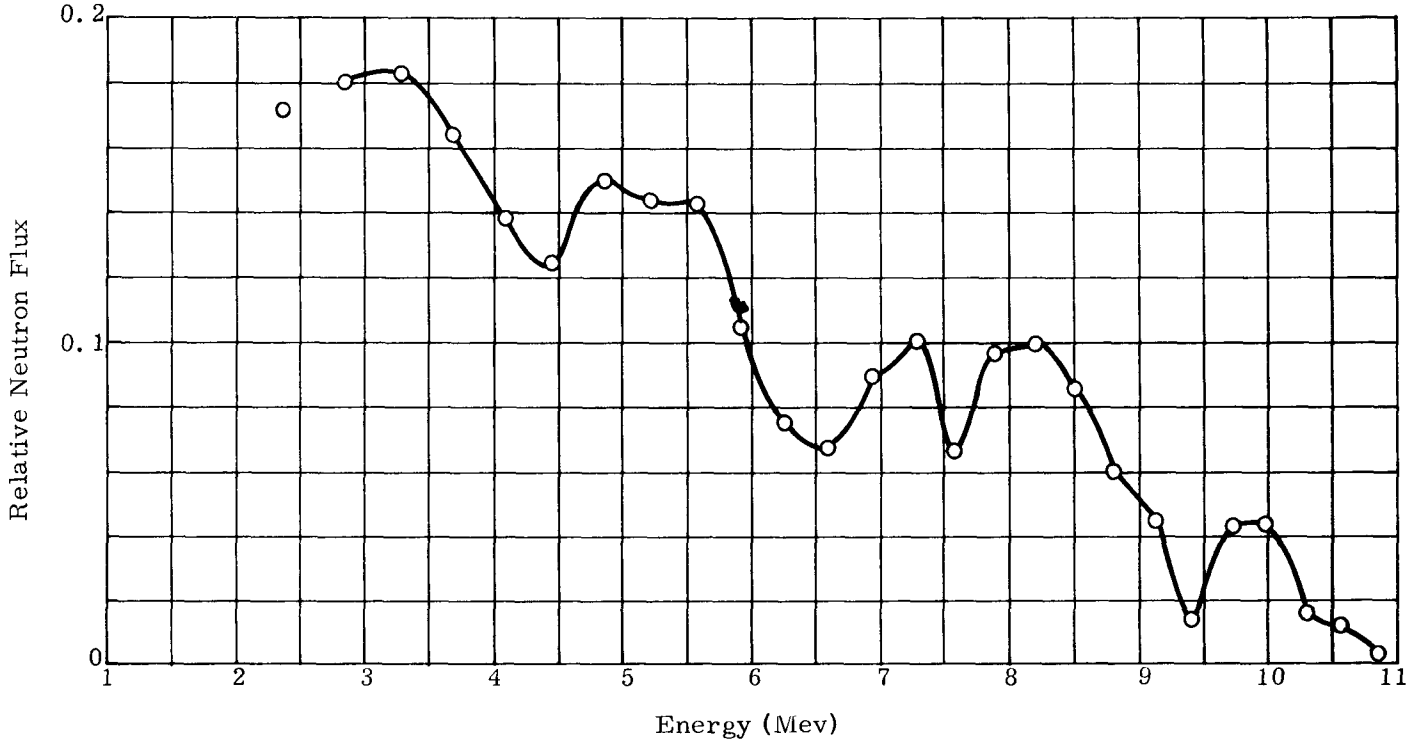

FIG. IV-2. BARE PuBe SOURCE GROSS COUNT RATE AT 250 CPS

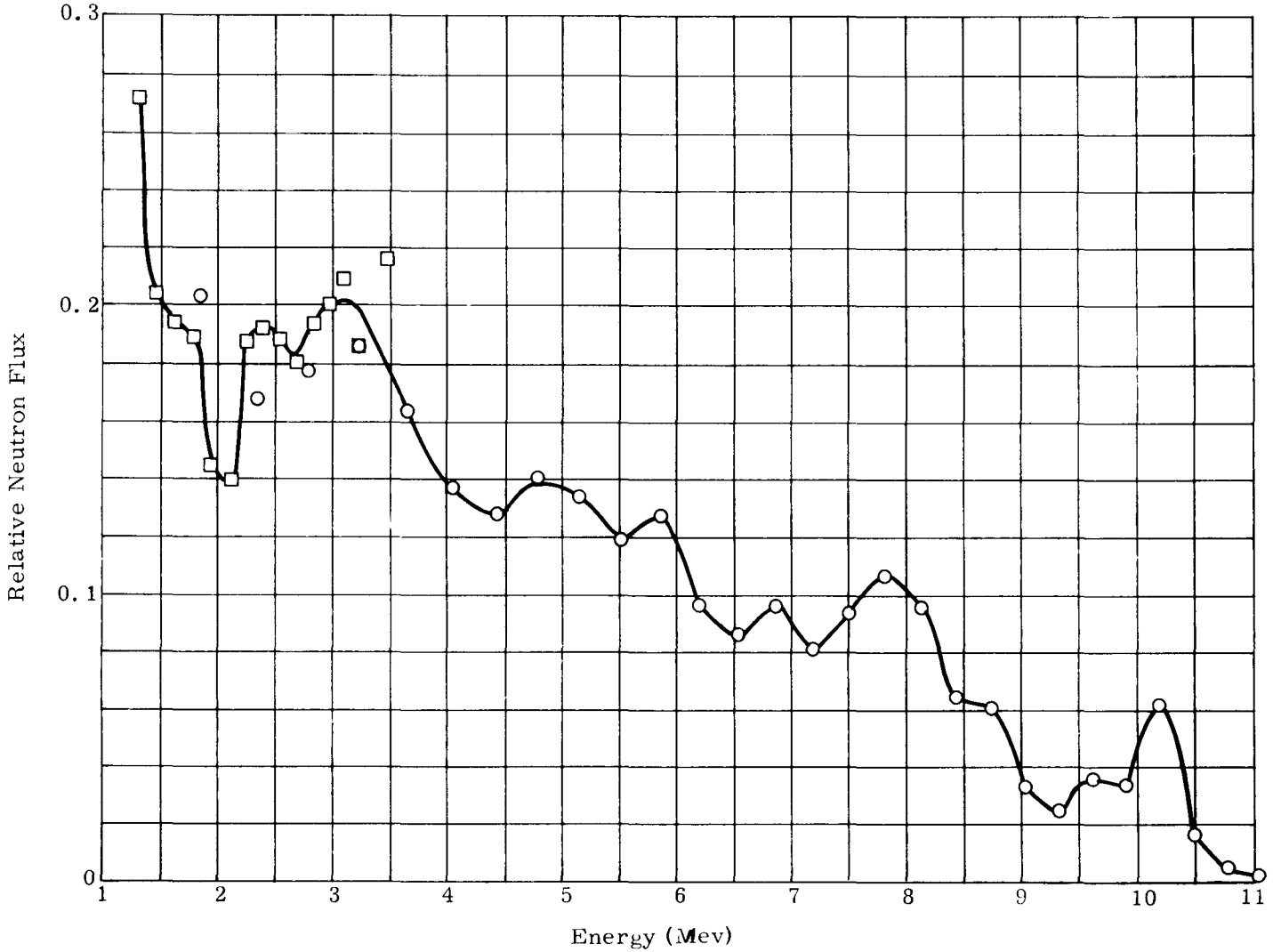

FIG. IV-3. BARE PuBe SOURCE GROSS COUNT RATE AT 1150 CPS

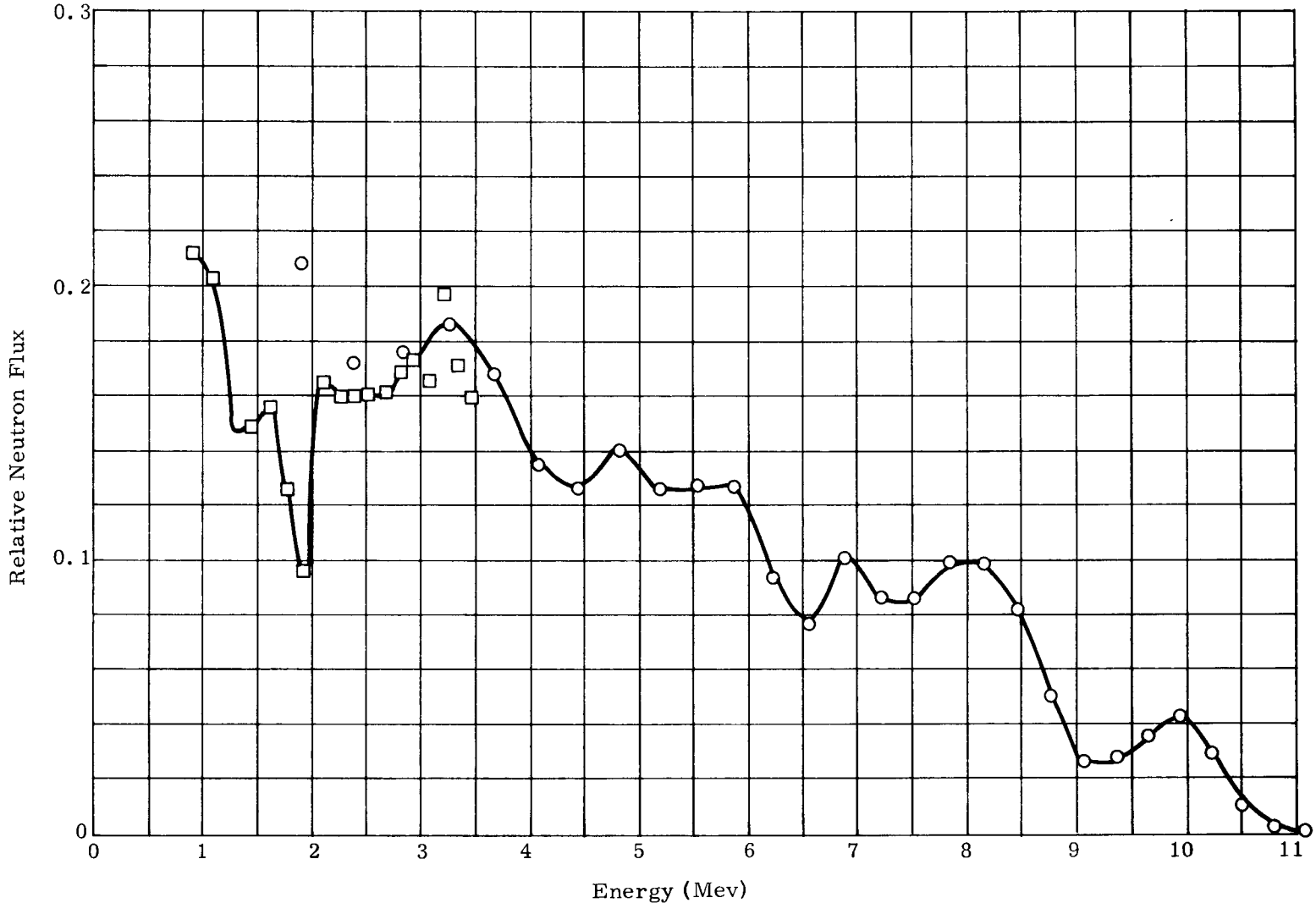

FIG. IV-4. BARE PuBe SOURCE GROSS COUNT RATE FOR HIGH ENERGY = 1700 CPS; LOW ENERGY = 2400 CPS

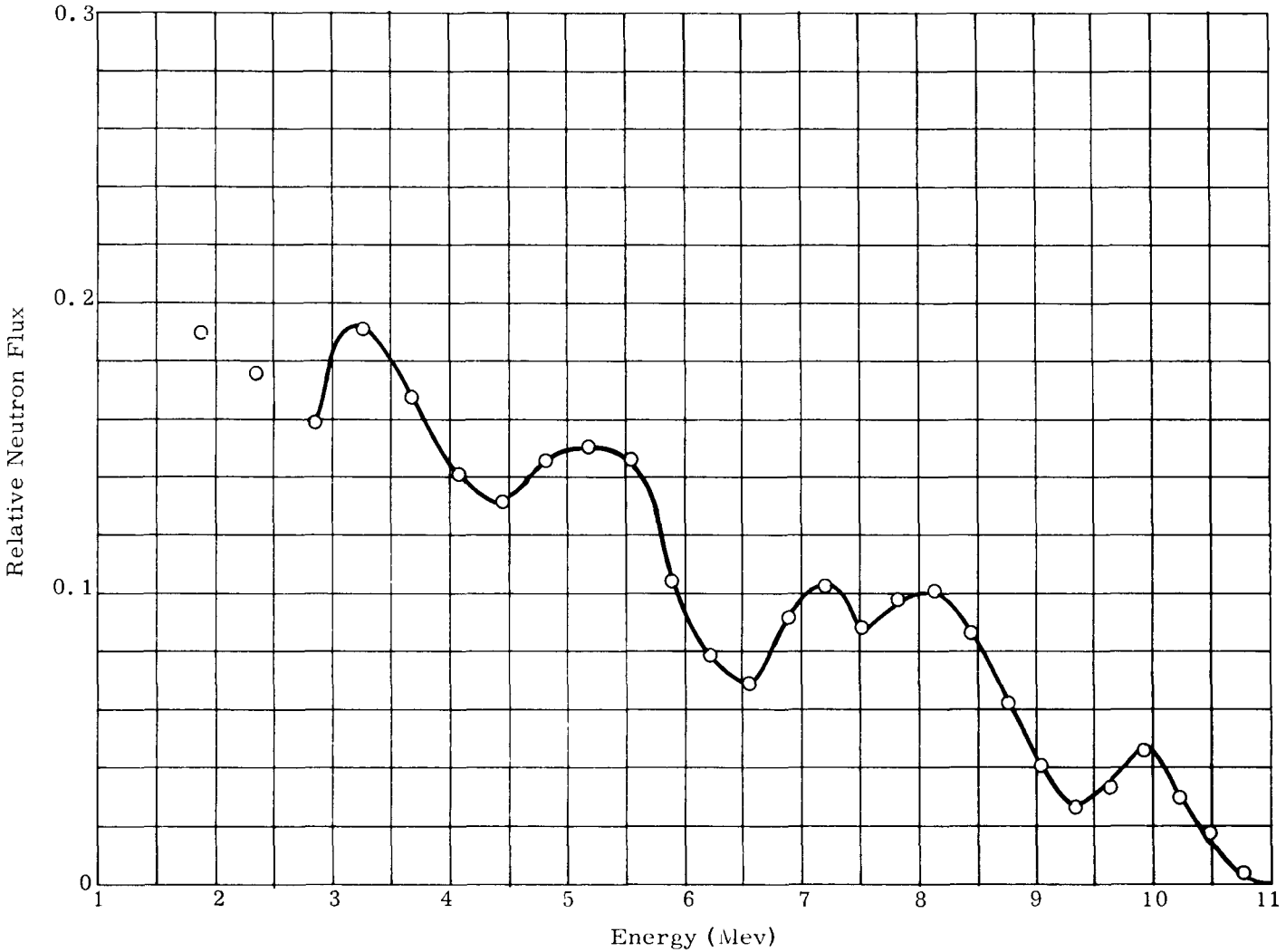

FIG. IV-5. BARE PuBe SOURCE GROSS COUNT RATE AT 3800 CPS

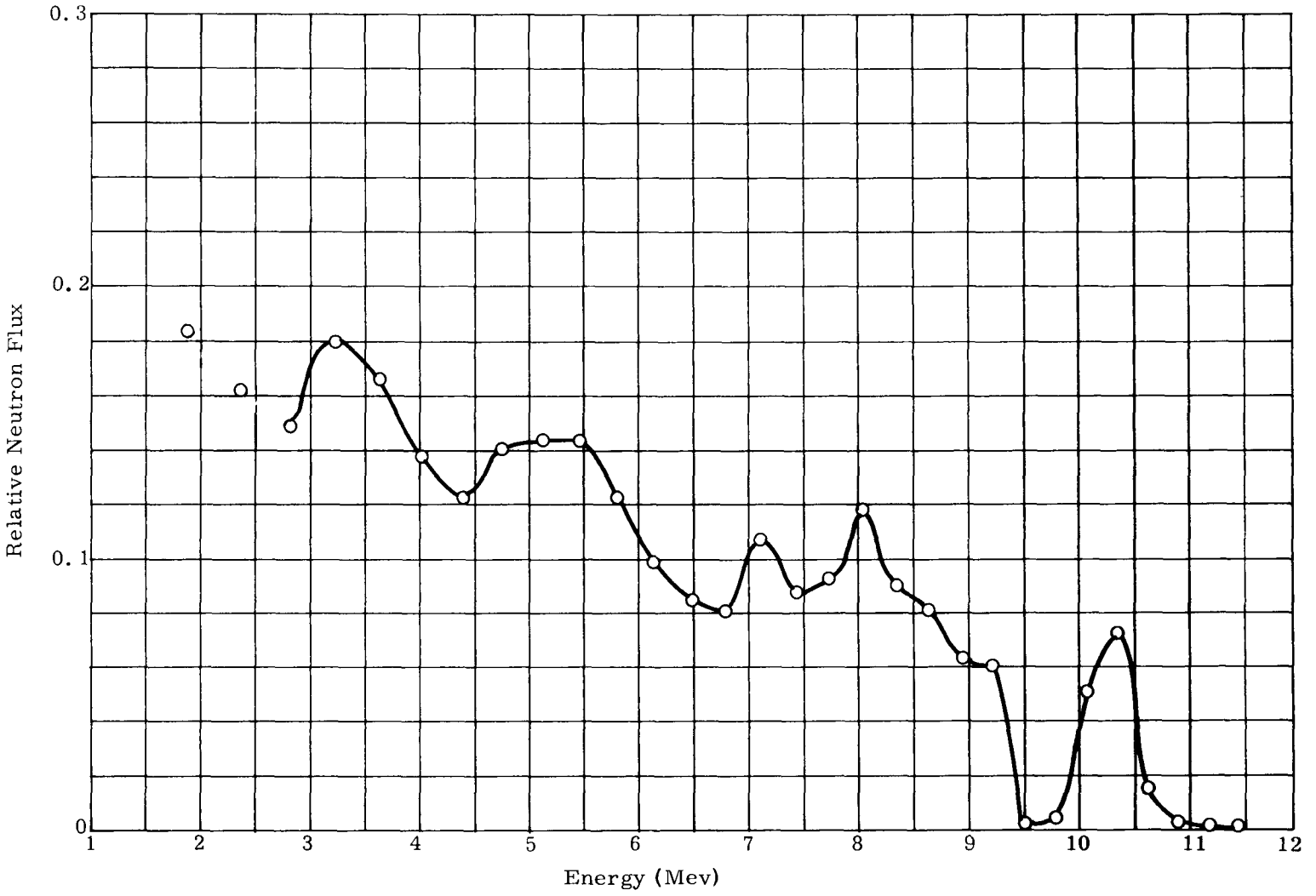

FIG. IV-6. BARE PuBe SOURCE GROSS COUNT RATE AT 8000 CPS

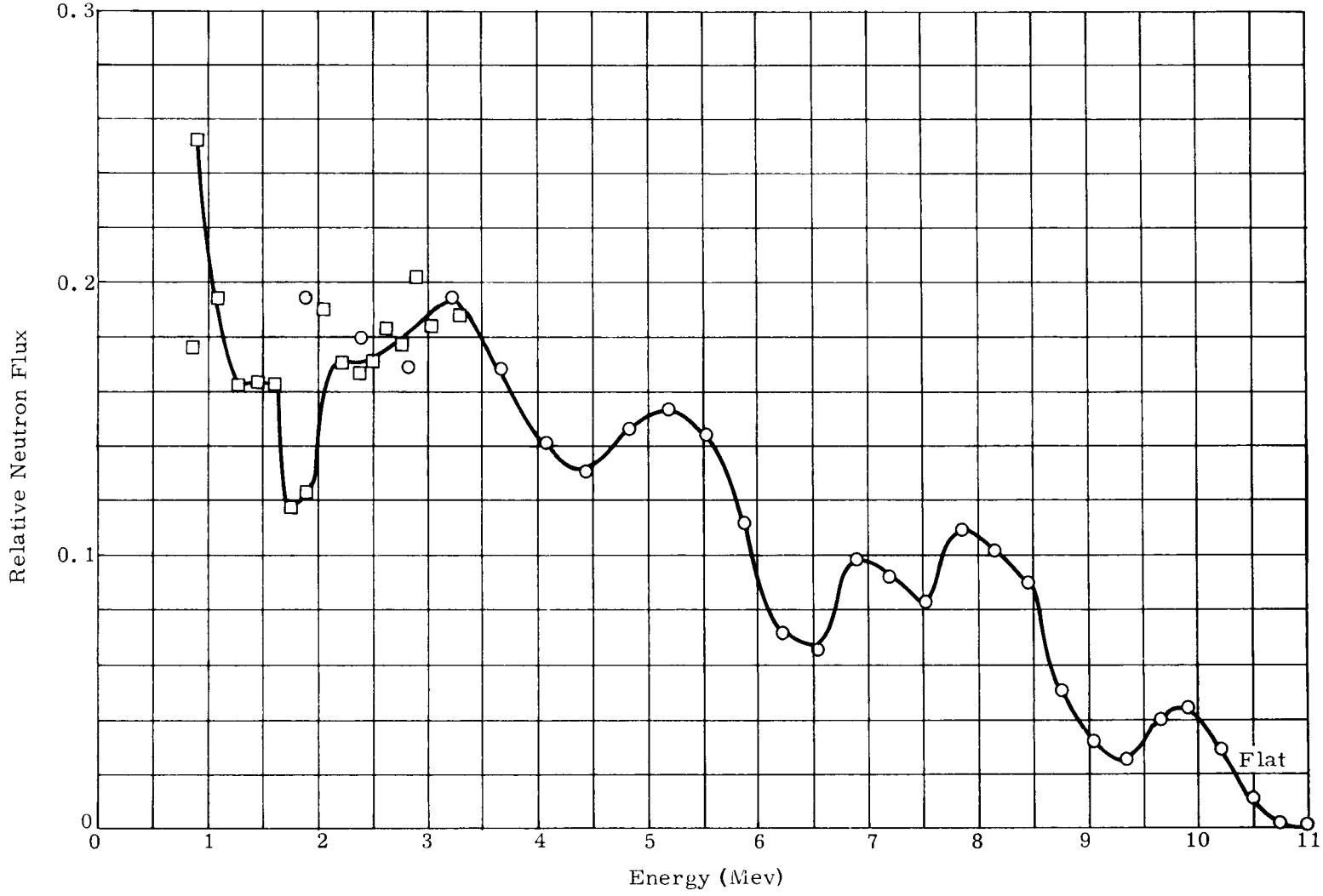

FIG. IV-7. BARE PuBe SOURCE GROSS COUNT RATE FOR HIGH ENERGY = 1700 CPS
LOW ENERGY = 2400 CPS

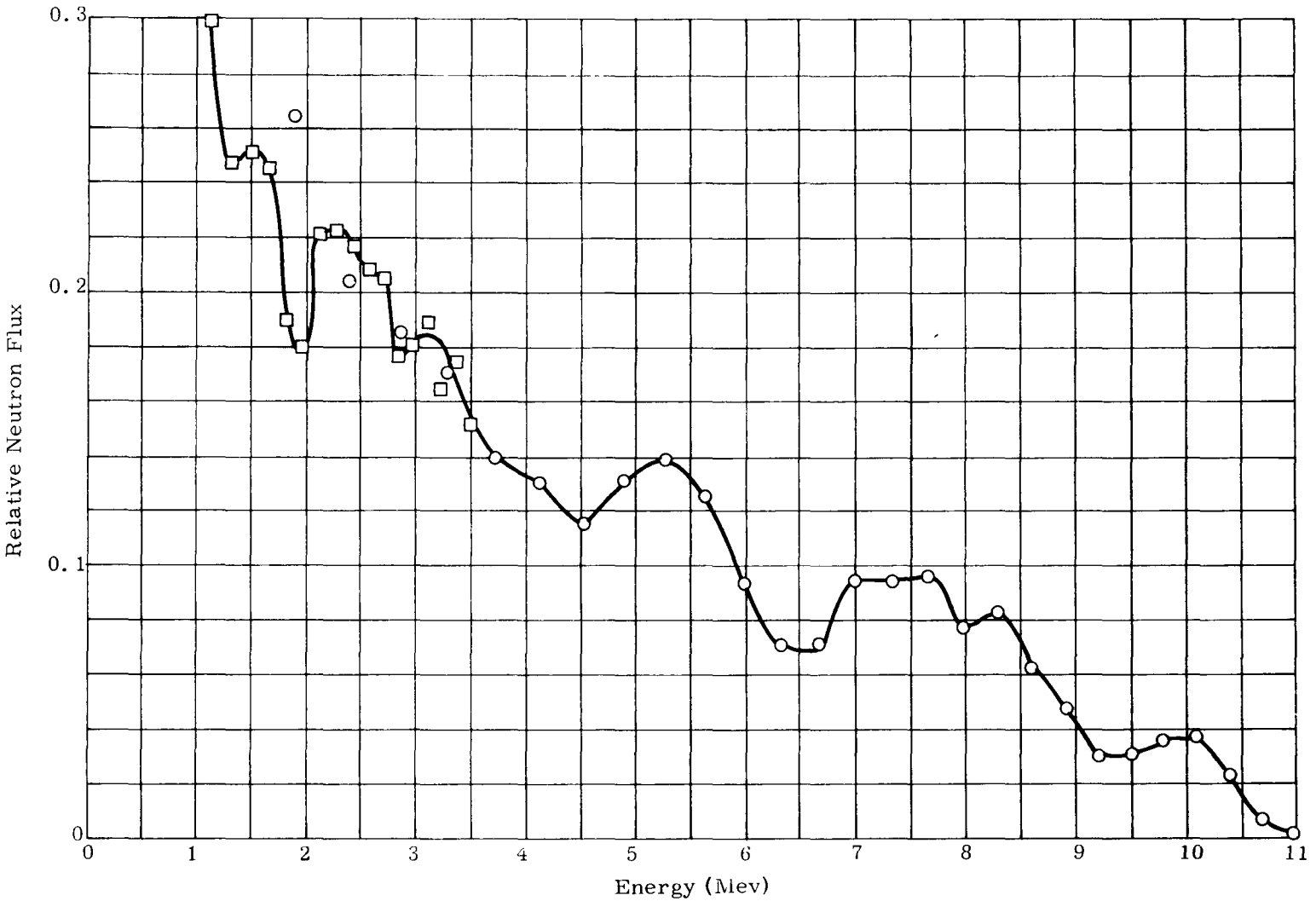

FIG. IV-8. PuBe SOURCE BEYOND THREE-INCH PARAFFIN SLAB SHIELD

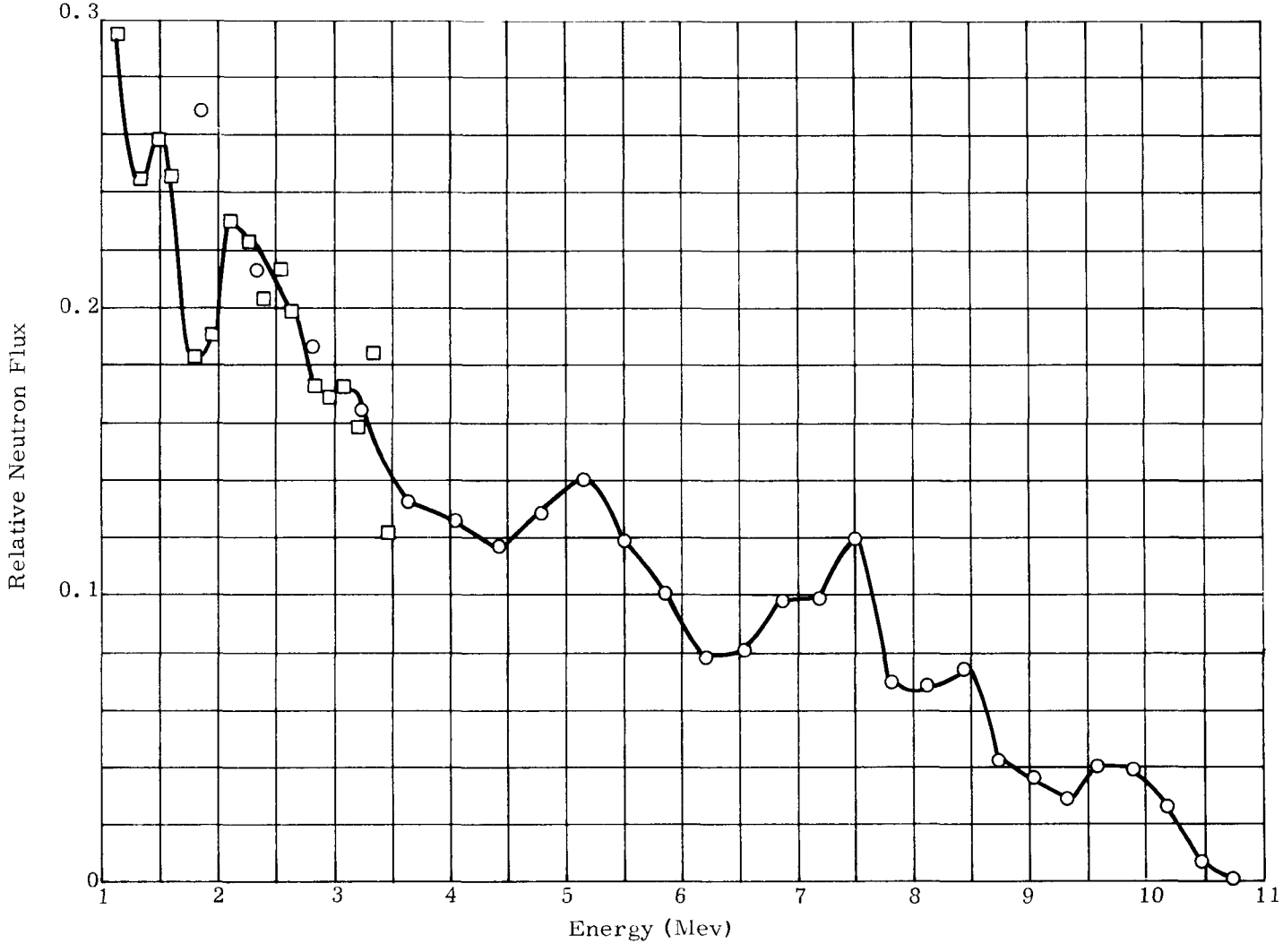

FIG. IV-9. PuBe SOURCE BEYOND SIX-INCH PARAFFIN SLAB SHIELD

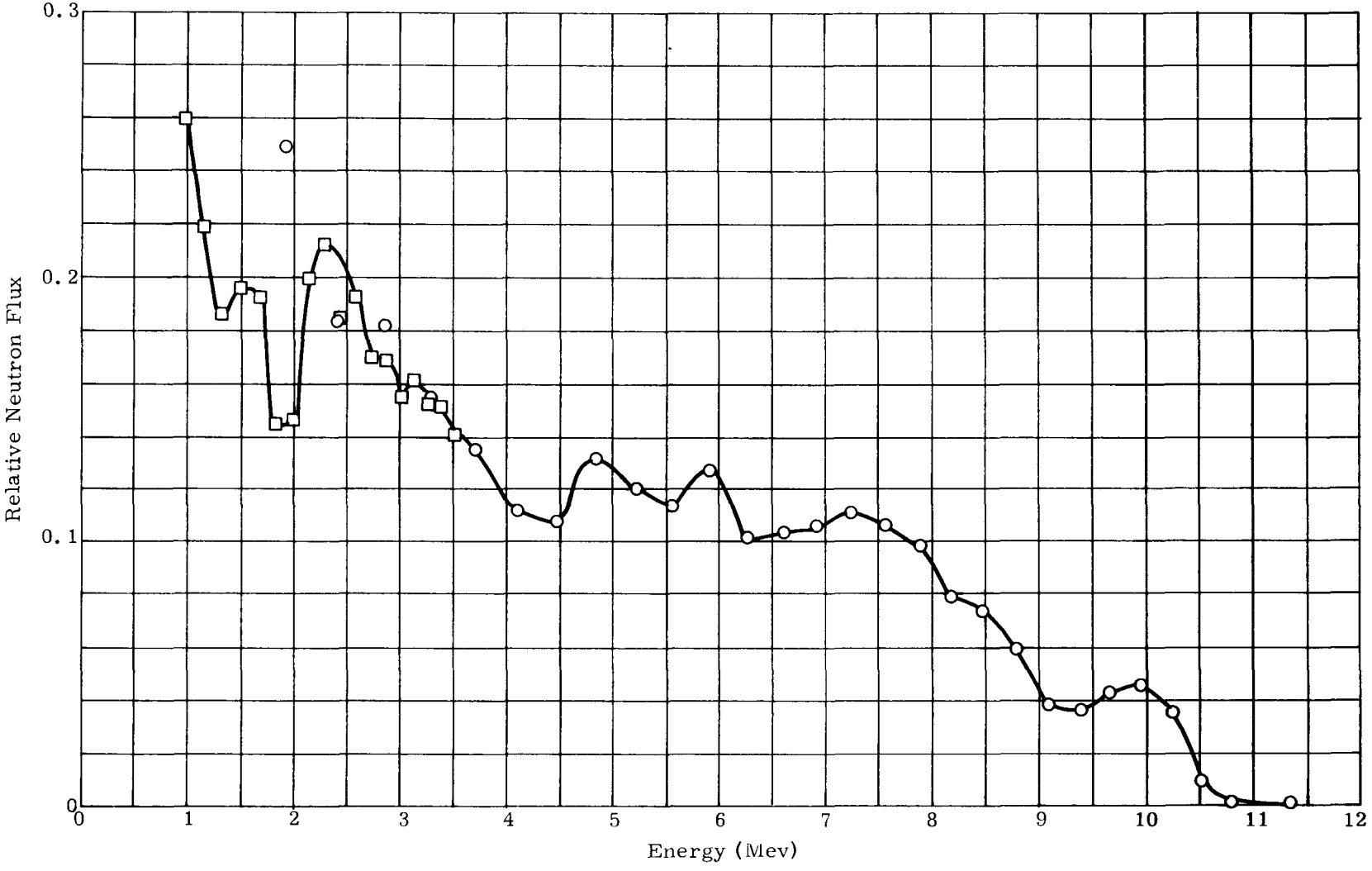

FIG. IV-10. PuBe SOURCE BEYOND SIX-INCH BLOCK SHIELD

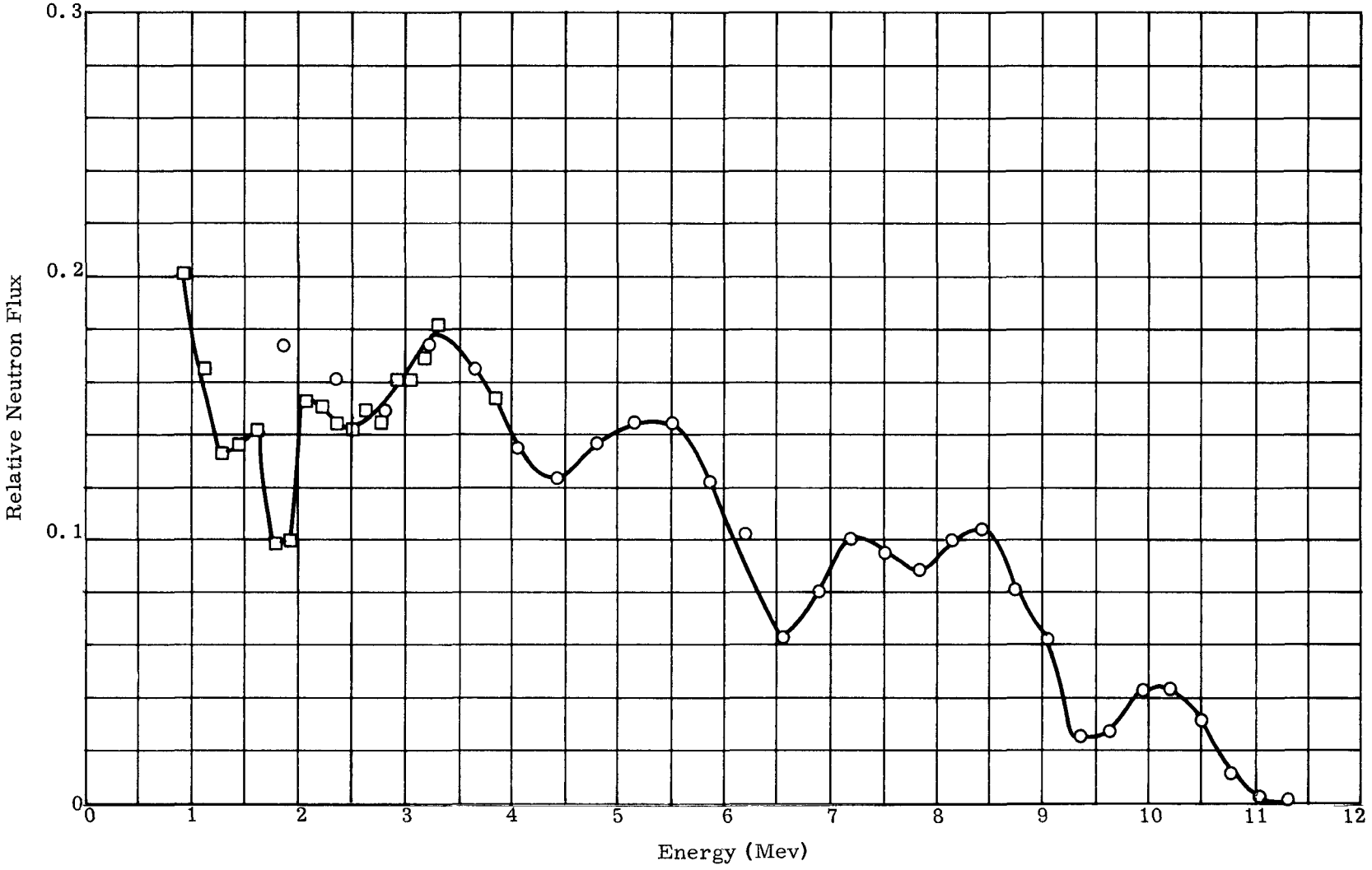

FIG. IV-11. BARE PuBe SOURCE CURVED STILBENE CRYSTAL ORIENTATION

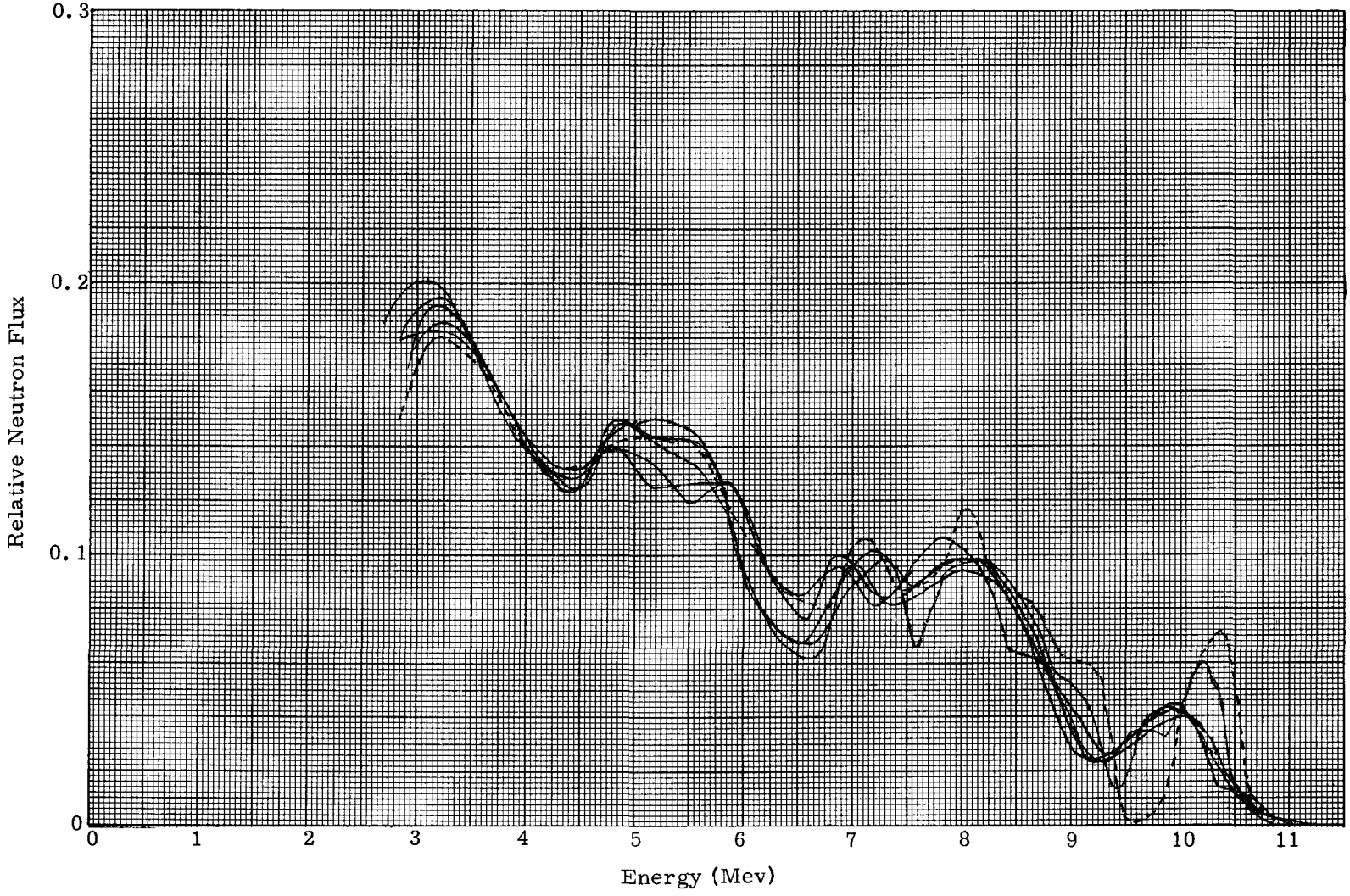

FIG. IV-12. DETECTOR COUNT RATE EXPERIMENT

(2) Uncertainty in the assignment of neutron energy to channels may lead to large variations in energy regions where the flux shows greatest variations. This consideration is particularly important for high neutron energies since the relationship is nonlinear. An uncertainty of 0.3 Mev at a neutron energy of 1.4 Mev corresponds to an uncertainty of 2.5 Mev at an energy of 10.9 Mev. Evidence of this type of variation is shown on Fig. IV-12 in the intervals of 6, 6.5 Mev and 8.5, 9.5 Mev.

Consideration (2) indicates the importance of energy considerations. A standard procedure includes the use of two standard line gamma sources, Cs-137 and Na-22, to more definitely ascertain the gamma energy relationships used in assigning neutron energies.

Results for the highest count rate show some apparently erratic behavior when compared to the other results. Some of this variation may be due to the extreme closeness of the detector to the source and its surrounding support equipment (less than 3-in. separation distance). However, the ability of the counting equipment to adequately handle high count rates was suspect. Therefore, it was concluded that capsule and generator measurements should be restricted to gross count rates of less than 8000 cps.

2. Reproducibility

In this experiment, a measurement was repeated after numerous adjustments of the counting instrument for intervening high and low energy measurements. A comparison of the results shows the same type of variation reported for the count rate experiment. Variations of ±10% for neutron energies less than 3.2 Mev appear to be mainly due to the normalization technique. Closer agreement would have been indicated if results had been normalized to the peak at 3.2 Mev. For the intended use of the stilbene system, the agreement was considered satisfactory.

3. Scattering

In this experiment, two measurements were made which compared the attenuation of an essentially infinite slab of paraffin to a finite slab of paraffin of sufficient extent to attenuate only neutrons emitted in the direction of the detector. In the absence of a significant number of neutrons scattered from facility walls and support equipment reaching the detector, there was a decrease as expected, in the total flux at the detector for the block shield. This decrease was recorded as a deficiency in low energy neutrons due to a loss of neutrons through the sides of the block, these neutrons might otherwise have been scattered back to the detector. A comparison of the results revealed this expected behavior. The disproportionate decrease in the low energies was observed both in the spectral and absolute flux comparison. Absolute fluxes were as follows:

	Flux		
	A	B	Ratio
Shield	Neutrons < 3.2 Mev	Neutrons > 3.2 Mev	B/A
Slab	3.6×10^2	4.8×10^2	1.33
Block	2.8×10^2	4.2×10^2	1.50

These results indicated that wall- or structure-scattered neutrons were not significantly influencing these measurements. However, later measurements performed on Subsystem S/N 4 tended to indicate that the results were influenced by scattered neutrons. The apparent anomaly is readily resolved when it is recognized that the

preliminary measurements were restricted to placement of the detector only six inches from the source, while the subsystem measurements were made at distances varying between 12 and 30 inches. The effect of scattered neutrons was quite small for the short separation between source and detector, but increased with increasing separation distance.

4. Crystal Orientation

A comparison of the normalized spectra for the two measurements indicated no differences attributable to the differing crystal orientation. The ratio of absolute neutron count for the curved orientation measurement to that for the flat orientation was approximately 0.7. It is significant to note that this factor may be directly related to the geometry of the experiment. Assuming the curved orientation to present an effective area of 2 cm^2 to the source (the product of the crystal diameter and height, the ratio of curved area to flat area (3.14 cm^2) is 0.65. The comparison is not rigorous because analysis of the data involves factors derived from experiments in which only the flat orientation is assumed. All measurements performed on the generator were performed with the flat orientation.

5. Perturbed Spectrum Measurements

This experiment was run with a fixed source-detector distance of 6.5 inches. Spectral variations and variations in absolute total flux were totally attributable to the attenuating properties of the paraffin slabs. Comparison of the spectra showed the expected buildup of neutrons in the lower energy regions from neutron scatter. The total fluxes for the three measurements of bare source, three- and six-inch thickness of paraffin were in the ratios 1.0, 0.50 and 0.20, respectively. A removal cross section $\sum_r$ (cm^{-1}), computed from these data as

$$\sum_r = -\frac{1}{x} \ln \frac{\phi(x)}{\phi(o)} = \frac{1}{15.24} \ln 0.20 = 0.106 \text{ cm}^{-1}$$

compares favorably with the measured neutron removal cross section for paraffin of $\sum_r = 0.109 \text{ cm}^{-1}$. (Density = 0.952 gm/cm^3). Here, x is the slab thickness (cm) and $\phi_{(x)}$ and $\phi_{(o)}$ are the total neutron fluxes (n/cm^2-sec) measured with and without the paraffin slab, respectively. This comparison was not completely valid since two different quantities were involved: a flux removal cross section for a Pu-Be source and a dose removal cross section for a fission source. For larger attentuation, the expected behavior is a lower cross section for Pu-Be neutrons than for fission neutrons due to the relative hardness of the Pu-Be emission spectrum. The results do, however, demonstrate adequate behavior of the stilbene system.

This experiment was a preliminary to the perturbation experiment in water, which was analyzed in much greater detail. The results of this experiment are given in Section IV-B.

B. DETAILED EXAMINATION OF SPECTRAL RESPONSE

A set of experiments was performed to explore the utility of the stilbene detecting system for the general application of absolute measurement of the neutron energy spectrum. In constrast to the experiments of the preceding section, experimental emphasis was on precise determination of those quantities which determine the absolute number scale associated with a spectrum measurement. Two experiments were performed with the Pu-Be source: spectral measurements in air and measurements of the perturbed spectra in water. The experiments were set up to nearly approximate a condition for which precise analysis is possible· that of a point source in an infinite medium. Analysis and experiment were then compared.

Correlative analyses utilized the moments method solution of the transport equation to determine fast and epithermal flux spectra and a technique for determination of thermal flux from results of the moments calculation. The first step in the analysis was to verify the accuracy of these mathods, associated techniques for generation of scattering matrices and selected cross section. This was achieved by comparison of analysis with experiments and previous calculations performed for a fission neutron source. This analysis is reported in Section IV-B.

A prime quantity associated with the intent of the experiments is the absolute emission rate of the Pu-Be source. Results of long counter measurements performed at Mound Research Corporation are verified by comparison of measured and calculated thermal flux distributions for the source in water. This source normalization is reported in Section IV-B.

Spectral measurements were made at selected distances in air. Results were integrated to determine absolute dose rates which were compared to calculated values and other measurements (Section IV-B).

Measurements of the perturbed spectra through varying amounts of water serve to verify the correctness of the measured source neutron emission spectrum. The measured spectrum was as input to moments calculations of the energy dependent neutron flux in water. Here, good comparison of the experimental and analytically determined spectra after perturbation by water reflects the ability of the spectrometer system for absolute spectral measurement.

As evidenced by the results of this chapter, the spectrometer system is, for neutrons of energies greater than 1 Mev, capable of yielding absolute neutron spectra to within the limits required for biological dose rate and radiation damage studies. Particularly, the integral of the measured spectrum appears to be correct to within 10% and, in this respect, the system represents a precision dosimeter. More uncertainty exists in individual details of the energy dependent spectrum. Here, error in the magnitude is probably around 20%. Part of this variation is due to the uncertainty in assignment of energy values according to the gamma calibration method.

1. Fission Source Calculations

The investigation of measurements performed with the stilbene detecting system required comparison with a theoretical analysis of fast neutron spectra and thermal neutron flux from the Pu-Be source in water. The moments method (see Appendix B) and a technique for determining thermal flux from the moments and analytical representation of the epithermal flux (Ref. 10) were used for this analysis. Prior to performing calculations for the Pu-Be source, these techniques were used to calculate fast and epithermal spectra, age-to-indium resonance and thermal neutron flux from a point isotopic fission source in water. The objective of these calculations was to verify, by comparison with similar calculations and experiments that the analytical

techniques would give sufficient accuracy. The results of the calculations for the fission source are presented in this section.

a. Moments technique

Calculation of moments and reconstruction of the flux ϕ (n/cm^2-sec-Mev) for radius r (cm) as a sum of exponential terms

$$4\pi r^2 \phi (r, E) = \sum_{J}^{N} A_J (E) e^{-\alpha_J (E) \mu_o r} \qquad \text{(IV-1)}$$

where $N \geq 2$, was performed by a computer program (SPFRC) written in FORTRAN IV for the IBM 7094 and 360 computers. The quantities A_J (sec^{-1} Mev^{-1}) and α_J (cm^{-1}) are determined from the moments in the reconstruction phase. The dimensionless quantity, μ_o, is preselected to ease numerical calculations. To ensure an adequate representation of the neutron source spectrum and energy dependent cross section data, provisions were made in the program for allowance of up to 200 discrete points spanning the energy range of interest. Exact calculations of spatial moments $B^{(1)}_{n,\ell}$ (cm^{n+1}/Mev-sec) in a hydrogeneous medium through order n = N involves scattering integral expansion coefficients $M^{(\ell)}_{J,1}$ (cm^{-1}) through order ℓ = N/2 and an integral over moments $B^{(J)}_{n,\ell}$ for all energy indices $J \leq 1$ (all higher energies). The large demands for data storage necessitated the use of magnetic tape units (7094) or auxiliary disk units (360) for temporary storage of scattering matrices and computed moments for all energy points. Initial calculations were performed and compared to hand calculations for elimination of possible coding errors. Checks were made to determine the extent of and to eliminate excessive round-off error. In particular, the use of double precision arithmetic was found to be necessary in the subroutines for matrix inversion and polynomial root finding associated with the exponential flux reconstruction routine.

b. Cross sections and scattering matrices

An objective of the moments calculations was to predict accurately the detailed energy-dependent flux spectra over a broad spatial range. This objective required that considerable emphasis be placed on selection of the best available cross sectional data and the development of accurate, consistent scattering matrices from these data. A method had been developed for generation of neutron scattering matrices for heavy elements (defined for this purpose as atomic mass greater than one) (Ref. 11). This method assumes a pointwise spacing in uniform lethargy intervals[2] and uses the Lagrange interpolation formula for representation of the flux. A minimum of four lethargy points are used in evaluating the scattering integral. Thus, this procedure yields at least a tetradiagonal slowing down matrix

---

[2] Subsequent to analysis reported here, the formulation for heavy elements and hydrogen were generalized for computation of scattering matrices for an arbitrary nonuniform lethargy structure. This generalization reduces the number of energy points required for computation to low energies while allowing accurate source spectrum and cross section representation.

which is superior to the more usual linear approximation. Computations are performed by computer program ELASTIC which accepts cross sections and Legendre expansion coefficients (laboratory system) as input and provides scattering matrices as card output in a format accepted by the moments program. An auxiliary program is available for conversion of Legendre coefficients in the CM system to the laboratory system. For hydrogen, elastic scattering matrices are generated by the moments code according to the formulation of Certaine (Ref. 12) under the assumption that scattering is isotropic in the center of mass system. Cross section data and Legendre expansion coefficients for oxygen were taken from GA 2156 (Ref. 13), NDA 15C-15 (Ref. 14) and NDA 15C-40 (Ref. 15). Inelastic scattering was treated as pure absorption. Cross section data for hydrogen and oxygen used in all moment calculations are given in Table IV-2. Hydrogen cross sections are from BNL 325 (Ref. 16).

c. Selection of energy mesh spacing

Moments calculations for the fission source spanned the energy range of from 18.02 Mev to approximately 1 ev. Comparative calculations for varying numbers of lethargy points over this range were run to determine the minimum number of lethargy spacings which would adequately represent the fission spectrum, flux variations and variations in cross sectional data. Comparisons were made with prior moments calculations and a measurement of the indium resonance flux in water. Fast neutron spectra for a 34-energy point structure (a constant delta lethargy of $\Delta\mu = 0.5$) and a 68-energy point structure ($\Delta\mu = 0.25$) were compared to the data of Aronson, et. al., (Ref. 17). Table IV-3 presents this comparison over the range (0 to 120 cm) for various neutron energies. The comparison is made with the results of the NDA model for exact degradation in oxygen computed with a lethargy interval of $\Delta\mu = 0.1$ for integration of the scattering term.

Lacking detailed experimental data, the NDA moments calculations are taken as a standard for comparison. These data are correct to within the limitations imposed by the oxygen slowing down model and the basic cross section data. Variations between these data and the present calculations were expected due to use of different basic oxygen cross section data. An examination of the data in Table IV-3 shows that a decrease in the integration lethargy interval from 0.5 to 0.25 (34 to 68 energy points) generally decreases the flux and tends to give better comparison with the NDA data. Some variation is certainly due to the difference in integration intervals. Disregarding the other variables, it is expected that the NDA data would give better results than either of the two present calculations due to the use of the fine mesh structure afforded by the $\Delta\mu$ of 0.1. However, the development of scattering matrices using the Lagrangian weights for oxygen removes the implied assumption of linearity in flux, source and cross sections between successive mesh points and should yield a more exact integration for a given lethargy mesh spacing. Therefore, the use of this formulation for oxygen should tend to compensate for a relatively coarse mesh width. Care must still be taken, however, to properly account for cross section resonances. This was done by smoothing values at energy points in the neighborhood of resonances such that the total cross section (energy integral over the resonance) is preserved.

Of more importance to this study is the extension of calculations to low energies (~1.0 ev). On the basis of this comparison and results reported, the 68-energy point structure appeared adequate and was selected for moments calculations with the Pu-Be source. Results reported are for the 68-point calculation.

d. Comparison of indium resonance fluxes and age-to-indium resonance

Moments results for low energies were compared to the measurements of indium resonance flux from a fission source in water of Hill, Roberts and Fitch (reported by

TABLE IV-2

Cross Section Data and Legendre Expansion Coefficients

Energy (Mev)	Hydrogen $\sigma_T = \sigma_S$ (barns)	Oxygen[2] σ_T (barns)	Oxygen[2] σ_S (barns)	Oxygen[2] Legendre Expansion Coefficients[1] F_1	F_2	F_3	F_4	F_5	F_6
18.02	0.520	1.71	0.75	0.870	0.680	0.603	0.459	0.388	0.260
14.03	0.682	1.58	0.67	0.680	0.480	0.327	0.251	0.146	0.064
10.93	0.878	1.33	0.67	0.650	0.456	0.295	0.204	0.105	0.060
8.51	1.11	1.46	0.90	0.621	0.420	0.259	0.153	0.060	0.052
6.63	1.36	1.30	1.06	0.523	0.329	0.211	0.070	0.031	0.045
5.16	1.63	1.50	1.47	0.303	0.190	0.163	0.020	0.018	0.033
4.02	1.94	1.85	1.78	0.152	0.066	0.026	-0.013	0	0
3.13	2.28	1.70	1.70	0.253	0.169	0.092	-0.013	0	0
2.44	2.66	0.90	0.90	0.235	0.056	-0.006	0.006	0	0
1.90	3.09	3.00	3.00	0.034	0.062	0.015	0	0	0
1.48	3.58	2.21	2.21	0.044	0.090	0.041	0.016	0.006	0.004
1.15	4.14	3.15	3.15	-0.055	0.240	-0.022	0.015	-0.008	0.004
0.897	4.80	2.90	2.90	0.020	-0.010	-0.015	0.001	-0.005	0
0.699	5.54	2.85	2.85	0.135	-0.015	0.002	0	0.001	0
0.544	6.34	3.87	3.87	0.280	0	0.007	0	0.004	0
0.424	7.15	11.2	11.2	0.020	0.120	0.009	0	0	0
0.330	8.04	3.82	3.82	-0.0221	-0.017	0	0	-0.004	0
0.257		3.70	3.70	-0.126	-0.026	0	0	-0.005	0
0.200		3.70	3.70	-0.070	-0.020	0	0	-0.003	0
0.156		3.70	3.70	-0.038	-0.009	0	0	-0.001	0
0.121		3.70	3.70	-0.017	0	0	0	0	0
0.0946		3.70	3.70	-0.147	0.0069	0	0	0	0
0.0736		3.70	3.70	-0.133	0	0	0	0	0
0.0573		3.70	3.70	-0.127	0	0	0	0	0
0.0447		3.70	3.70	-0.102	0	0	0	0	0
0.0348		3.70	3.70	0	0	0	0	0	0

[1] Expansion coefficients are in center of mass system and normalized such that $F_0 = 1.0$.

[2] For oxygen, at all energies below 0.0348 Mev, $\sigma_T = \sigma_S = 3.70$ barns and $F_l = 0$ for all $l > 0$.

Cross Section Data for Hydrogen

Energy (Mev)	Hydrogen $\sigma_T = \sigma_S$ (barns)	Energy (Mev)	Hydrogen $\sigma_T = \sigma_S$ (barns)
2.71×10^{-2}	17.2	1.42×10^{-4}	20.2
2.11×10^{-2}	17.8	1.11×10^{-4}	20.3
1.64×10^{-2}	18.2	8.62×10^{-5}	20.3
1.28×10^{-2}	19.1	6.71×10^{-5}	20.4
9.97×10^{-3}	20.0	5.23×10^{-5}	20.4
7.76×10^{-3}	20.0	4.07×10^{-5}	20.5
6.05×10^{-3}	20.0	3.17×10^{-5}	20.5
4.71×10^{-3}	20.0	2.47×10^{-5}	20.5
3.67×10^{-3}	20.0	1.92×10^{-5}	20.5
2.86×10^{-3}	20.0	1.50×10^{-5}	20.5
2.22×10^{-3}	20.0	1.17×10^{-5}	20.5
1.73×10^{-3}	20.0	9.09×10^{-6}	20.6
1.35×10^{-3}	20.0	7.08×10^{-6}	20.6
1.05×10^{-3}	20.0	5.51×10^{-6}	20.7
8.18×10^{-4}	20.0	4.29×10^{-6}	20.7
6.37×10^{-4}	20.0	3.34×10^{-6}	20.8
4.96×10^{-4}	20.0	2.60×10^{-6}	20.8
3.86×10^{-4}	20.0	2.03×10^{-6}	20.9
3.01×10^{-4}	20.0	1.58×10^{-6}	21.0
2.34×10^{-4}	20.0	1.23×10^{-6}	21.0
1.83×10^{-4}	20.2	9.58×10^{-7}	21.0

TABLE IV-3

Fast Neutron Spectra Point Isotropic Fission Source in Water

$4\pi r^2 \phi(r, E)$ (n/sec/Mev-fission neutron)

E (Mev)		r = 0	10	20	30	60	90	120
10.9	A[1]	4.6-4	2.0-4	8.8-5	3.8-5	3.0-6	2.4-7	1.8-8
	B	(2)	--	--	--	--	--	--
	C	4.67-4 (1.02)	2.20-4 (1.10)	1.02-4 (1.16)	4.71-5 (1.24)	4.35-6 (1.45)	3.82-7 (1.59)	3.22-8 (1.79)
6.63	A	1.25-2	4.8-3	1.9-3	7.5-4	4.6-5	3.0-6	1.7-7
	B	1.22-2 (0.98)	5.54-3 (1.15)	2.39-3 (1.25)	9.97-4 (1.33)	6.58-5 (1.43)	4.08-6 (1.36)	2.47-7 (1.45)
	C	1.22-2 (0.98)	5.14-3 (1.07)	2.09-3 (1.10)	8.30-4 (1.11)	4.82-5 (1.05)	2.67-6 (0.89)	1.48-7 (0.87)
4.02	A	7.0-2	2.6-2	6.5-3	1.8-3	6.0-5	2.7-6	1.4-7
	B	6.72-2 (0.96)	2.60-2 (1.00)	7.71-3 (1.18)	2.33-3 (1.29	8.23-5 (1.37)	4.08-6 (1.51)	2.43-7 (1.74)
	C	7.42-2 (1.06)	2.53-2 (0.97)	7.69-3 (1.18)	2.32-3 (1.29)	7.51-5 (1.25)	3.16-6 (1.17)	1.56-7 (1.11)
2.44	A	1.8-1	7.3-2	2.0-2	5.3-3	1.3-4	4.7-6	2.2-7
	B	1.90-1 (1.06)	7.30-2 (1.00)	2.23-2 (1.12)	6.40-3 (1.21)	1.70-4 (1.30	6.9-6 (1.47)	3.88-7 (1.76)
	C	1.93-1 (1.07)	7.24-2 (0.99)	2.19-2 (1.10)	6.21-3 (1.17)	1.50-4 (1.15)	5.22-6 (1.11)	2.44-7 (1.11)
1.48	A	3.0-1	8.3-2	2.2-2	5.7-3	1.3-4	4.5-6	2.4-7
	B	3.05-1 (1.01)	9.60-2 (1.16)	2.62-2 (1.19)	7.01-3 (1.23)	1.73-4 (1.33)	7.05-6 (1.57)	3.88-7 (1.61)
	C	3.01-1 (1.00)	1.21-1 (1.46)	3.08-2 (1.40)	7.89-3 (1.38)	1.79-4 (1.38)	6.40-6 (1.42)	3.02-7 (1.26)
0.897	A	3.7-1	1.4-1	3.4-2	7.3-3	1.7-4	6.8-6	3.7-7
	B	3.53-1 (0.95)	1.43-1 (1.02)	3.65-2 (1.07)	9.52-3 (1.30)	2.33-4 (1.37)	9.59-6 (1.41)	5.29-7 (1.43)
	C	3.47-1 (0.94)	1.43-1 (1.02)	3.48-2 (1.02)	8.75-3 (1.20)	1.95-4 (1.15)	7.02-6 (1.03)	3.30-7 (0.89)
0.544	A	3.7-1	1.7-1	3.8-2	9.5-3	2.1-4	8.4-6	4.4-7
	B	2.26-1 (0.61)	1.97-1 (1.16)	4.91-2 (1.29)	1.26-2 (1.33)	3.04-4 (1.45)	1.25-5 (1.48)	6.88-7 (1.56)
	C	2.28-1 (0.62)	1.93-1 (1.14)	4.59-2 (1.21)	1.13-2 (1.19)	2.48-4 (1.18)	8.90-6 (1.06)	4.17-7 (0.95)
0.330	A	3.2-1	2.4-1	5.0-2	1.2-2	3.3-4	1.0-5	5.4-7
	B	4.00-2 (1.25)	2.42-1 (1.01)	5.99-2 (1.20)	1.53-2 (1.28)	3.67-4 (1.11)	1.51-5 (1.51)	8.28-7 (1.53)
	C	2.06-2 (0.64)	2.85-1 (1.19)	6.73-2 (1.35)	1.67-2 (1.39)	3.68-4 (1.12)	1.32-5 (1.32)	6.21-7 (1.15)

(1) Key ro results: A--NYO 6267,[16] exact degradation in oxygen, $\Delta\mu = 0.1$
B--Current results, 34-point, $\Delta\mu = 0.5$
C--Current results, 68-point, $\Delta\mu = 0.25$
{Numbers in parenthesis represent ratio $\frac{\text{result B or C}}{\text{result A}}$}

(2) Exponential reconstruction solution failed at 10.9 Mev

(3) Notation 4.6-4 = 4.6×10^{-4}

NDA 15C-40 (Ref. 15). The exponential form solution for the flux of 1.58 ev from the moments calculation, normalized to one fission neutron per second, is

$$4\pi r^2 \phi(r, 1.58) = \sum_{j=1}^{4} A_j e^{-\alpha_j \mu_o r}$$

where

$\mu_o = 0.1$

A_1	$= 1.88123 \times 10^4$ n/sec-Mev	α_1	$= 1.16980\ cm^{-1}$
A_2	$= 1.34539 \times 10^3$ n/sec-Mev	α_2	$= 0.900023\ cm^{-1}$
A_3	$= 1.16819 \times 10^5$ n/sec-Mev	α_3	$= 1.71469\ cm^{-1}$
A_4	$= -2.15175 \times 10^5$ n/sec-Mev	α_4	$= 5.19761\ cm^{-1}$

Fluxes computed from this expression are compared to the experiment described in Table IV-4. The experimental flux has been arbitrarily normalized to the calculated flux at r = 20 centimeters. Good shape agreement occurs when r is greater than 10 centimeters; the maximum deviation of 14% occurs at 90 centimeters. The large discrepancies for radii less than 10 centimeters are, in part, a consequence of the assumed exponential form for the flux which is not valid close to the source.

TABLE IV-4

Comparison of Indium Resonance Flux Experiment and Moments Calculations

r (cm)	$4\pi r^2 \phi(r)$ (n/sec) Experiment	Calculated E = 1.58 ev	$R = \frac{\phi_{calc}}{\phi_{exp}}$
3	1.36×10^4	3.89×10^4	2.86
5	2.58×10^4	4.49×10^4	1.74
10	2.50×10^4	2.62×10^4	1.05
15	1.25×10^4	1.24×10^4	0.99
20	5.82×10^3	5.82×10^3	1.00
30	1.32×10^3	1.34×10^3	1.02
40	3.74×10^2	3.36×10^2	0.90
50	9.78×10^1	9.18×10^1	0.94
60	2.65×10^1	2.71×10^1	1.02
70	8.87×10^0	8.50×10^0	0.96
80	2.61×10^0	2.79×10^0	1.07
90	8.34×10^{-1}	9.50×10^{-1}	1.14

The computed moments, $B_{0,0}$ and $B_{2,0}$, may be used to determine the neutron age τ (E) (cm^2), which is defined as

$$\tau(E) = \frac{1}{6} \frac{\int_0^\infty r^2 \cdot 4\pi r^2 \phi(r, E)\, dr}{\int_0^\infty 4\pi r^2 \phi(r, E)\, dr} \qquad \text{(IV-2)}$$

According to the definition of the moments (Appendix B), the age of neutrons to energy, E, is computed as

$$\tau(E) = \frac{1}{3\mu_0^2} \frac{B_{2,0}(E)}{B_{0,0}(E)} \qquad \text{(IV-3)}$$

Neutron ages, computed from this expression are:

E (ev)	τ (cm^2)
2.03	26.4
1.58	26.5
1.23	26.6
0.957	26.7

These results are in good agreement with the more recent measurements of the age-to-indium resonance which range from 26.7 $\pm$ 0.9 to 27.68 $\pm$ 0.10 as reported by Joanau, Goodjohn and Wikner (Ref. 18). The unweighted average of these measurements is 27.17 $\pm$ 0.78. Joanau, Goodjohn and Wikner used the moments method to compute a value of 26.4 cm^2 to indium resonance (1.46 ev) which is in very good agreement with the present calculations.

e. Thermal neutron flux comparison

The final objective of the fission source studies was to obtain a solution for the thermal neutron flux (2200 m/sec). The method of Anderson (Ref. 10) was used (see Appendix B) which utilizes the zeroth moment and exponential representation of the epithermal flux to solve for the thermal flux. This technique emphasizes the importance of obtaining a good solution for the epithermal flux. The moments result at 2.03 ev is as follows:

$$\mu_0^{-1} B_{0,0} = 3.47256 \times 10^5 \text{ n-cm/sec-Mev}$$

$$4\pi r^2 \phi(r, 2.03) = \sum_{J=1}^{4} A_J e^{-\alpha_J \mu_0 r}$$

$\mu_0 = 0.1$

A_1	$= 1.45950 \times 10^4$ n/sec-Mev	α_1	$= 1.16887$ cm^{-1}
A_2	$= 1.08702 \times 10^3$ n/sec-Mev	α_2	$= 0.899866$ cm^{-1}
A_3	$= 9.05673 \times 10^4$ n/sec-Mev	α_3	$= 1.71183$ cm^{-1}
A_4	$= 1.67696 \times 10^5$ n/sec-Mev	α_4	$= 5.26098$ cm^{-1}

This result was used to solve for the thermal flux at $E_0 = 0.025$ ev assuming a thermal cutoff energy $E_1 = 0.625$ ev. A macroscopic thermal neutron cross section of $\sum_a = 0.0221\ cm^{-1}$ and a thermal neutron diffusion length of L = 2.72 centimeters were used. Results are compared to the kernel for water deduced by Trubey, et. al. (Ref. 19), from the experimental data taken at the Lid Tank Shielding Facility of ORNL. This comparison is given in Table IV-5. The results are absolute, experimental and calculated fluxes are independently normalized to one fission neutron.

TABLE IV-5

Comparison of Experimental and Analytical Thermal Neutron Fluxes for a Fission Source

$4\pi r^2 \phi(r)$ (thermal neutrons/fission neutrons)

r	Experimental	Calculated	$R = \frac{\phi_{calc}}{\phi_{exp}}$
5	1.53	6.31	4.12
10	2.54	4.21	1.66
15	1.72	2.04	1.19
20	8.2×10^{-1}	9.10×10^{-1}	1.11
25	3.8×10^{-1}	4.06×10^{-1}	1.07
30	1.83×10^{-1}	1.86×10^{-1}	1.02
35	9.0×10^{-2}	8.82×10^{-2}	0.976
40	4.2×10^{-2}	4.32×10^{-2}	1.03
50	1.14×10^{-2}	1.13×10^{-2}	0.991
60	3.1×10^{-3}	3.22×10^{-3}	1.04
70	9.0×10^{-3}	9.88×10^{-4}	1.10
80	2.8×10^{-4}	3.20×10^{-4}	1.14
90	8.9×10^{-5}	1.08×10^{-4}	1.21
100	3.1×10^{-5}	3.74×10^{-5}	1.22
120	4.0×10^{-6}	4.85×10^{-6}	1.20

The comparison shows good agreement over the range $15 \leq r \leq 120$ centimeters, the maximum deviation being + 22% at 110 centimeters. Of particular interest for the present work is the range from 20 to 40 centimeters, where a maximum deviation of 11% occurs. These results once again illustrate the failure of the exponential solution to adequately represent the flux very close to the source as indicated by the poor comparison for $r \leq 10$ centimeters.

The derivation of the solution for the thermal flux assumes that the macroscopic absorption cross section of the water medium varies as 1/v and that the moments $B_{0,0}(E)$ vary as 1/E over the energy regions of importance (the effective source region for thermal neutrons). A check of the zeroth moments for energies from 9.97 kev to 0.96 ev showed less than 5% variation from the 1/E condition (i.e., moments per unit lethargy were constant over this range to within the quoted

variation). Above 9.97 kev to the Mev range, the moment per unit lethargy shows a gradual increase. This is probably due to the inclusion in the calculation of the fission source per unit lethargy s (u) as given by (neutrons/fission neutron) for energy E (Mev)

$$s(u) = ES(E) = 0.484\, e^{-E} \sinh \sqrt{2E} \qquad \text{(IV-4)}$$

over the entire range of energies down to 0.96 ev.

It should be noted that the particular form of the equation for the thermal flux (Appendix B, Eq B-15) is valid only for the condition that the epithermal relaxation length $b = 1/u_o\alpha$ (cm) be greater than the thermal diffusion length L (cm). This condition is not met in the fourth exponential term of the solution for the epithermal flux. This term, although the coefficient A is negative, gives rise to an erroneous position flux component which introduces significant error in the total result for very small r. (This difficulty has not been completely resolved.) Possibly, a better result would have been obtained by applying the exponential least squares reconstruction technique (Appendix B).

f. Discussion

The intent of the calculations for the fission source was to examine the accuracy of the techniques and data employed. The choice of the 68-energy point for moments calculations utilizing scattering matrices generated with the Lagrange weighting technique is shown to yield sufficiently accurate results. When calculations are extended to thermal energies, comparison with an experimentally derived kernel shows small variation (20%) over a wide spatial range. In particular, over the range of 20 to 40 centimeters, the maximum deviation is 11%. Differences in fast neutron spectra (when compared to NDA data) are probably, for the most part, caused by revised cross section data and some smoothing of the oxygen cross section over the coarser energy interval.

In succeeding sections, the moments method and thermal flux calculation will be used to derive fast neutron spectra and thermal flux in water from a Pu-Be source. These calculations use the same 68-point energy structure and scattering matrices.

2. Plutonium Beryllium Source Normalization

Calibration experiments involving neutron spectral measurements with the stilbene system in air and through water were performed with the Martin Marietta standard Pu-Be source, M-740. An objective of these experiments was to determine the degree of accuracy to which the spectral measurements and associated data reduction techniques could reproduce the absolute magnitude of the neutron flux. Hence, a knowledge of the absolute emission rate of the neutron source was essential.

Two independent techniques were used to measure the source emission rate·

(1) Long counter measurements and comparison with a standard source (performed at Mound Research Corporation).

(2) Spatial measurement of the thermal neutron flux in water and comparison with analytically determined thermal neutron flux.

During the initial phases of this study, the Pu-Be source was sent to MRC for measurement of the fast spectrum with a stilbene system and for recalibration. Long counter measurements, performed at Mound(Ref. 20), indicated a total

neutron emission rate of 1.99×10^7 neutron/sec (4/18/66) with an absolute accuracy of ±3. The following anistropy of the source, measured with respect to its axis was reported

ϵ (0°)	0.71 ± 0.01
ϵ (90°)	1.084 ± 0.005
ϵ (180°)	0.66 ± 0.01

The basis for the normalization was comparison with MRC source M-591. The Pu-Be sources experience a buildup of neutron emission rate given by the approximate formula (from Mound) (Ref. 20).

$$Q(t) = Q(0)\ [1.0 + (0.31 \pm 0.04)\ (e^{-1.51 \times 10^{-3} t} - e^{-5.25 \times 10^{-2} t})] \qquad \text{(IV-5)}$$

where t is time in years and Q (t) is the absolute emission rate (n/sec). The original calibration of this source gives a base of $Q(0) = 1.84 \times 10^7$ n/sec as of January 1 1960.

A second calibration was performed at Martin Marietta, Nuclear Division. The technique employed was comparison of the measured spatially dependent thermal neutron flux in water from the source with thermal fluxes calculated by the technique described in Section IV-C. A description of the calculation and comparison with experiment follows.

a. Moments and thermal flux calculations

The moments method was utilized to determine fast and epithermal neutron spectra from a point isotropic Pu-Be source in water. The 68-energy point structure and scattering matrices for hydrogen and oxygen described in Section IV-B was used for this calculation. The relative, energy dependent, fast spectrum used for the calculation was based on the spectrum as measured by the stilbene system. A relative sparsity of points at high energies in the 68-point structure necessitated some smoothing of the data. Care was taken to retain the dominant features of the measured spectrum. The source spectrum normalized to one neutron per second, is given in Table IV-6. An extrapolation of the measurements from 0.9 to 0.5 Mev was necessary due to the limitations on the measurement. In this region the source per unit energy was assumed constant and equal in the value at 0.9 Mev. Below 0.5 Mev the source was assumed to be zero.

The moments calculation yielded fast and epithermal neutron spectra for the point isotropic Pu-Be source in water at specific energy values down to 0.9 ev. Fast neutrons spectral results are discussed in Section IV-B. Moments for the flux at 2.03 ev were used to reconstruct the spatial flux. For this case, the exponential reconstruction technique which uses 2N moments to solve exactly for the 2N coefficients A_j α_j $j = 1, 2, \ldots N$ failed to produce a solution for N = 3 and 4 (see discussion in Appendix B). In the solution for N = 2 (a two-exponential fit) one of the coefficients A was negative. This term has a significant influence on results through r = 20 centimeters and the existence of a negative coefficient of rather large magnitude would have an effect on the magnitude of the remaining positive coefficient. Rather than reject the negative term and use the remaining positive term (as was done for the fission source where the perturbation was small), the Gaussian least square technique was used to reconstruct the flux as a single exponential term. The first five even moments of the flux with unit weighting at 2.03 ev were used to determine in the least squares sense, the best values of the coefficients A and α for the flux as

$$4\pi r^2 \phi(2.03 \text{ ev}, r) = A e^{-\alpha \mu_o r} \text{ n/cm}^2\text{-sec-Mev}$$

Moments for this calculation (according to the definition in Appendix B) and the solution are as follows:

$B_{0,0} = 3.28347 \times 10^4$ n $(cm)^{n+1}$/sec-Mev
$B_{2,0} = 5.36382 \times 10^4$ n $(cm)^{n+1}$/sec-Mev
$B_{4,0} = 5.56999 \times 10^4$ n $(cm)^{n+1}$/sec-Mev
$B_{6,0} = 5.67927 \times 10^4$ n $(cm)^{n+1}$/sec-Mev
$B_{8,0} = 5.81794 \times 10^4$ n $(cm)^{n+1}$/sec-Mev
$B_{10,0} = 5.95103 \times 10^4$ n $(cm)^{n+1}$/sec-Mev

$\mu_o = 0.100$
$A = 4.0000 \times 10^4$ n/sec-Mev
$\alpha = 0.95262$

TABLE IV-6

Pu-Be Source Spectrum for Moments Calculations*

Energy E (Mev)	Lethargy u	S (E) (n/sec/Mev-source neutron)	S (u) = E S (E) (n/sec/source neutron)
10.93	0.5	0	0
8.51	0.75	0.07588	0.6457
6.63	1.0	0.07071	0.4688
5.16	1.25	0.1214	0.6264
4.02	1.50	0.1147	0.4609
3.13	1.75	0.1585	0.4961
2.44	2.0	0.1416	0.3456
1.90	2.25	0.1079	0.2050
1.48	2.50	0.1517	0.2246
1.15	2.75	0.1517	0.1745
0.897	3.00	0.1517	0.1361
0.699	3.25	0.1517	0.1060
0.544	3.50	0.1517	0.08255
0.424	3.75	0	0

Spectrum is based on stilbene spectral measurements of Pu-Be source, M-740.

A comparison of Fermie age was made to check the validity of the epithermal moments and flux calculations. The age of Pu-Be neutrons to epithermal energies computed from the moments according to Eq (IV-3) are as follows:

Energy (ev)	τ (cm^2)
2.03	54.5
1.58	54.6
1.23	54.7
0.958	54.8

These results are in good agreement with experimentally determined ages to In-115 (E = 1.46 ev) and Rh-103 (E = 1.25 ev) resonances of 52.8 and 53.7 cm^2, respectively, found in Ref. 21.

The single exponential solution was used to compute the thermal flux in water according to Eq (B-15), Appendix B. Thermal constants and L used in this calculation were the same as for the fission source calculations. Results are given in Table IV-7 as the thermal flux (2200 m/sec) in water resulting from a point isotropic Pu-Be neutron source in water which emits 1 n/sec.

TABLE IV-7

Calculated Thermal Neutron Flux (2200 m/sec) from Point Isotropic Pu-Be Neutron Source in Water

r (cm)	$4\pi r^2 \phi_{th}(r)$ (n/source neutron)
14	1.92
16	1.56
18	1.26
20	1.02
22	0.827
24	0.673
26	0.548
28	0.448
30	0.367
32	0.301
34	0.247
36	0.203
38	0.167
40	0.137
42	0.113
44	0.0931
46	0.0768
48	0.0632
50	0.0522

b. Source geometry investigation

The comparison of analysis with experimentally determined fluxes assumes that the finite source may be represented as a point source at the center of the actual source. To determine the validity of this assumption, a point kernel technique was employed to integrate over the finite volume of the source to obtain a fast dose rate and epithermal flux in water. The fast dose and the epithermal flux kernels were obtained from the moments solution.

The Pu-Be source is a right circular cylinder which initially contained a mixture of approximately 159 grams of Pu-239 and 79 grams of Be. The source-containing region diameter is 1.36 inches and the height is 2.69 inches. This source is encapsulated in stainless steel with overall dimensions of 1.543 inches in diameter and 3.389 inches high.

The kernels were integrated over the volume of the actual source to determine fast dose and epithermal flux in the radial midplane at various distances from the source. Source strength per unit volume was assumed uniform and was normalized such that the integral over the source volume was equivalent to the normalization of the kernels (1 n/sec). Hence, the ratio of the results of the volume integration to the kernel is a direct measure of perturbation due to finite geometry. The ratios are given in Table IV-8.

For small radii, the expected result is observed, the volume source gives lower values. For radii greater than 15 centimeters, the two results agree to within 1%. (Small variations noted are probably due to inherent errors in the point kernel technique.) As a result of these calculations, it is concluded that for radii greater than or equal to 15 centimeters, the source is equivalent to a point isotropic source in water at the center of the actual source and having a source strength (n/sec) equal to the total emission rate of the finite source in the same units.

TABLE IV-8

Ratio of Results for Point Source to Finite Volume Source

r (cm)	Fast Dose Rate $\frac{\text{Point Kernel}}{\text{Cylindrical Volume}}$	Epithermal Flux (2.03 ev) $\frac{\text{Point Kernel}}{\text{Cylindrical Volume}}$
3	0.812	0.788
4	0.871	0.859
5	0.908	0.899
6	0.932	0.924
8	0.958	0.954
10	0.972	0.970
12	0.972	0.973
15	0.987	0.987
20	0.993	1.001
25	0.996	0.997
30	0.998	0.998
40	1.000	1.000
50	1.001	1.001
60	1.002	1.002
80	1.002	1.002
100	1.002	1.003

c. Experimental determination of thermal flux

Thermal flux in water beyond the Pu-Be source was measured by determination of thermal gold foil actuators. Thermal activations were obtained from the total foil activation by applying cadmium ratio corrections. An infinite water medium was simulated by placing the source in a water tank of dimensions sufficient to have at least one foot of water separating the source from the water surface, tank walls or bottom. Accurate positioning of the foils was assured by use of a plastic holder placed so that the foils were in the radial midplane of the source. The same restriction of a minimum of one foot of water from the surface, bottom and walls applied to foil positions. Measurements of bare and cadmium-covered foils were made at various distances from the source, ranging from 1 to 15.75 inches from the center of the source. Small foils, approximately 0.1875 inch in diameter and weighing approximately 0.0211 gram were used for distances of up to 8 inches from the source surface. Beyond this distance, large foils approximately 0.75 inch in diameter and weighing approximately 0.27 gram were used.

Neutron absorption by gold leads to the formation of Au-198. The major portion (98.6%) of the decay scheme of Au-198 is by emission of a 0.960 Mev beta and a 0.412 Mev gamma according to

$$0n^1 + {}_{79}Au^{197} \rightarrow {}_{79}Au^{198} \xrightarrow{T_{1/2} = 64.8\ hr} {}_{80}Hg^{198}\ (\text{stable}) + \beta^- + \gamma$$

For the conditions under which this experiment was conducted (counting from much shorter than the half-life of the activity so that no appreciable decay occurs during counting and low fluxes) the activity due to thermal neutron (2200 m/sec) is given by

$$\lambda_2 N_2 = N_1 \sigma_{a_{th}} \phi_{th} \left[1 - e^{-\lambda T}\right] e^{-\lambda t} \qquad \text{(IV-6)}$$

where

λ = $\frac{\ell n\, 2}{T_{1/2}}$ decay constant (sec^{-1})

λN_2 = $_{79}Au^{198}$ activity (disintegrations/unit time) and N_2 = number of atoms of Au-198 in the foil

σ_a = 98.8 barns = the thermal activation cross section.

T = irradiation time (sec)

t = time elapsed after removal from the flux no counting (sec)

N_1 = the number of atoms of Au-197 in the foil.

$N_1 = \frac{6.025 \times 10^{23}}{197.0} W$

where

W = the weight of the foil (gm)

The thermal activity may be equated to the proportional counter thermal count rate C_{th} (sec^{-1}) divided by the counter efficiency, ϵ. The thermal count rate is determined from the total count rate, C (sec^{-1}) (after correction for background) by use of the cadmium ratio, R, defined as the ratio of the total activity to the activity induced by neutrons other than thermal. (The cadmium covers absorb all neutrons up to about 0.4 ev.) Thus,

$$\lambda_2 N_2 = \frac{C_{th}}{\epsilon} \frac{C}{\epsilon} \left[\frac{R - 1}{R}\right] \qquad \text{(IV-7)}$$

Equations (IV-6 and IV-7) may be combined to give the solution for the thermal flux in terms of the observed proportional counter count rate and efficiency as

$$\phi_{th} = \frac{C}{\epsilon} \left[\frac{R - 1}{R}\right] \cdot \frac{1}{N_1 \sigma_{a_{th}} \left[1 - e^{-\lambda T}\right] e^{-\lambda t}} \qquad \text{(IV-8)}$$

The cadmium correction factor, R - 1/R, is given by the smooth curve through the data points of Fig. IV-13.

The counter efficiency was determined from gold foils identical to those used in the experiment. These foils were sent to Brookhaven National Laboratory for activation in a known flux. At Brookhaven, small and large foils were placed in the graphite sigma pile and exposed to neutrons from a Ra-Be source for 8.1 days (3.0 half-lives). Pile Position 1-5 was used for which the absolute thermal flux is 1.552×10^4 n/cm^2-sec and the cadmium ratio is 5.7. Absolute activation of these foils is proportional to R/(R - 1). The efficiency of the Martin Marietta proportional counter was then determined from the observed count rate for the standard foils or

$$\epsilon = \frac{C}{\phi_{th}} \left[\frac{R - 1}{R}\right] \frac{1}{N_1 \sigma_{a_{th}} \left[1 - e^{-\lambda T}\right] e^{-\lambda t}}$$

$$= \frac{C}{1.552 \times 10^4} \left[\frac{4.7}{5.7}\right] \frac{1}{N_1 \sigma_{a_{th}} \left[1 - e^{-\lambda T}\right] e^{-\lambda t}} \qquad \text{(IV-9)}$$

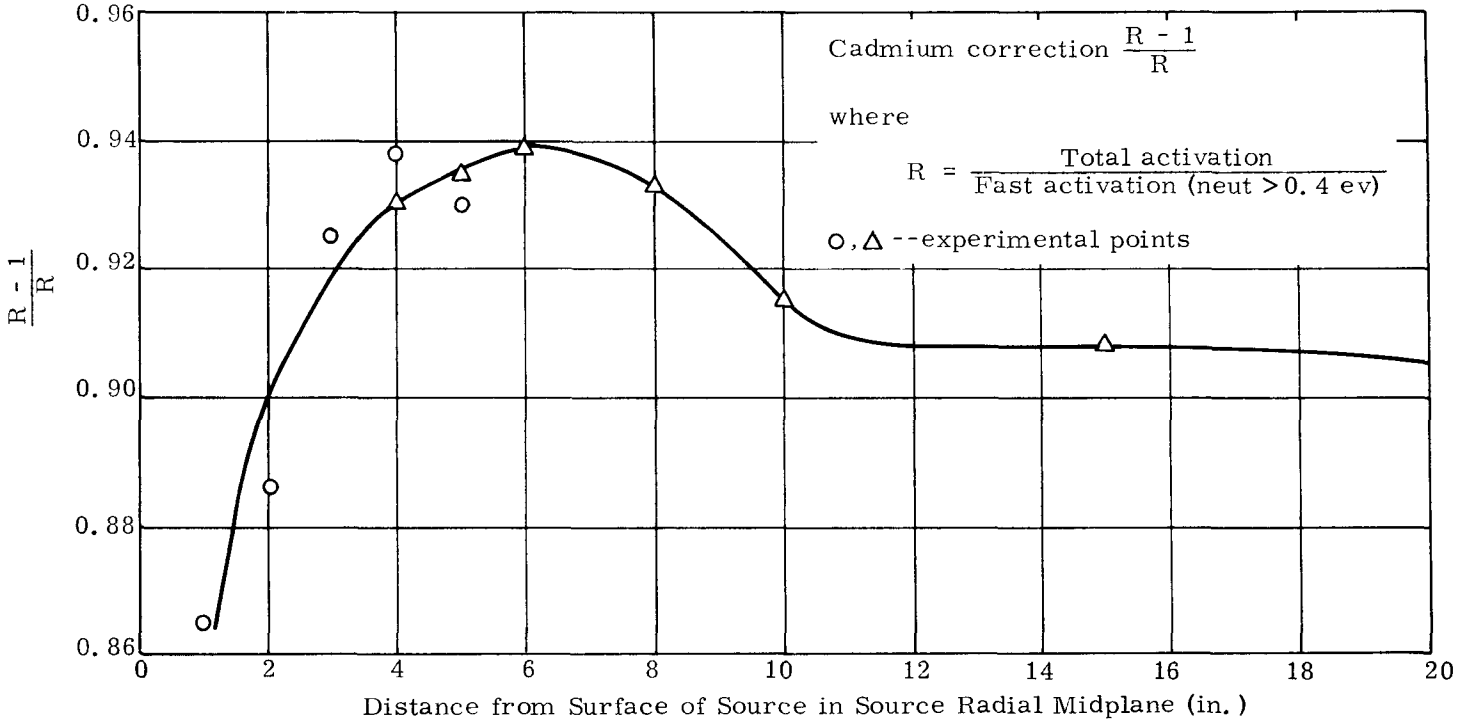

FIG. IV-13. CADMIUM CORRECTION FACTOR

Hence, all factors are known and the absolute thermal flux may be determined from Eq (IV-8).

Note that this procedure has eliminated the necessity of correction for flux perturbations in the vicinity of individual foils. Since the standard foils were the same as those used in the experiment, error introduced by this effect is approximately equal and self-cancelling. The second order effect of additional perturbation of one foil on another was not examined. Due to size and placement of foils in this experiment, corrections due to this effect are believed to be negligibly small (less than 1%).

d. Comparison of experiment and theory

Experimental results were initially normalized to the calculated values by assuming the source emission rate as measured by Mound of 1.99×10^7 n/sec. These data, for all foil positions, are given in Table IV-9. Over the range 14.66 centimeters to 40.06 centimeters, where the calculation applies, the observed maximum variation is 9.7%. The emission rate which normalized the experimental data to the calculated values was 2.06×10^7 n/sec. Hence, this experiment yields an absolute emission rate for the Pu-Be source of 2.06×10^7 n/sec. This value is to be compared to the Mound measurement, as corrected according to Eq (IV-5) for the elapsed time of approximately 270 days between the Mound measurement and the gold foil actuator. The corrected Mound value is 2.01×10^7 n/sec which is within 2.5% of the gold foil experimental value.

TABLE IV-9

Comparison of Calculated and Experimental Thermal Fluxes

$4\pi r^2 \phi_{th}(r)$ (n/sec/source neutron)

r (cm)	A = Calculated Values	B = Experimental / 1.99×10^7	R = B/A
4.50	3.21	0.844	
7.04	3.37	1.84	
9.08	2.91	2.03	
12.12	2.32	2.06	
14.66	1.79	1.82	1.017
17.20	1.37	1.39	1.015
19.74	1.05	1.13	1.076
22.28	0.803	0.863	1.074
24.82	0.618	0.621	1.005
29.90	0.370	0.406	1.097
32.44	0.288	0.281	0.976
40.06	0.136	0.138	1.015

' r = distance in water, source radial midplane, from center of source.

Without further analysis, an absolute error on the gold foil experiment cannot be assigned. Since the observed variance is small, the Mound result is accepted as correct. Analysis of stilbene measurements of fast spectra and dose rate in air and water (reported in Section IV-C) is based on an emission rate of 1.99×10^7 n/sec.

3. Spectrum Measurements in Air

Neutron spectrum measurements were made with the stilbene system at two points in the radial midplane of the Pu-Be source. A specific objective of this experiment was to test the ability of the system and data reduction technique to correctly predict the absolute magnitude of the energy dependent spectra. The experimentally derived spectra are integrated to determine the neutron dose rate. These dose rates are compared to calculated values based on the known emission rate of the source.

Spectral measurements were made using separation distances of 5.625 and 12.125 inches between the source surface to crystal cover surface. Long counts were taken to ensure good counting statistics. Count rate data were analyzed using the Stilbene Data Reduction Code (Appendix A) to determine the absolute neutron spectral data. The resulting neutron spectra are shown in Fig. IV-14. The distance, R, of Fig. IV-14 is the radial distance from the center of the source to the face of the stilbene crystal. The spectral shape is essentially the same as previous measurements in air for this source.

Neutron dose rates in mrem/hr were calculated as

$$D(r) = \int_{E = 0.2\ \text{Mev}}^{E = 10.4\ \text{Mev}} C(E)\, \phi(r, E)\, dE \qquad \text{(IV-10)}$$

where

$\phi(E, r)$ = measured spectrum (n/cm^2-sec-Mev), Fig. IV-14

$C(E)$ = flux-to-dose rate conversion factor (mrem/hr per n/cm^2-sec) as derived from 10 CFR 20 and listed in Table IV-10.

To compute total neutron dose, it was necessary to extrapolate the experimental data below 1.0 Mev (as shown by the dashed portion of the curves of Fig. IV-14). Since the dose rate conversion function decreases rapidly in this region, the resultant uncertainty in the computed dose rate due to the extrapolation is relatively small. The computed dose rates for neutrons with energies less than 1.0 Mev are 8 and 9% of the total dose rate for the two points. The experimentally determined dose rates are as follows:

Radial Distance (cm)	Neutron Dose Rate (mrem/hr)	
	Neutrons < 1.0 Mev	Total
16.41	62	776
32.92	20	221

The radial distance includes the source radius (1.96 cm) and the thickness of the stilbene crystal aluminum cover plate (0.16 cm). Attenuation of neutrons in the thin crystal cover plate was not considered in computing these results or in the theoretical analysis.

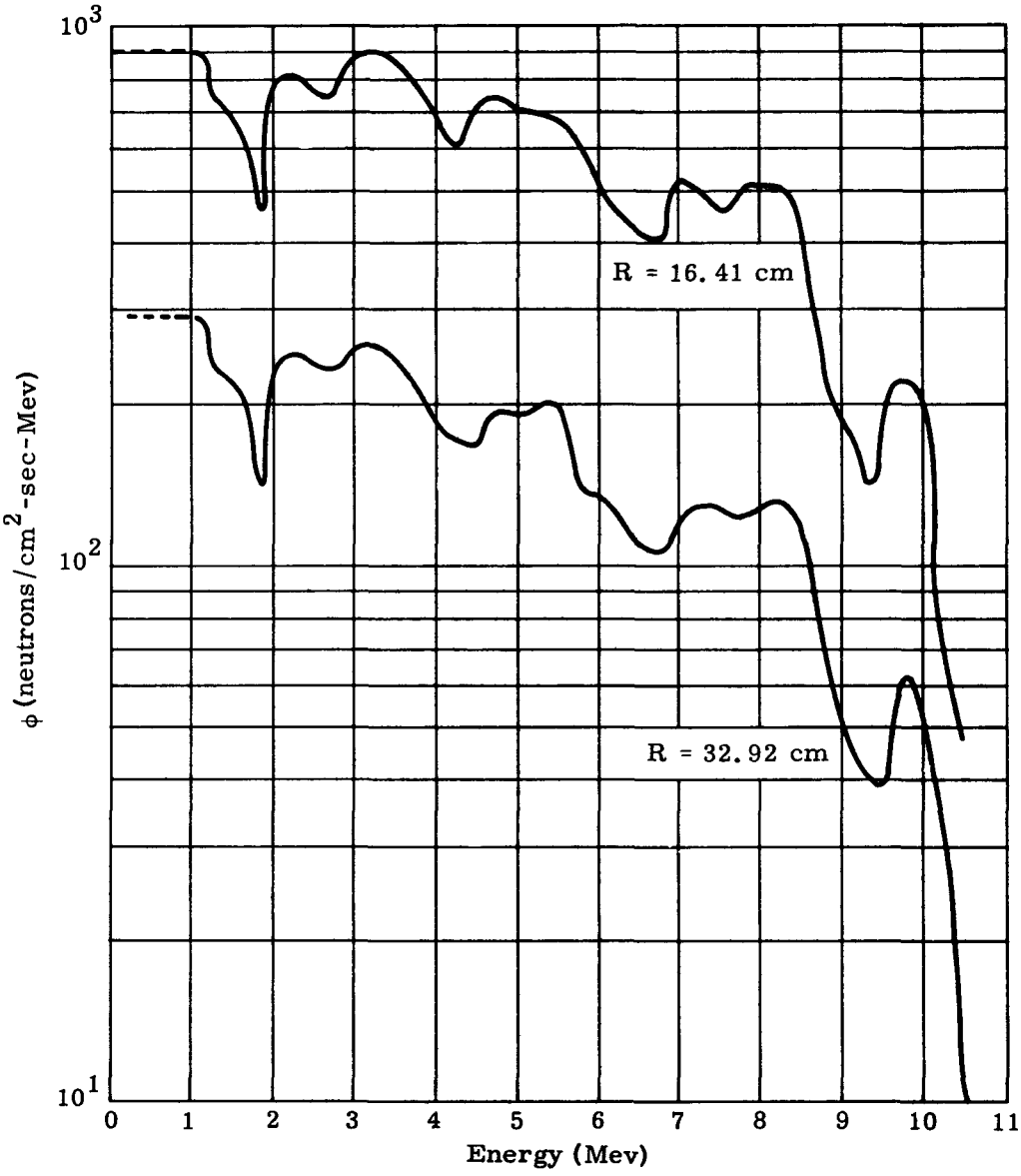

FIG. IV-14. NEUTRON FLUX FROM PuBe SOURCE IN AIR

TABLE IV-10

Neutron Flux to Dose Rate Conversion Factor

E (Mev)	C (E)	E (Mev)	C (E)
0.2	0.0345	5.8	0.141
0.4	0.0595	6.0	0.141
0.6	0.0909	6.2	0.143
0.8	0.111	6.4	0.143
1.0	0.133	6.6	0.145
1.2	0.139	6.8	0.145
1.4	0.135	7.0	0.145
1.6	0.133	7.2	0.147
1.8	0.132	7.4	0.147
2.0	0.130	7.6	0.147
2.2	0.128	7.8	0.147
2.4	0.125	8.0	0.147
2.6	0.125	8.2	0.147
2.8	0.127	8.4	0.147
3.0	0.128	8.6	0.147
3.2	0.128	8.8	0.147
3.4	0.130	9.0	0.147
3.6	0.132	9.2	0.147
3.8	0.133	9.4	0.147
4.0	0.133	9.6	0.147
4.2	0.135	9.8	0.147
4.4	0.135	10.0	0.147
4.6	0.137	10.2	0.149
4.8	0.139	10.4	0.152
5.0	0.139	10.6	0.152
5.2	0.139	10.8	0.154
5.4	0.139	11.0	0.156
5.6	0.141	11.2	0.156

Experimental data were compared to results of an analytical model for computation of dose rates which employs a point kernel integration over this source volume using neutron effective removal cross sections. This model employs program SPEND, an IBM computer program, for point kernel integration over volume distributed sources and shield regions in cylindrical geometry. The physical representation of the source geometry is exact, it is a cylindrical source region containing a homogeneous mixture of 159 grams of Pu-239 and 79.1 grams of Be with a radius of 1.73 centimeters and a height of 6.83 centimeters encapsulated by a stainless steel cylindrical annulus and cylindrical end plates. The source and encapsulation have an outer radius of 1.96 centimeters and a height of 8.61 centimeters. Neutron removal cross sections used for the calculations are as follows:

Material	Σ_R (cm^{-1})
Homogenized source region	0.134
Stainless steel	0.168
Air	5.168×10^{-5}

Since only the source neutron emission rate (and not the source strength) is known, a preliminary calculation was performed to adjust calculations to the measured emission rate. The emission rate of the source was taken as 1.99×10^7 n/sec (see Section IV-C) as measured at Mound using a BF_3 long counter. To simulate this long counter technique, a SPEND calculation was performed to determine the neutron flux, ϕ_s (n/cm^2-sec), at all points on a spherical surface of radius R with a center at the source center. The neutron emission rate, Q (n/sec), is then given by the integral of the flux over this surface. Thus,

$$Q = \int_A \phi_s \, dA = 4\pi R^2 \int_0^{\frac{\pi}{2}} \phi_s(\theta) \sin\theta d\theta \text{ (n/sec)} \qquad \text{(IV-11)}$$

where θ is the polar angle measured from the axis of the cylinder

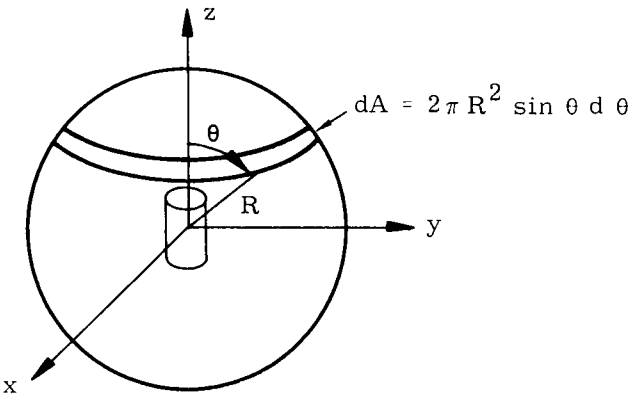

The equivalent source strength, S, is that which yields an emission rate Q = 1.99×10^7 n/sec as measured by Mound Laboratory. The uniform volumetric source strength used for subsequent calculation is:

$$S_V = \frac{S}{V}_{source} = \frac{2.76 \times 10^7 \text{ n/sec}}{64.04 \text{ cm}^3} = 4.31 \times 10^5 \text{ n/cm}^3\text{-sec}$$

Neutron dose rates exterior to and in the radial midplane of the source were computed using this source strength and a conversion factor (consistent with removal cross section theory) of 0.1428 mrem/hr.

Results of this calculation are shown on Fig. IV-15 along with the experimental results. Comparison is as follows:

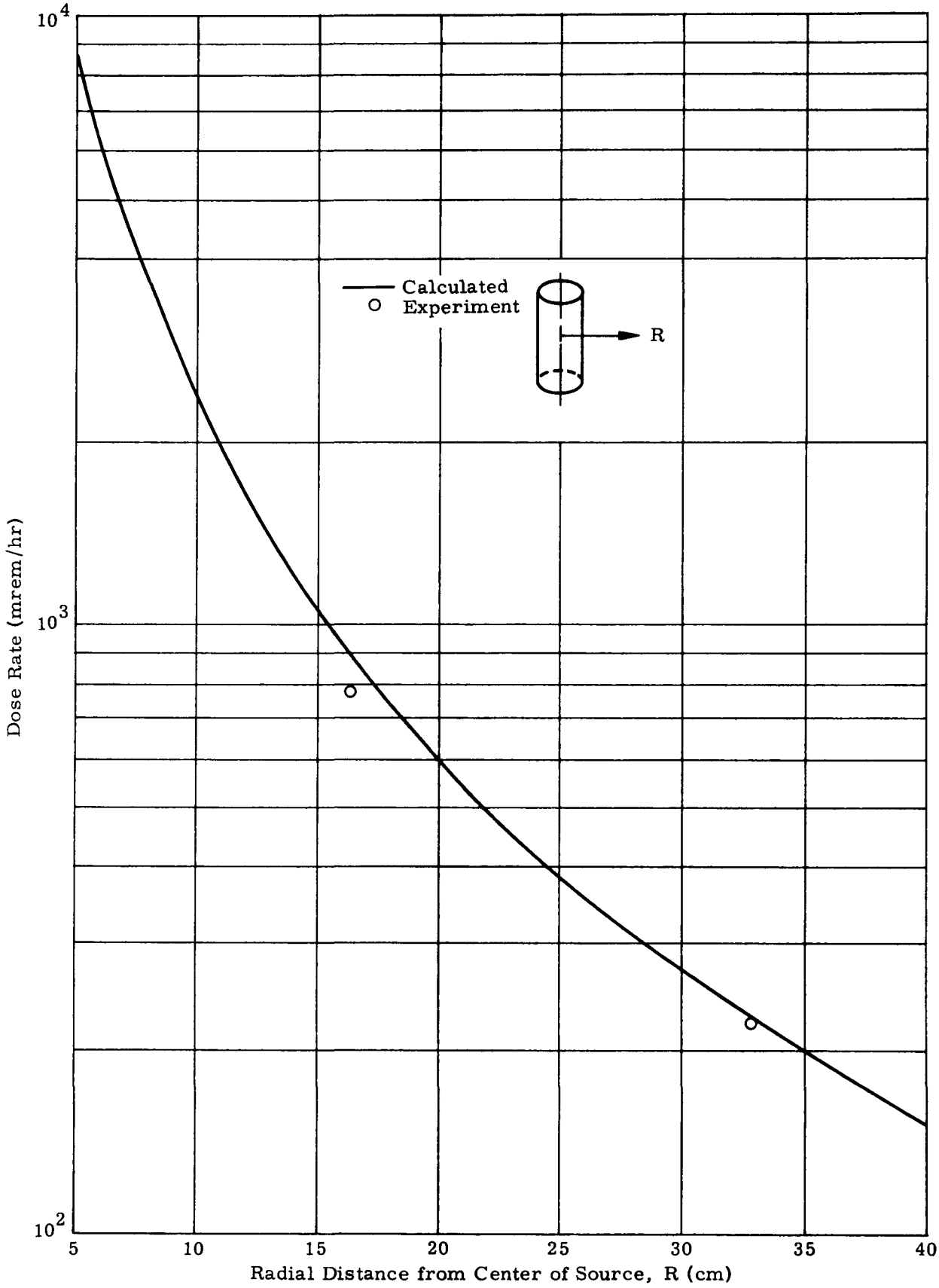

FIG. IV-15. NEUTRON DOSE RATES FROM PuBe SOURCE IN AIR

Radial Distance (cm)	Neutron Dose Rate (mrem/hr) Experiment	Calculation	Ratio: Experiment-to-Calculation
16.41	776	895	0.87
32.92	221	225	0.98

The maximum discrepancy of 12% is within experimental and analytical uncertainties, which are mainly due to experimental statistical deviation, uncertainty in measurement of ϵ, extrapolation of spectrum below 1.0 Mev and uncertainty in the use of removal cross sections in the absence of hydrogenous materials. These results tend to validate the use of the stilbene system including the normalized data reduction program for measurement of absolute neutron energy spectra and neutron dose rates.

4. Spectrum Measurements in Water

An experiment and analysis were performed in which spectral results of the Pu-Be source in water obtained with the stilbene system are compared with moments method calculations. The objective of the experiment and analysis was to demonstrate the ability of the measurement technique to correctly determine the absolute magnitude and energy dependence of the spectrum as perturbed by water.

Spectral measurements were made with the stilbene system in the radial midplane of the Pu-Be source beyond two different thicknesses of water. Source detector geometry was arranged to simulate the source in infinite water. A perturbation to the desired geometry was introduced by the necessity of placing the broad face of the detector crystal exterior to, but in contact with, the water tank containing the source. The uncertainty introduced by this perturbation is believed to be small due to the forward peaking of neutron angular distributions through water shields. Two measurements were made with water thickness of 5.625 and 8.0 inches. The corresponding radial distances from the center of the source to the detector crystal face of 16.89 and 22.92 centimeters include a source radius of 1.96 centimeters, tank wall thickness of 0.16 centimeter, an air gap of 0.32 centimeter and an aluminum crystal face cover with a thickness of 0.16 centimeter.

Verification of the ability of the stilbene system to measure spectra and dose rates through shield materials accurately was achieved by comparison of experimental results with moments calculations for a point source in water. The solution for the moments employs a scattering matrix for oxygen based on a heavy element treatment which utilizes an accurate N point quadrature to represent the scattered source. Moments thus calculated are exact to within the numerical limits imposed by the energy point spacing and machine computer program limitations. Reconstruction of the scalar energy flux from the moments is accomplished by assuming the exponential flux or dose function of the form of Eq IV-1 and solving for the constants A_i and α_i which may be expressed in terms of the known moments. This exponential form yields more accurate results for deep penetration when compared to the more conventional spatial polynominal representation. (For further discussion of moments calculations see Section IV-C and Appendix B.)

The first 20 energy points of the 68-point energy structure were used for reconstruction of the energy dependent fast flux over the interval from 18.02 to 0.1559 Mev. The input source spectrum approximated the measured emission spectrum of the Pu-Be source (see Section IV-C-3 and Table IV-6). Some smoothing was necessary for high energies due to a lack of a sufficient number of energy points in the representation to represent adequately the fine detail exhibited by this source. Dose moments

were formed as the energy integral of the product of the flux moments and conversion factor. The spatially dependent dose function is then formed according to a form similar to Eq. (IV-1). The solution yielded a two-exponential dose rate function for the point Pu-Be source in water which is valid for r > 12 cm:

$$4\pi r^2 \frac{D(r)}{S} = 0.28157e^{-0.097023r} - 0.13916e^{-0.188743r} \quad \frac{\text{mrem/hr}}{\text{n/sec}}$$

A check of this function was made by comparison of moments of higher order (not used in the reconstruction solution) calculated from Eq. (IV-12) with the exact higher order moments. The comparison shows good agreement. Additional checks have been made by comparing solutions for a point fission source using the same program and same hydrogen and oxygen scattering matrices which show good agreement with similar calculations performed at other laboratories and experimental data (Section IV-B).

An additional calculation was performed to investigate the effects of the finite geometry of the source. Program SPEND was used to integrate the dose rate kernel (Eq. (IV-12)) over a cylinder of dimensions equal to the Pu-Be source region to determine dose rates in the radial midplane of the source. Attenuation, according to Eq. (IV-12), was included in the source region. Results were normalized to and compared to the point source solution (see Section IV-B and Table IV-8). These calculations indicated that, for r >15 cm, the dose rate from a point source of S (n/sec) is equivalent to the dose rates from the volume distributed source with dimensions equivalent to the Pu-Be source and with a source strength $S_V = S/V_{source}$ (n/cm^3-sec).

Neutron spectral data and dose rates were normalized to a source strength of 1.99×10^7 n/sec (the Mound measured emission rate) and compared to experimental results. Figure IV-16 presents the measured and calculated neutron spectra. The experimental spectras were integrated according to Eq. (IV-10) to determine the neutron dose rate. Note that an extrapolation was made for neutrons with energies less than 1.0 Mev. Results and comparison are as follows.

	Neutron Dose Rate (mrem/hr)		
Radial Distance (cm)	Experiment E > 1.0 Mev	Total	Calculated (moments) Total
16.89	43	271	273
22.92	12	87	86

Calculated and experimental dose rates are also shown in Fig. IV-17.

The agreement in spectral shape and dose rate data is well within experimental and computational error. The relatively smooth calculated spectrum for high neutron energies (as compared with the experiment) is a direct result of the scarcity of energy points in this range and the resultant smoothing of the input spectrum. Better resolution could be obtained by increasing the number of energy points. However, in this case, it is believed that little new knowledge would be gained and that the present results are sufficient to demonstrate the capabilities of the stilbene detecting system.

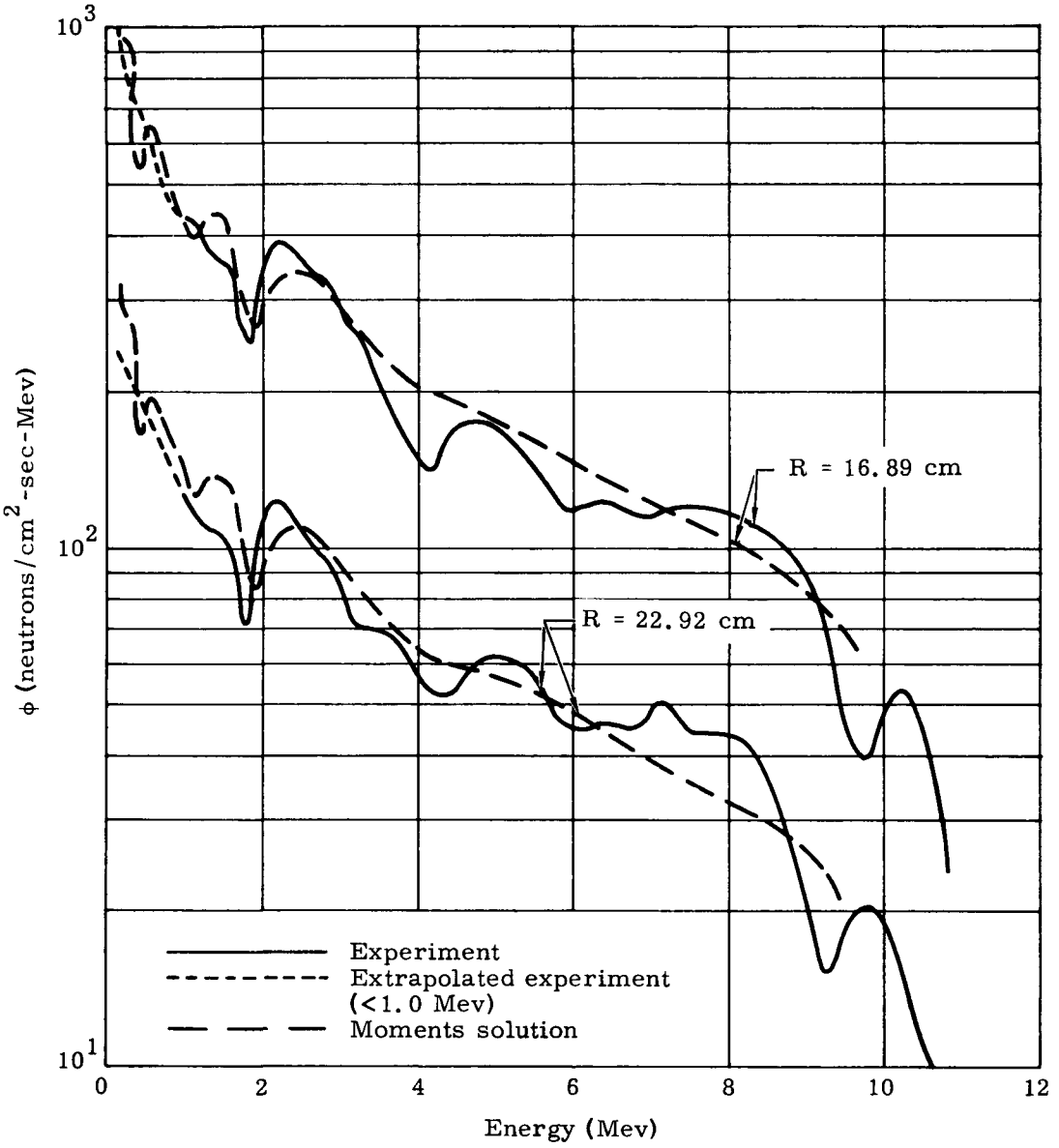

FIG. IV-16. NEUTRON FLUX FROM PuBe SOURCE IN WATER

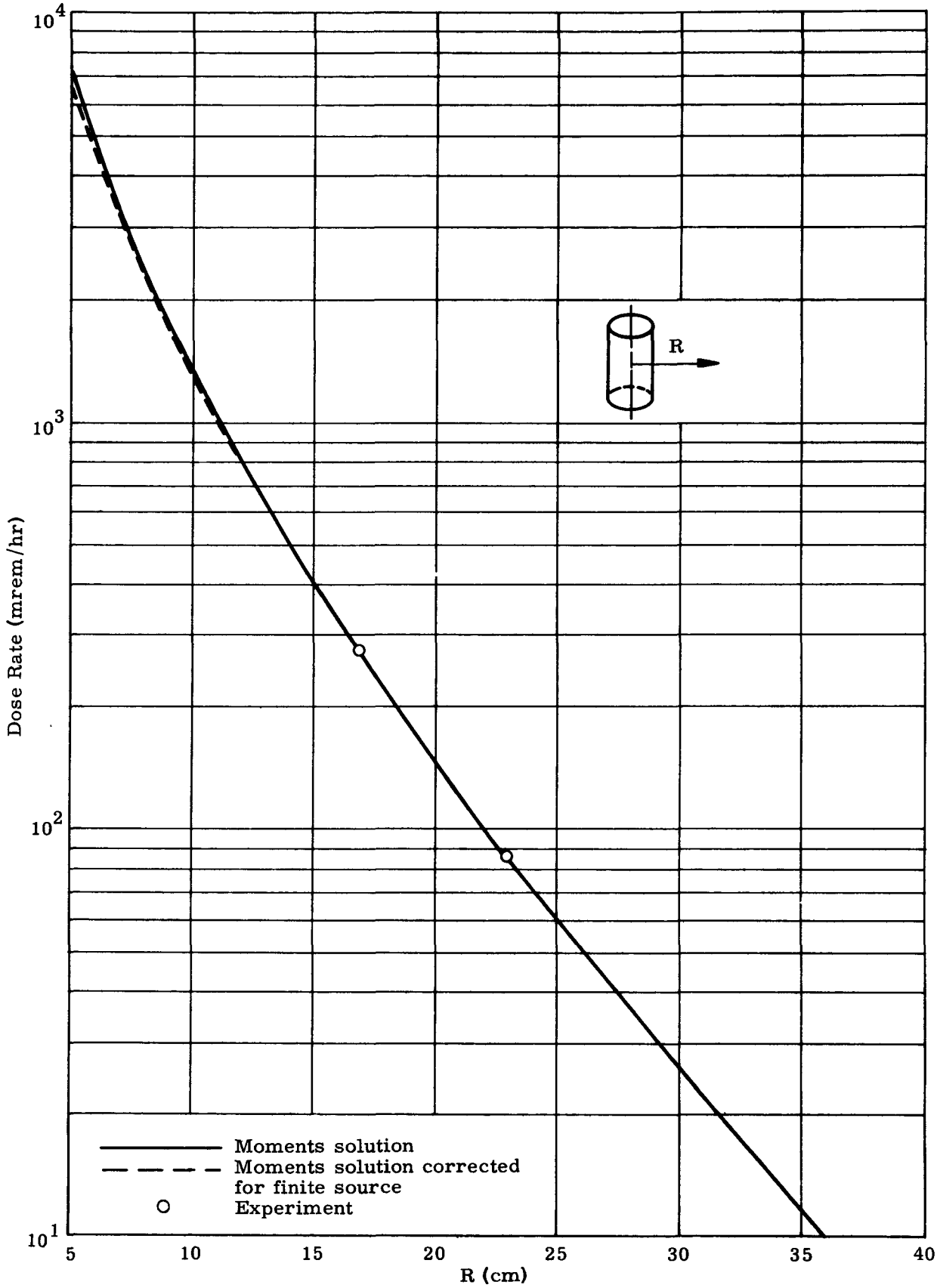

FIG. IV-17. NEUTRON DOSE RATES FROM PuBe SOURCE IN WATER

BLANK

V. SUBSYSTEM NEUTRON MEASUREMENTS

A. EXPERIMENTAL MEASUREMENTS

Neutron spectrum and dose rate measurements were made on the SNAP 19 System 4 generator subsystem. The measurements were made in Test Cell 2 of the Martin Marietta Critical Facility, using the procedures defined in Test Procedure 452B1900019, "Subsystem Radiation Measurements".

For the measurements, the subsystem was mounted in a fixed position on the test stand in the center of the test cell, a room approximately 20 by 20 by 20 feet with reinforced concrete walls and ceiling (Ref. 22). To measure neutron spectra at various locations, the detector was positioned at the proper spatial orientation using the mounting fixture shown in Fig. V-1.

To obtain a continuous spectrum from 1.0 to 12.5 Mev, measurements were made with high voltage settings of 1535 and 1650 volts as described in Chapter III-B.

Calibrations were performed before and after each spectrum measurement, using the Compton recoil spectra of Cs-137 and Na-22 gamma sources as described in Chapter IV-A.

Neutron spectra were measured at six locations around the subsystem as shown in Fig. V-2. The three radial locations were on the midplane of the subsystem at radial distances of 13.1, 17.1 and 29.1 inches from the subsystem axis. The two locations of the measurements on the subsystem axis were 13.8 and 15.8 inches from the midplane of the subsystem. The sixth point was an off-axis location approximately 15 degrees from the subsystem midplane.

The experimental data points were reduced using the data reduction program presented in Appendix A. The spectral shapes for all measured locations were essentially the same. Figure V-3 shows a typical spectrum, measured at Location 1 on Fig. V-2. The measured spectrum covers the energy range from approximately 1.0 to 12.5 Mev. For the dose rate evaluation discussed in Chapter V-B, it was necessary to extrapolate the spectrum data to include the energy range from 0 to 1.0 Mev. Two such extrapolations are shown in Fig. V-3. The one marked Approximation 1 is essentially a linear extrapolation of the lower energy portion of the measured data. Approximation 2 assumes that the spectrum is essentially flat below 1.0 Mev. The actual value logically falls somewhere between the two extrapolations. Using these extrapolations increases the neutron dose rate 22 or 29%, depending on which approximation is used. The difference between these two increases represents the range of uncertainty in total neutron dose rate contributed by neutrons below 1.0 Mev. Therefore, the uncertainty would be only 7%.

The neutron spectrum data for all six locations evaluated in this experiment are presented in Figs. V-5 through V-10. The two sets of data points, obtained from the data reduction, are shown using the symbols Δ for the high energy and O for the low energy measurement. The smooth curves are believed to be the best representation of the data. These curves were integrated to determine the dose rates reported in Chapter V-B. Figure V-2 shows the location of the points with respect to the subsystem.

The measurement of Dose Point 2 was repeated (see Figs. V-5 and V-6). A comparison of data points for these two measurements indicates good experimental reproducibility.

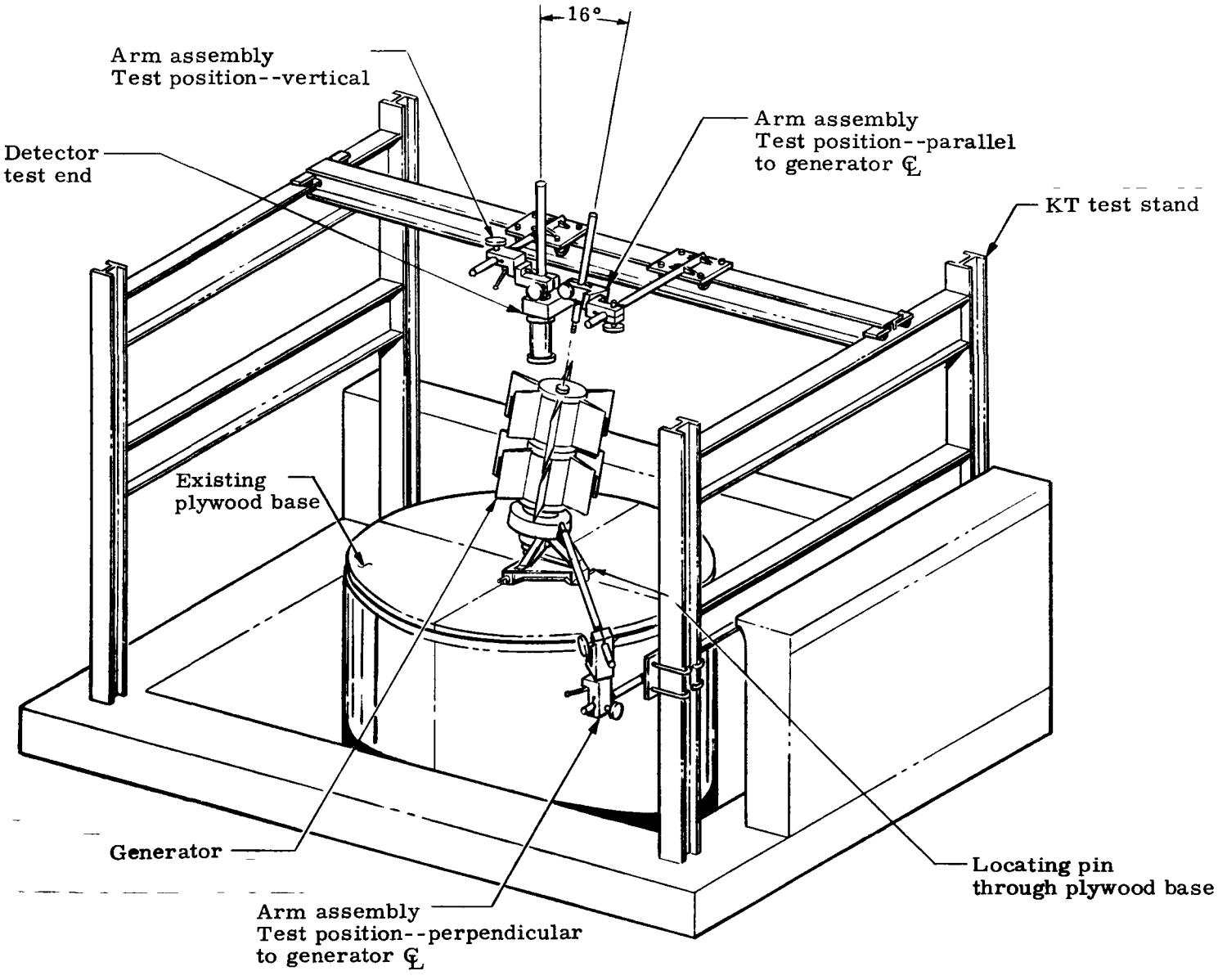

FIG. V-1. CAPSULE SPECTRA MEASUREMENT MOUNTING BRACKET

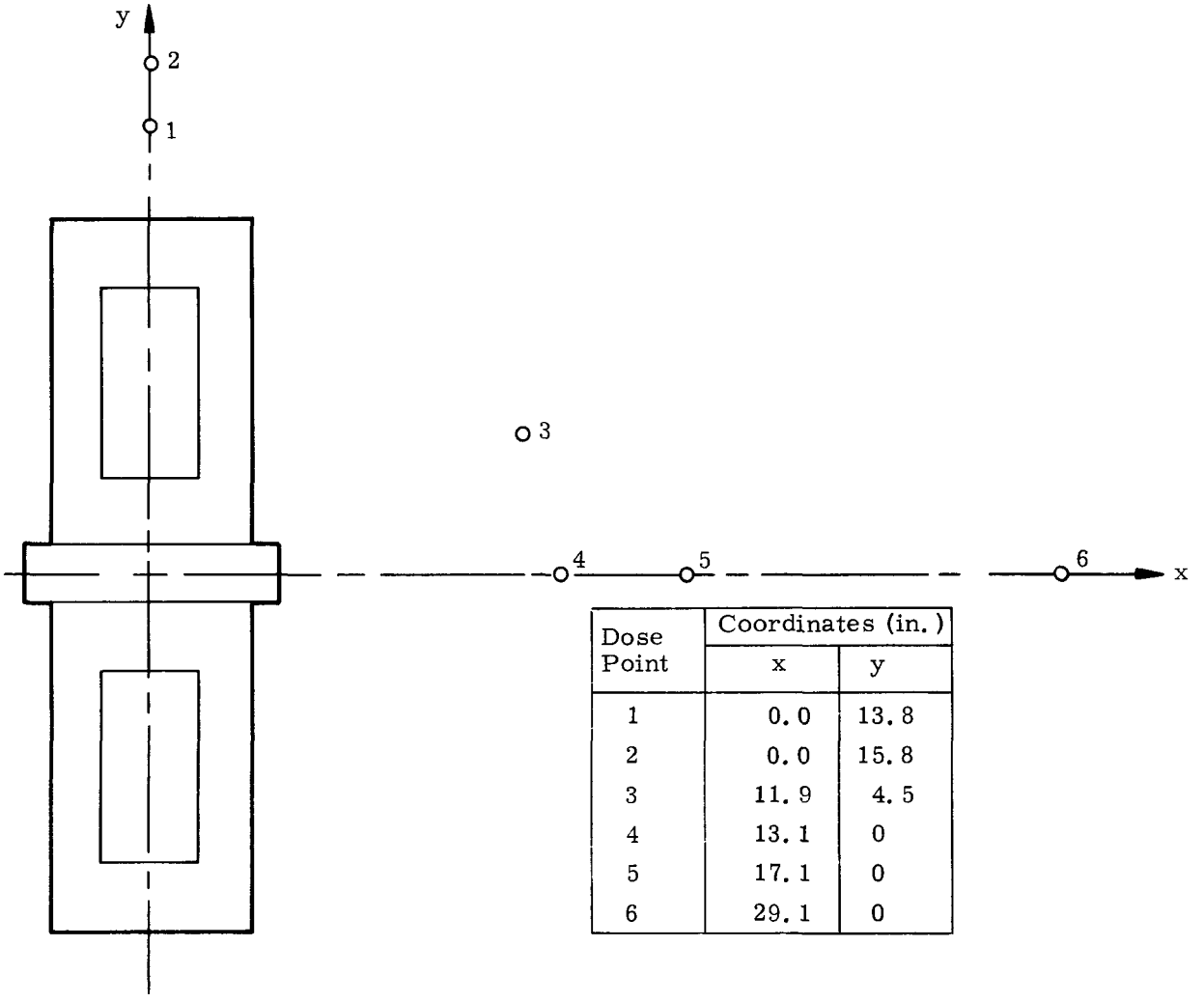

Dose Point	Coordinates (in.)	
	x	y
1	0.0	13.8
2	0.0	15.8
3	11.9	4.5
4	13.1	0
5	17.1	0
6	29.1	0

FIG. V-2. LOCATION OF DOSE POINTS IN RELATION TO SUBSYSTEM

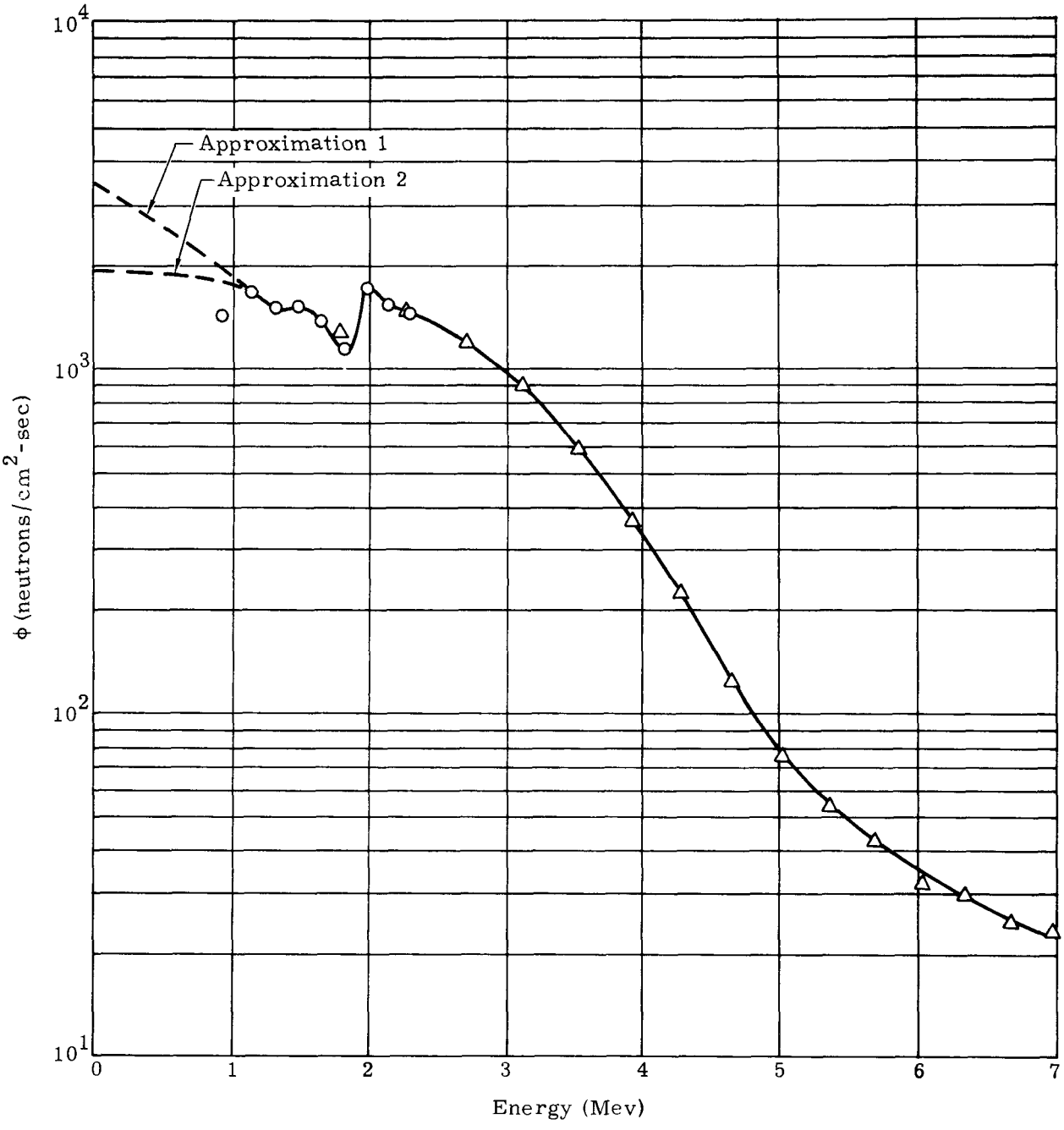

FIG. V-3. NEUTRON SPECTRUM MEASURED AT A POINT 13.8 INCHES ABOVE THE CENTER OF THE SUBSYSTEM

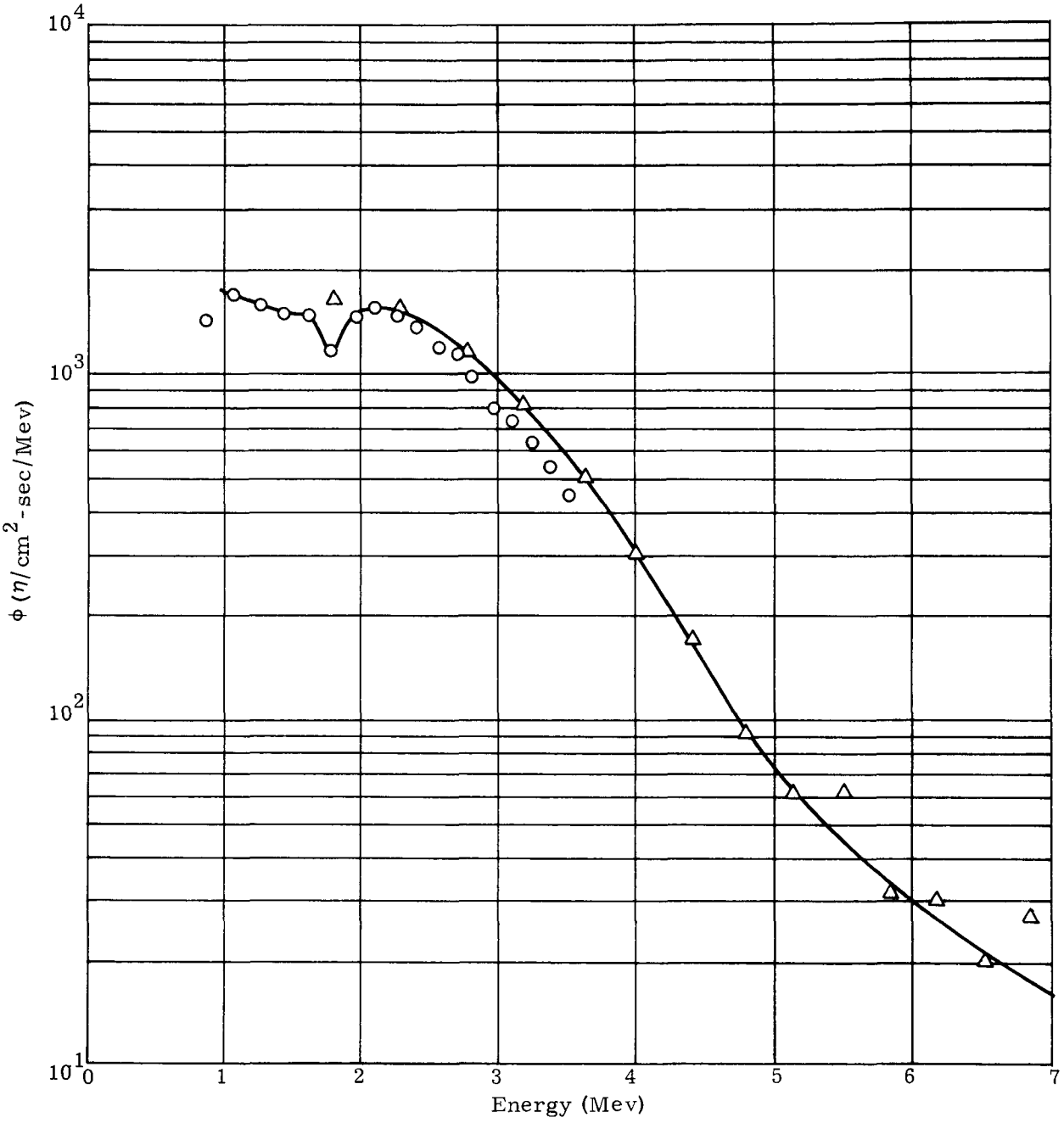

FIG. V-4. NEUTRON SPECTRAL MEASUREMENT--POINT 1

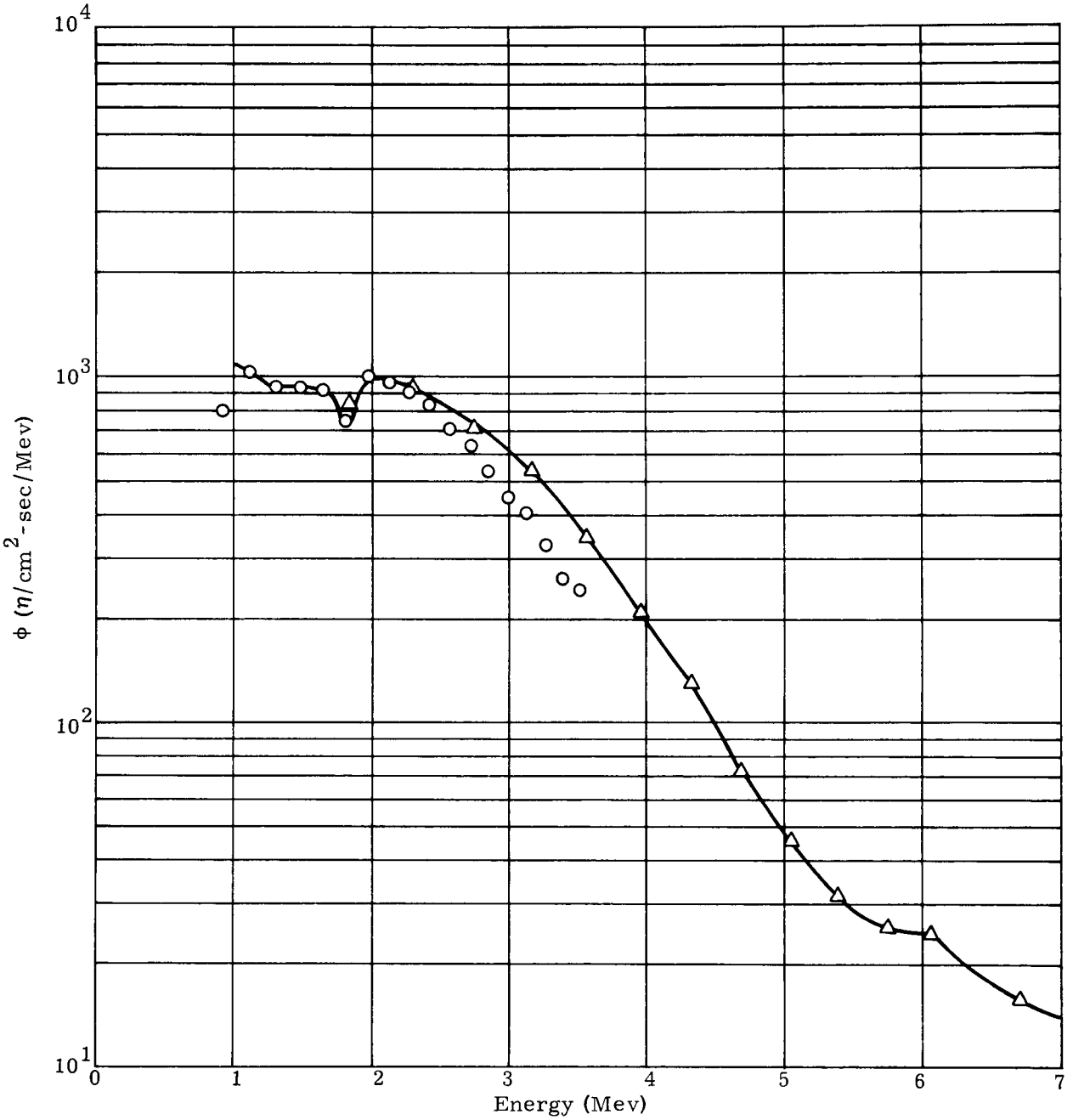

FIG. V-5. NEUTRON SPECTRAL MEASUREMENT--POINT 2

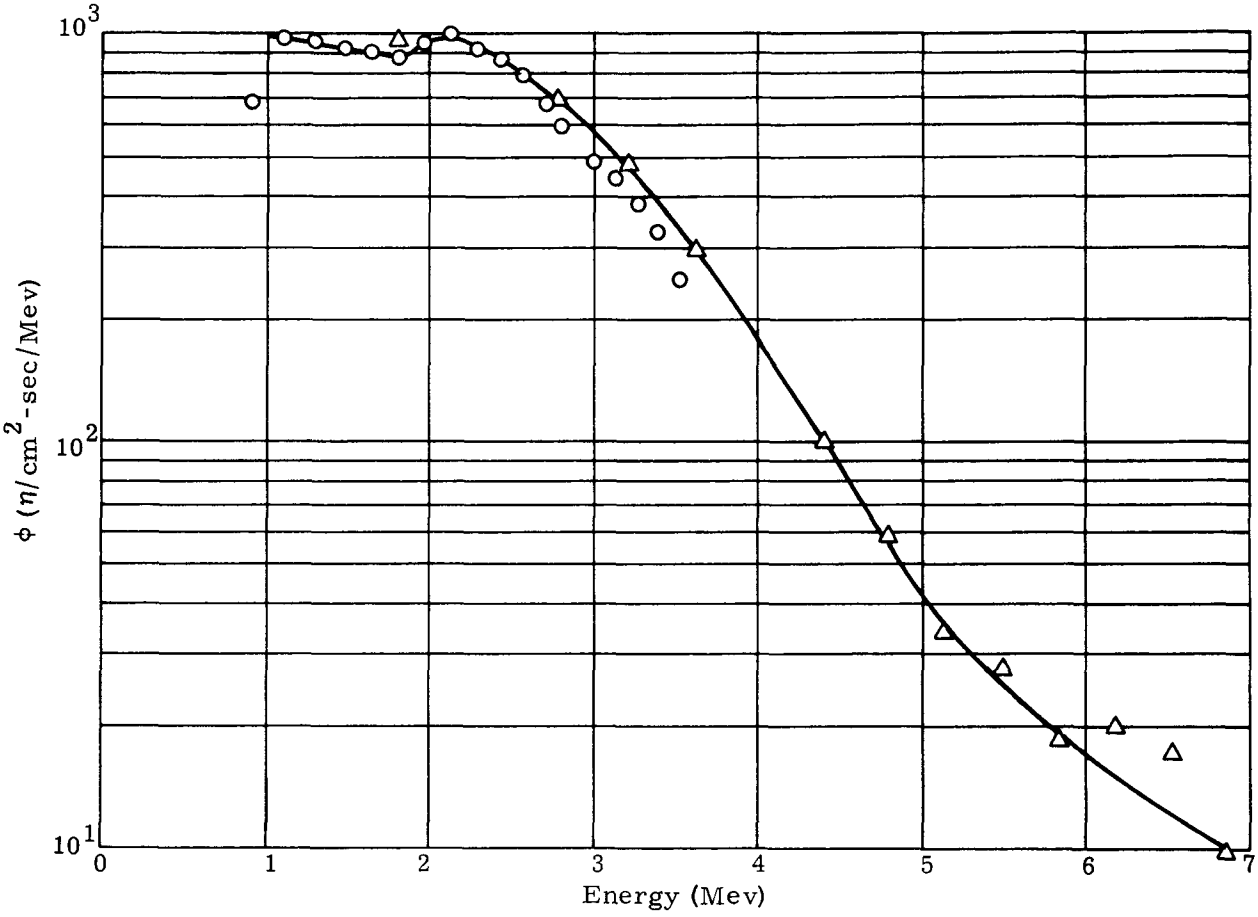

FIG. V-6. NEUTRON SPECTRAL MEASUREMENT--POIN T 2
(REPEAT OF MEASUREMENT)

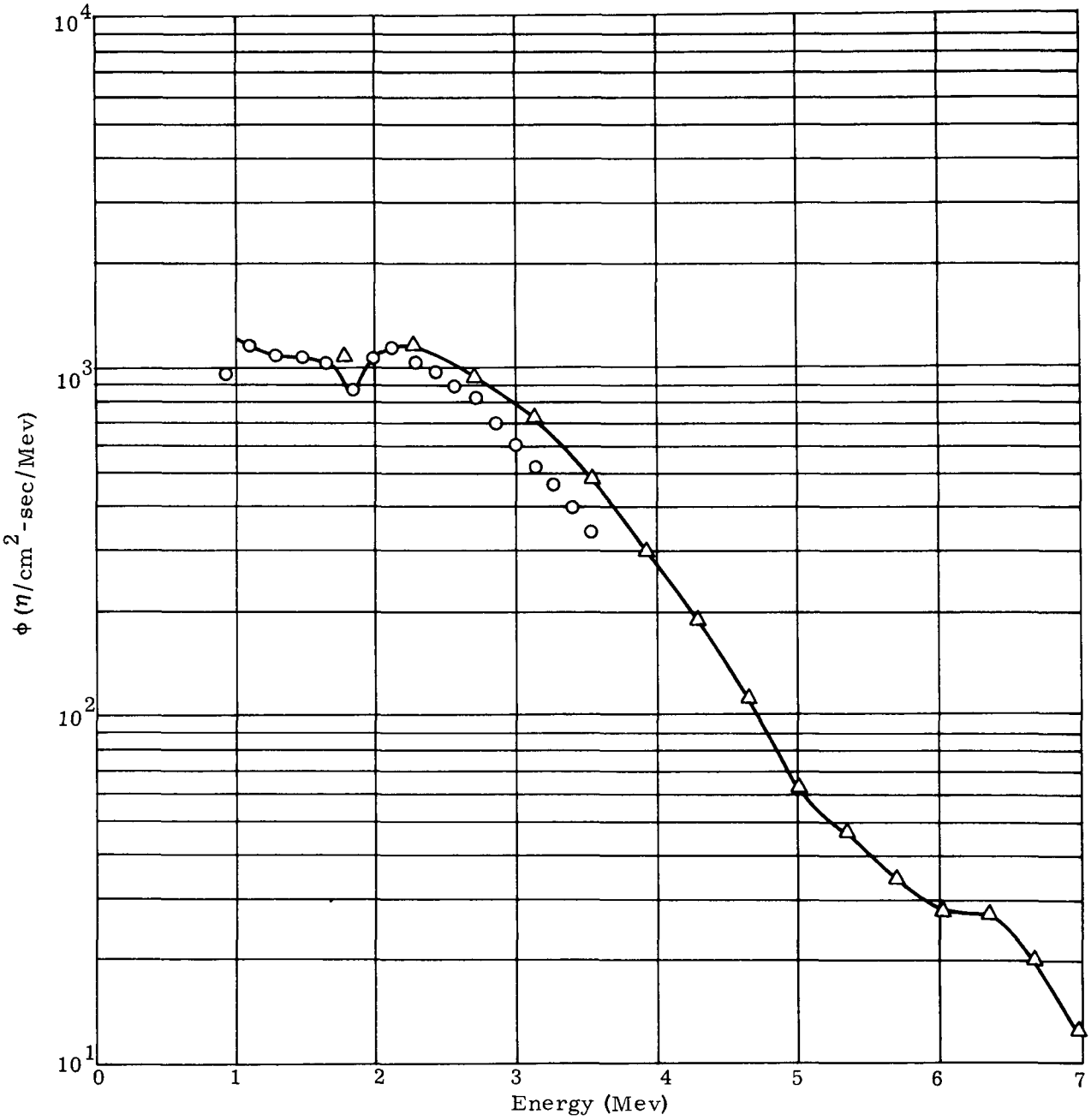

FIG. V-7. NEUTRON SPECTRAL MEASUREMENT--POINT 3

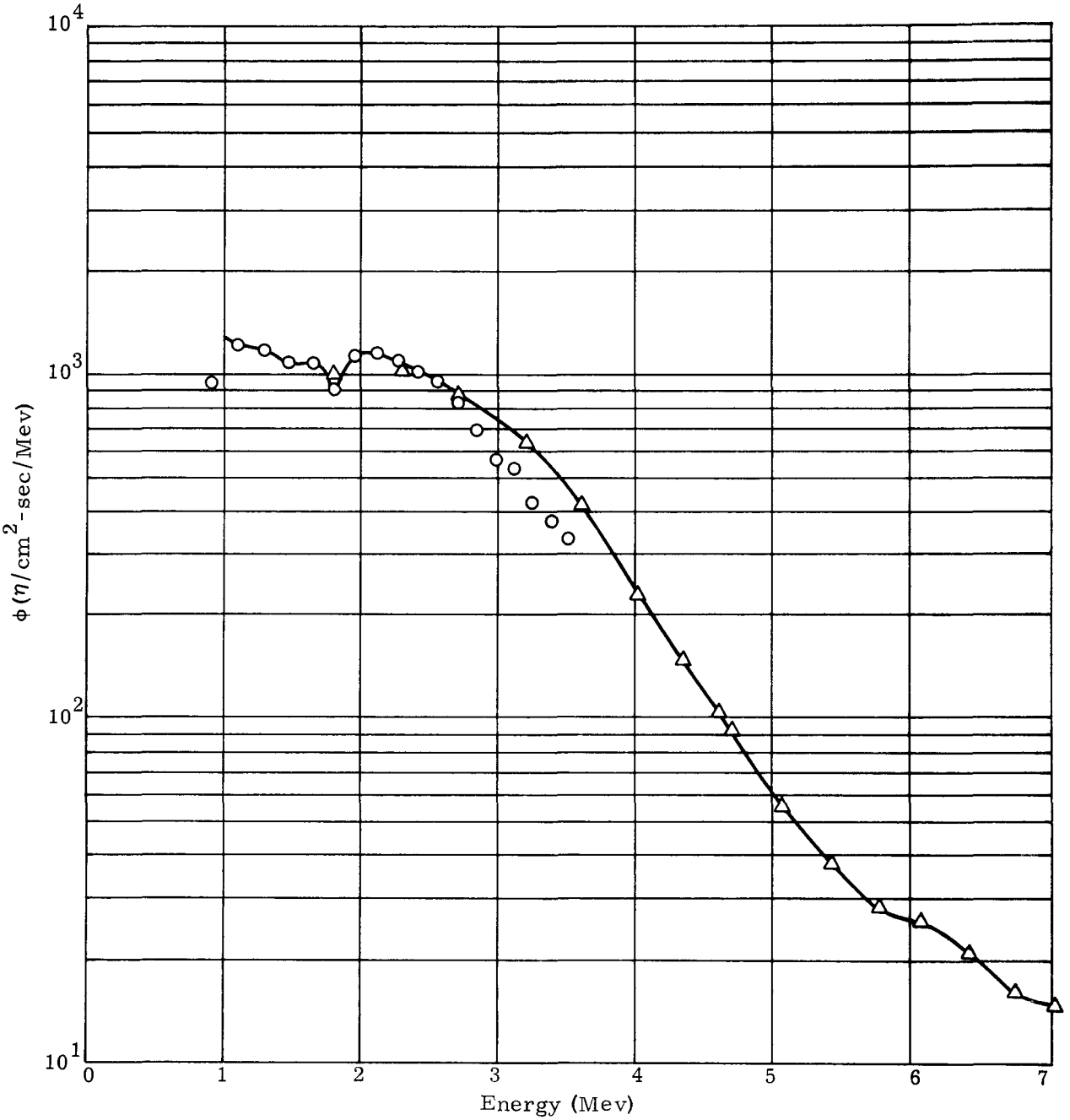

FIG. V-8. NEUTRON SPECTRAL MEASUREMENT--POINT 4

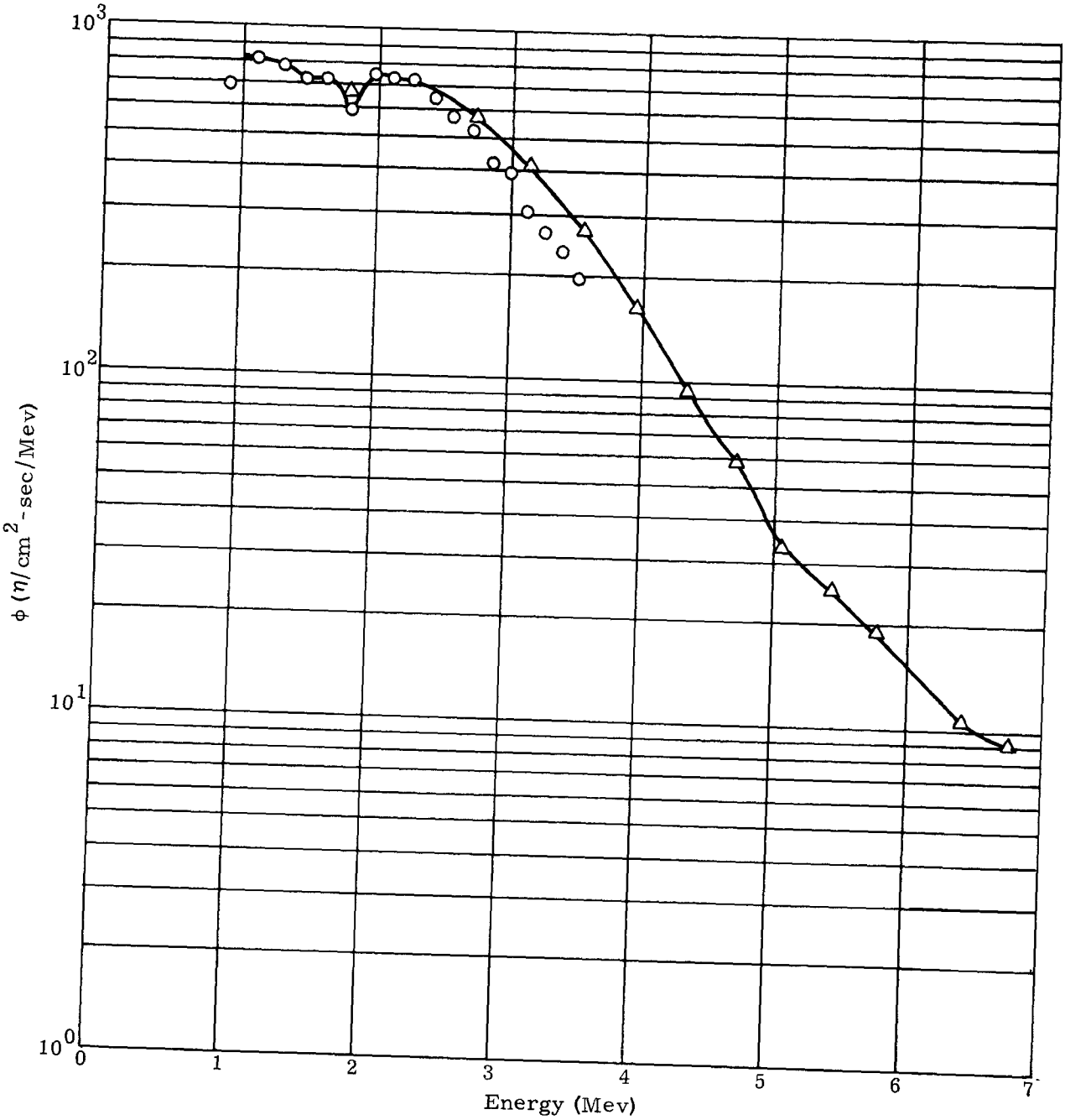

FIG. V-9. NEUTRON SPECTRAL MEASUREMENT--POINT 5

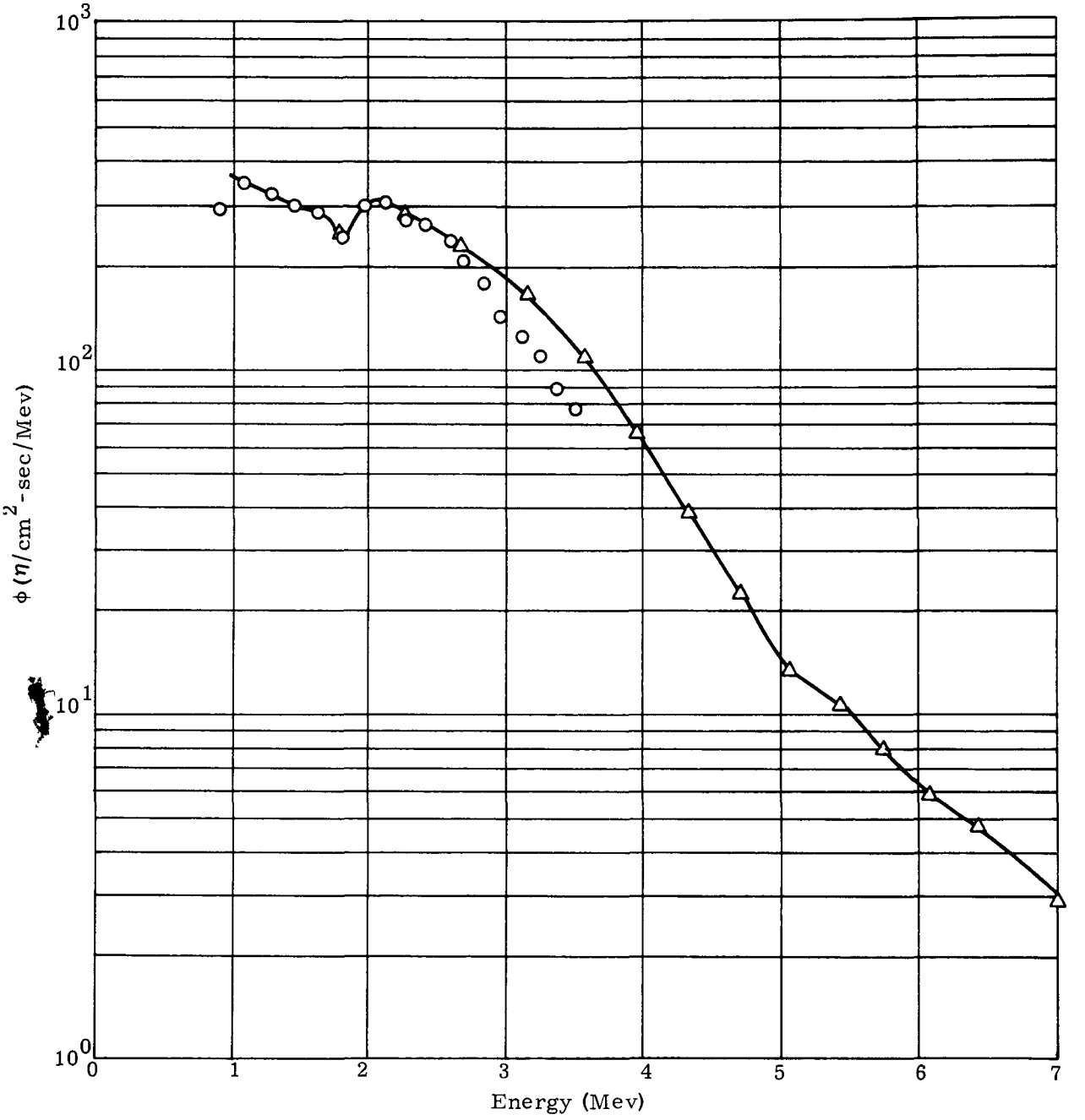

FIG. V-10. NEUTRON SPECTRAL MEASUREMENT--POINT 6

B. DOSE RATES

The energy spectrum at each measured point shown in Fig. V-2 was numerically integrated to find the neutron dose rate at that point. In the analysis of the data, the measured neutron dose rates at every point were increased by 30% to account for the energy spectrum in the 0.0 to 1.0 Mev range as discussed in Section V-A. Table V-1 gives the neutron dose rates at each point prior to and after this increase.

Neutron dose rates from a subsystem are also calculated using program SPEND (Shield Penetration and Energy Deposition) for comparison with those determined from the measured energy spectra. The neutron dose rates as computed by program SPEND are based on the original 625-watt(t) inventory of the SNAP 19 fuel capsule and a 3.33×10^4 n/sec-gm of Pu-238 neutron generation rate. This generation rate was derived from the maximum neutron generation (2.5×10^4) n/sec-gm of Pu-238) measured by Mound Laboratory on small samples of the capsule fuel (Ref. 23) and an 0.25 effective multiplication factor, k_{eff}, to account for the increase due to fast fissioning in the capsule. The thermal inventory and neutron generation rate quoted correspond to a source production rate of 3.75×10^7 n/sec.

TABLE V-1

Measured Dose Rates

Dose* Point	Location X (in.)	Location Y (in.)	Measured (mrem/hr)	1.30 Measured (mrem/hr)
1	0.0	13.8	509	662
2	0.0	15.8	316	411
3	11.9	4.5	378	491
4	13.1	0.0	374	486
5	17.1	0.0	242	315
6	29.1	0.0	99	129

*From Fig. V-2

Before a valid comparison between measured and calculated neutron dose rates can be made, a comparison must be made between the emission rate on which the calculated dose rates are based and the emission rates on which the measured dose rates are based. An integration was performed for the calculated neutron fluxes at a distance of 50 centimeters from the center of a SNAP 19 fuel capsule. It was found that the ratio of the source production rate to the emitted production rate is 1.29; i.e., 29% of the neutrons are attenuated in the fuel capsule. Therefore, the calculated neutron dose rates are based on an emission rate of

$$\frac{3.75 \times 10^7 \text{ n/sec}}{1.29} = 2.90 \times 10^7 \text{ n/sec}$$

The calculated neutron dose rates are given in Table V-2 for the points at which the neutron spectra are measured.

TABLE V-2

Calculated Neutron Dose Rates

Dose Point	Dose Rate (mrem/hr)
1	810
2	502
3	550
4	480
5	300
6	111

The emission rates for the two fuel capsules used in Subsystem S/N 4 were measured at Mound Research Corporation. These emission rates were 2.52×10^7 and 2.96×10^7 n/sec, respectively, for Capsules 300 and 307 (Ref. 24). Since Capsule 307 is in the top generator of Subsystem S/N 4 and it was found from the calculations that greater than 80% of the neutron dose rate at points on the axis above and within 10 inches of the top of the subsystem are due to the top capsule, an approximate correction factor for calculated dose rates on the system axis (Points 1 and 2, Fig. V-2) is

$$\frac{2.96 \times 10^7 \text{ n/sec}}{2.90 \times 10^7 \text{ n/sec}} = 1.02$$

An approximate correction factor for radial points (Points 4, 5 and 6, Fig. V-2), based on the average emission rate for the two capsules, is

$$\frac{2.96 \times 10^7 + 2.52 \times 10^7}{2 \times 2.90 \times 10^7} = 0.94$$

The correction factor for Point 3 of Fig. V-2 lies somewhere between 1.02 and 0.94. From Fig. V-2, it appears that the correction factor would be closer to 0.94 and, hence, this value is used. Table V-3 compares the corrected calculated neutron dose rates with extrapolated (1.30 measured) measured values.

Health physics measurements were made of total dose rates (neutron and gamma) above and to the side of SNAP 19 Subsystem S/N 4. Figures V-11 and V-12 give these total dose rates as a function of distance from the centers of the subsystem. Also plotted are the stilbene dose rates, which have been increased by 30% as previously discussed, and the corrected calculated dose rates. Previous calculations indicated that, for the six stilbene detector positions, approximately 90% or more of the total dose rate is neutron dose rate.

TABLE V-3

Comparison of Measured and Calculated Dose Rates

Dose Point	1.30 Measured (mrem/hr)	Corrected Calculated (mrem/hr)
1	662	826
2	411	512
3	491	517
4	486	451
5	315	282
6	129	104

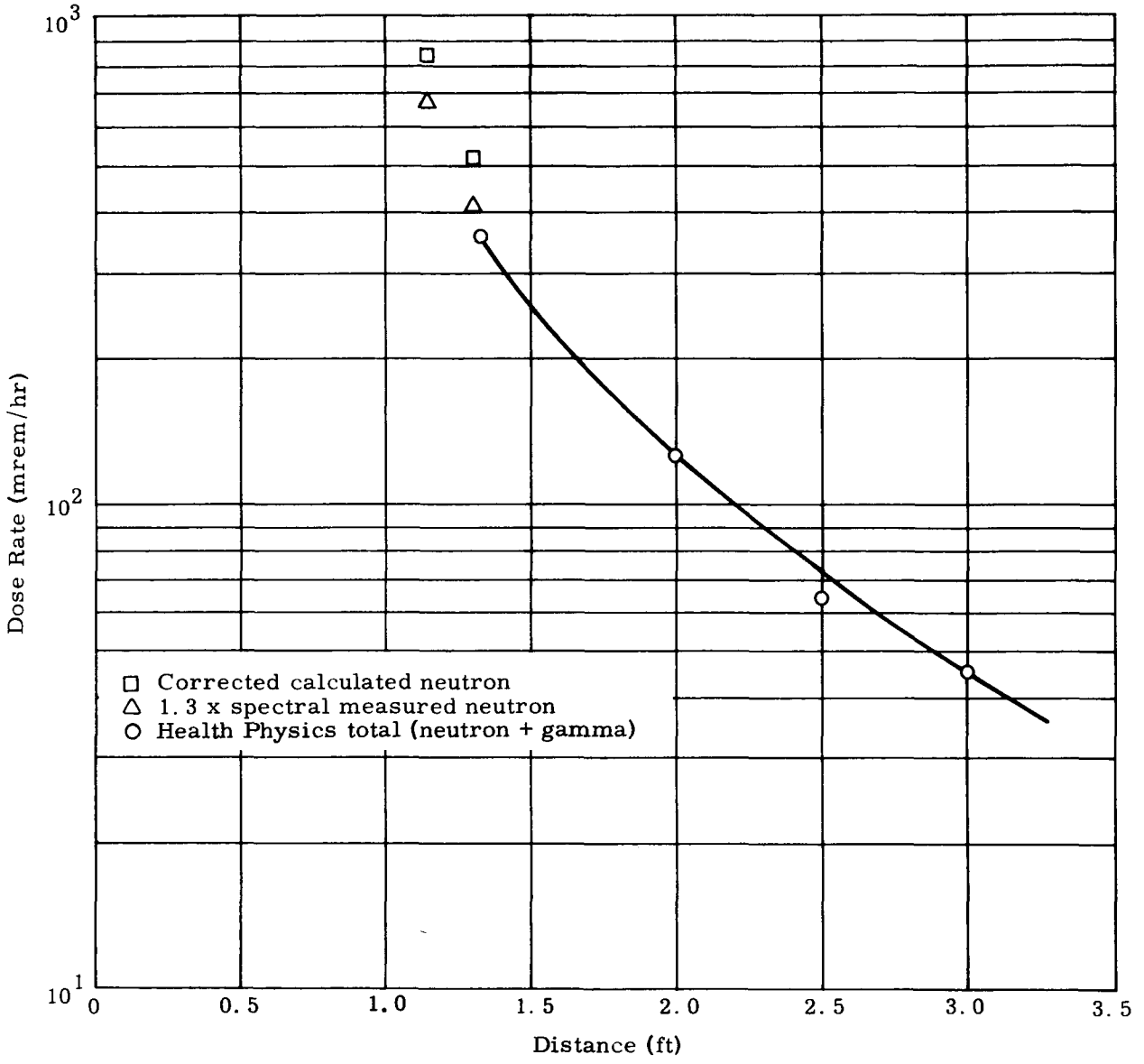

FIG. V-11. DOSE RATE ALONG THE AXIS AS FUNCTION OF DISTANCE FROM THE CENTER OF THE SUBSYSTEM

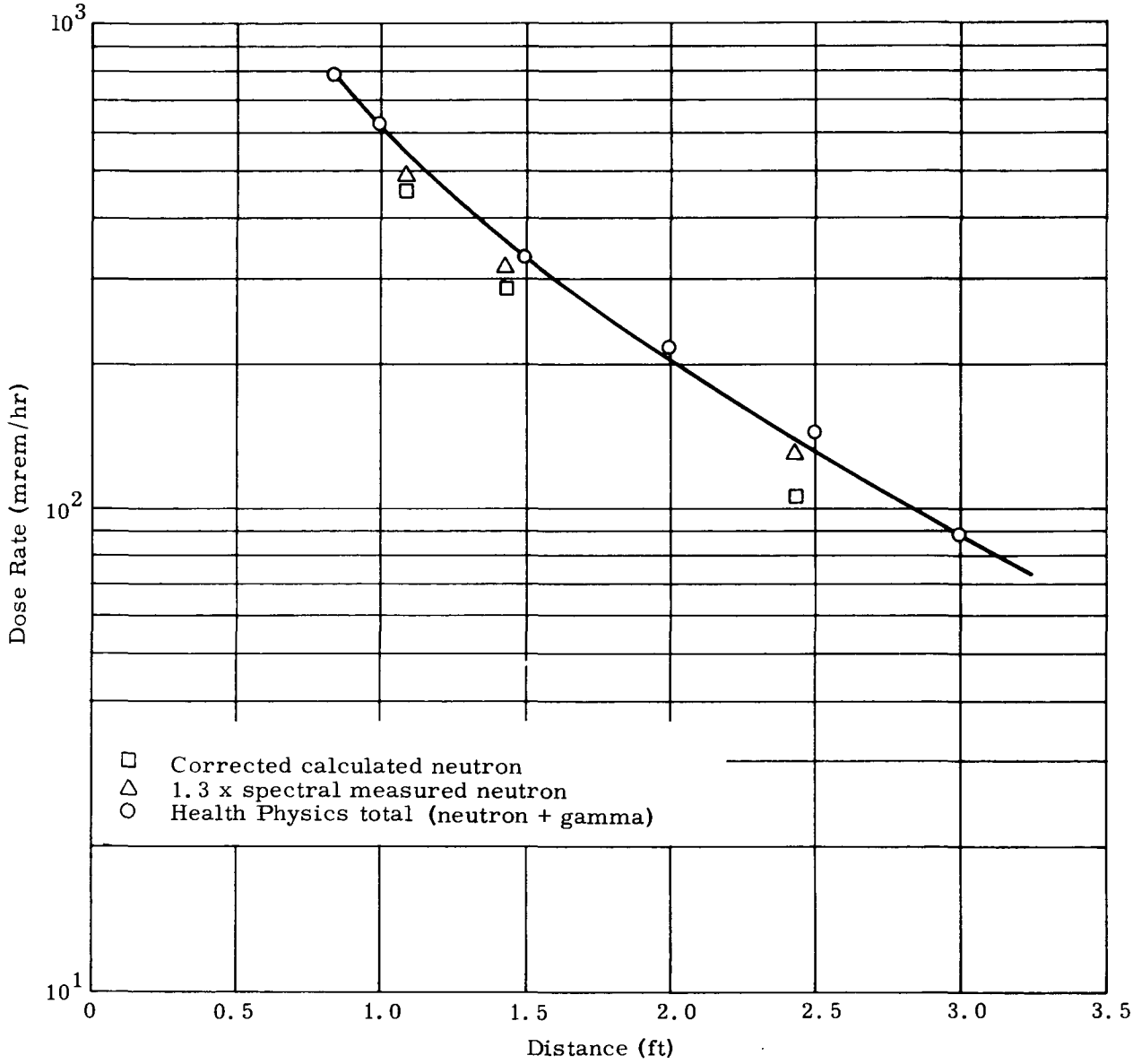

FIG. V-12. DOSE RATE TO SIDE OF THE SUBSYSTEM AS FUNCTION OF DISTANCE FROM AXIS

BLANK

VI. GAMMA MEASUREMENTS

A. MEASUREMENT TECHNIQUES

In measuring the gamma spectrum emitted by SNAP 19 Subsystem S/N 4, conventional gamma spectrometry techniques were employed (Ref 25). Gamma spectrum was measured with a scintillation counter, using a 1-1/2-inch diameter sodium iodide crystal and a TMC 256-channel multichannel analyzer with a pulse height plug-in unit. Figure VI-1 shows a block diagram of the circuit used.

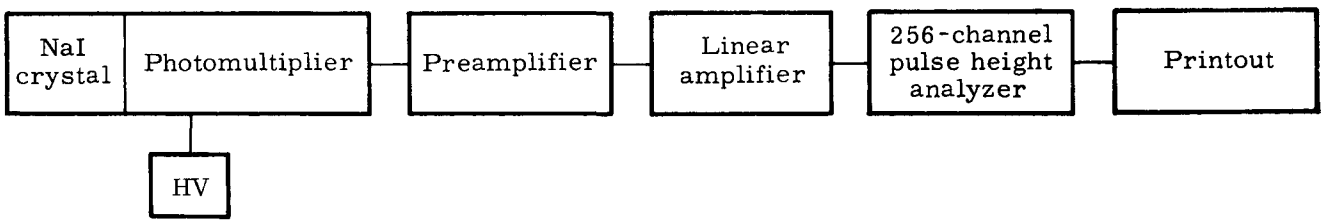

FIG. VI-1. BLOCK DIAGRAM AND PHOTO OF GAMMA SPECTROMETER

Measurements were made in Test Cell 2 of the Martin Marietta Critical Facility using the procedures defined in Test Procedure 452B1900019, "Subsystem Radiation Measurements", which is reproduced in Appendix C. The same test stand and detector mounting fixture described in Section V-A were employed.

Because of scattering problems, measurements were made at only one location--on the midplane of the subsystem, 29 inches from the subsystem axis.

To calibrate the system, it was first necessary to determine the response of the NaI crystal to gamma energies. Standard sources listed in Table VI-1 were used in this calibration.

TABLE VI-1

Standard Sources Used in NaI Calibration

Source	Gamma Energy (Mev)
Na-22	0.511
Cs-137	0.662
Mn-54	0.84
Co-60	1.17, 1.33

The response of the spectrometer was found to be linear in the range covered by these sources. By recording the channel of the 256-channel analyzer in which the characteristic gamma energy for each of the sources fell, the system was calibrated for the various energy ranges of interest to these measurements.

B. SPECTRUM MEASUREMENTS

Measurements were difficult to make due to the low energy gammas resulting from scatterings within the generator, from the walls and floors and from structures in the measuring room. This low energy spectrum results in poor resolution in the definition of the low energy gamma spectrum. To overcome this, spectral measurements were made using three different energy ranges. These energy ranges and the resolution attributable to each one are shown in Table VI-2.

TABLE VI-2

Energy Ranges and Resolutions

Energy Range (Mev)	Resolution (Kev)
0 to 1.55	6
0 to 3	11.7
0 to 4.70	20

By performing the measurements in more than one range, better resolution was obtained in the low energy part of the spectra, the part most affected by scattered radiation. Better resolution was also obtained as the distance between the generator and the detector was increased. The resultant gamma spectrum measured on the subsystem midplane 29 inches from the axis is shown in Figs. VI-2 and VI-3. In Fig. VI-2, the counting scale was calibrated so that Channel 256 of the TMC was equivalent to 1.55 Mev. Therefore, the low energy spectrum of the generator was better defined since the spectrum was then spread out, thus increasing resolution. The TMC was then calibrated to make Channel 256 equivalent to 4.7 Mev and the high energy component of the spectrum was defined as shown in Fig. VI-3. The data compare favorably with the spectrum measured by Mound Laboratories on System 6 capsules.

C. GAMMA DOSE

The gamma dose rate could not be accurately computed because of the scattering of gammas and the resultant increase in the magnitude of the low energy spectrum. Gamma doses computed from spectral data were high by as much as a factor of 5.

Low energy gammas result from the Compton scattering of higher energy gamma rays in various materials surrounding the capsules. In Compton scattering, an incident gamma, E_γ, is scattered with a decrease in energy and the production of a lower energy photon, E_e. The energy loss between the incident gamma and the resulting photon is a function of the angle between them, θ. The resultant photon has an energy equal to

$$E_e = E_\gamma - E_\gamma / 1 + E_o (1 - \cos \theta) \qquad \text{(VI-1)}$$

In this manner, a single energy incident gamma can produce an energy distribution from 0 Mev up to near the energy of the incident gamma. Because of this effect of scattering on spectrum, gamma dose rates are not reported for Subsystem S/N 4.

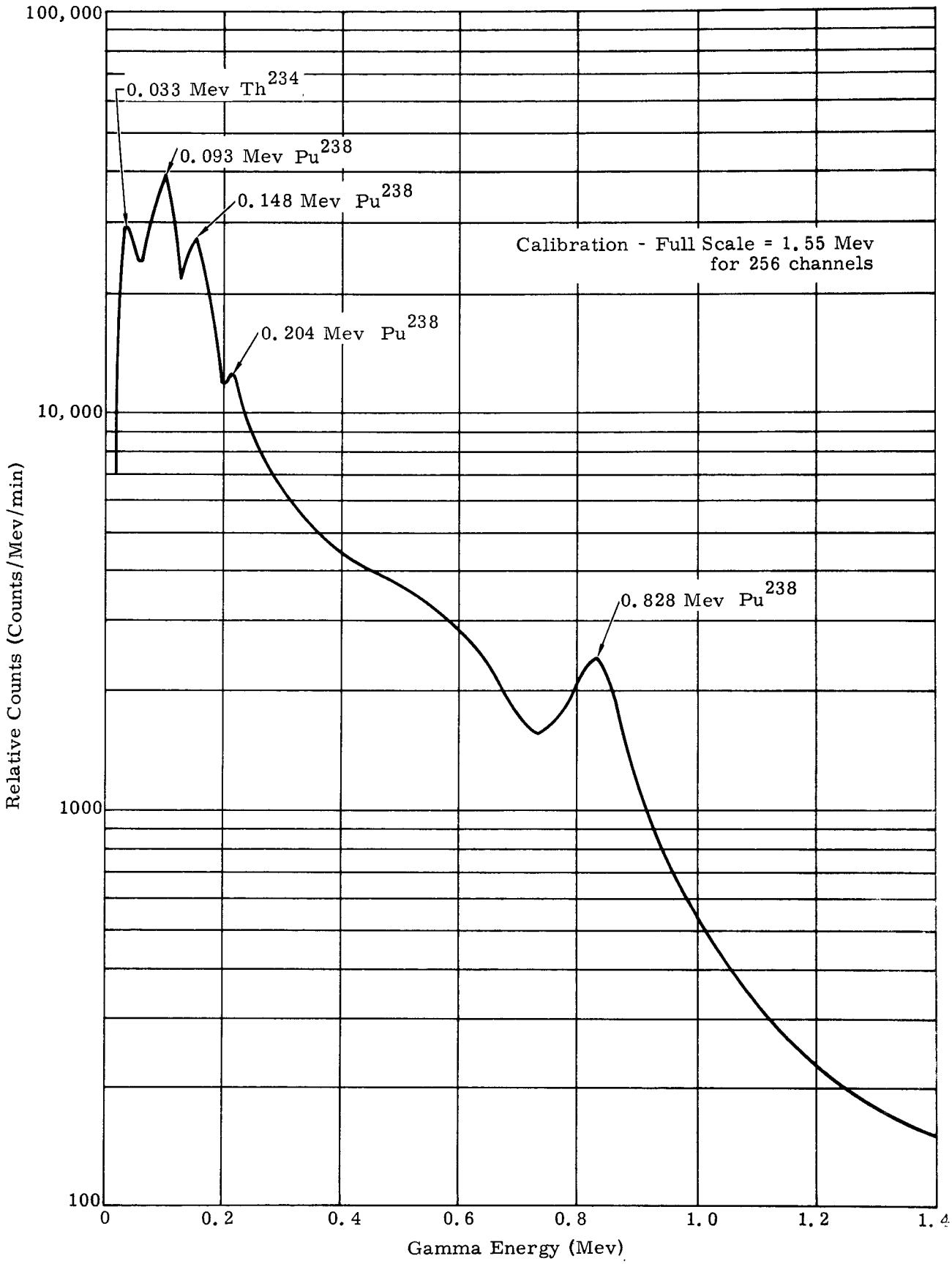

FIG. VI-2. GAMMA SPECTRUM

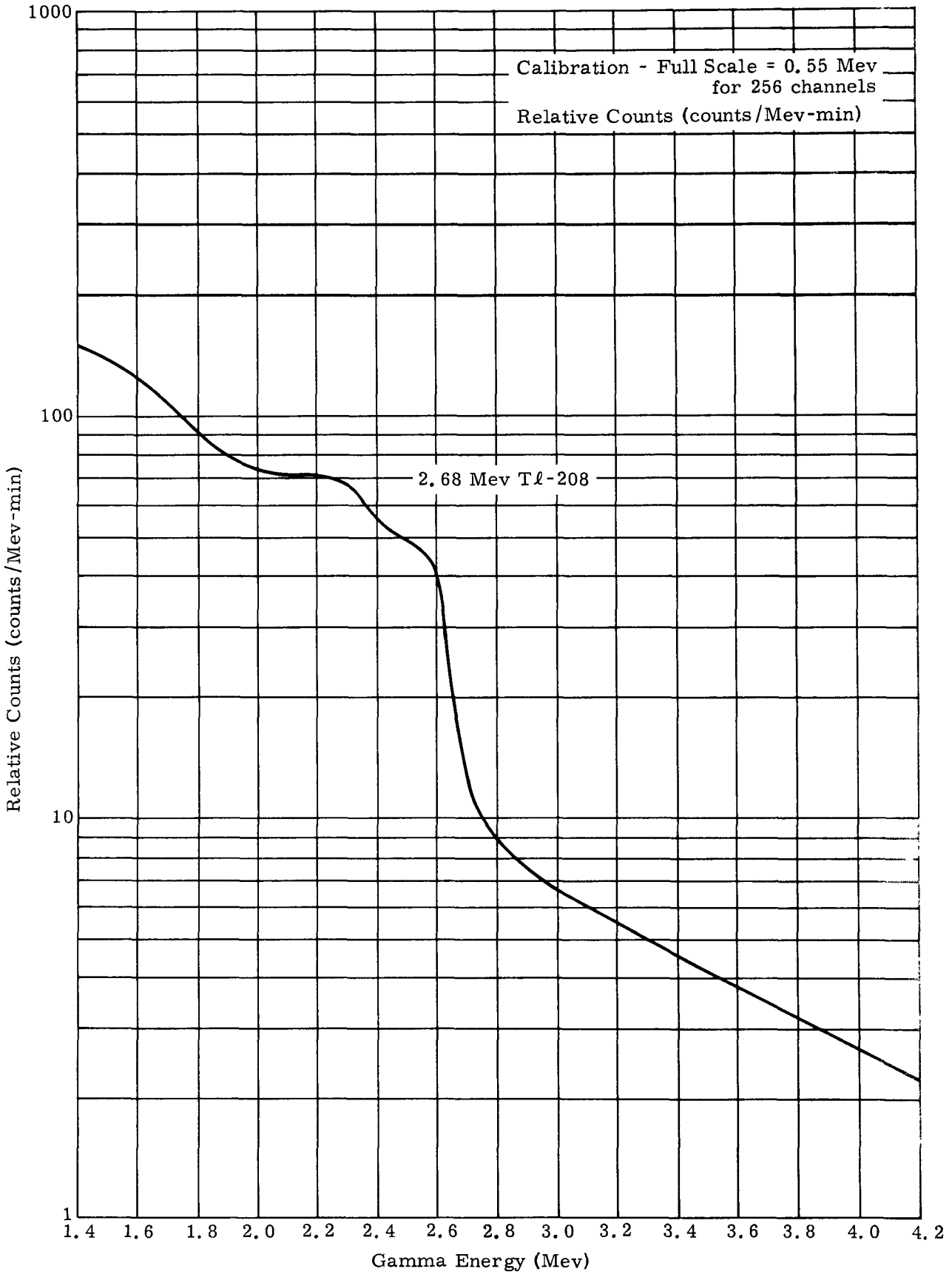

FIG. VI-3. GAMMA SPECTRUM

VII. CONCLUSIONS

The program described herein determined the neutron spectrum and dose rate at various locations in the vicinity of SNAP 19 Subsystem S/N 4. It also determined the gamma spectrum on the subsystem midplane at a radial distance of 29 inches from the subsystem axis. Comparison of neutron dose rate data shows good agreement among data obtained experimentally with the stilbene detection system dose rates, determined analytically, and dose rates measured using health physics techniques.

Preliminary experiments and theoretical analyses, both described in Chapter IV, validate the use of the stilbene detection system as a reliable means of determining neutron spectrum and dose rates. The most significant conclusion to be drawn from the program is that the stilbene system provides an accurate means of determining absolute dose rates in addition to its more conventional application of determining relative spectra.

In establishing the validity of the absolute dose rate measurements using the stilbene spectrometer, three independent approaches were used:

(1) Calibration of the spectrometer against a Pu-Be neutron source of known mission

(2) Determination of dose rates when the Pu-Be neutron spectrum was perturbed by water

(3) Comparison of the Pu-Be neutron spectrum in air and in water.

To determine the neutron emission of the source, absolute thermal and epithermal fluxes were measured through various thicknesses of water using gold foils. The emission thus obtained was compared with a calibration performed at MRC using a BF_3 long counter. These emission rates agreed within 2.5%.

Comparison of experimental and analytical data verified that the stilbene neutron spectrometer was a reliable system for determining both relative neutron spectra and absolute dose rate.

The demonstrated validity of the stilbene spectrometer in measuring both shape and magnitude of neutron spectra should be of significant utility in the field of biological dosimeter calibration. Therefore, in the energy region in which confidence exists in the spectral measurements (1.0 to 10 Mev), the flux-to-dose conversion function varies by about 50%. The probable error in measuring a soft spectrum (that from a fission source, for example) may be as large as 10 to 20% if dosimeter measurements are performed with an instrument calibrated with a source having a hard spectrum.

While a systematic error of this magnitude is not normally a source of great concern among health physicists, experience has shown that dosimeter accuracy, particularly when applied in control of the extensive operations performed on SNAP generators during assembly and test, can be advantageous with respect to economics and convenience.

The observed accuracy of the spectrometer is, moreover, well within requirements imposed in determining radiation effects on instrumentation. Similar conclusions apply also in determining competition between nuclear radiation emanating from the SNAP source and radiation to be detected in some space experiments. Elimination of this competition may dictate shielding requirements or influence craft design for such experimental missions.

BLANK

VIII. REFERENCES

1. "Neutron, Gamma Spectra, Absolute Dose Rates." Martin Marietta Corporation, MND-3607-73, March 1966.

2. Swartz, C. D., and Owen, G. E., Fast Neutron Physics, Part I, Chapter II-3, Interscience Publishers, Inc., 1960.

3. Swartz, C. D., "Spectrometry of Fast Neutrons," NYO-3863, The Johns Hopkins University, September 1954.

4. Johnson, F. A., "The Application of Neutron Identification Circuit to the Study of Fast Neutron Interactions in Stilbene." Am. J. of Physics, 41, 1963.

5. Batchelor, Gilboy, Packer, "The Response of Organic Scintillation to Fast Neutrons." Nuc. Instruments and Methods, 13, 1961.

6. Swartz, Owen, Ames, "The Stilbene Scintillation Crystal as a Neutron Spectrometer." NYO 2053, August 1957.

7. Brodsky, A., "The Pulsed Distributions in Stilbene Produced by 1-15 Mev Neutrons Corrected for End Effect." TID 13075, June 1961.

8. Broek, H. W., and Anderson, C. E., "The Stilbene Scintillation Crystal as A Spectrometer for Continuous Fast-Neutron Spectra." Rev. of Scientific Instruments, 31, No. 10, October 1960.

9. Wasson, H. McN., "The Use of Stilbene with Decay Time Discriminator, as a Fast Neutron Spectrometer." AERE-R-4269, June 1963.

10. Anderson, D. C., "On the Temperature Dependence of the Thermal Neutron Flux Kernel." Nuc. Sci. and Engineering, 7, 468, 1960.

11. Anderson, D. C., "Heavy Element Scattering Formulation." Unpublished.

12. Certaine, J., "A Solution of the Neutron Transport Equation, Part II: NDA Univac Moments Calculations." NYO 6268, May 1955.

13. Joanau, G. D., Goodjohn, A. J. and Wikner, N. F., "Legendre Expansion Coefficients for the Angular Distribution of Elastically Scattered Neutrons and Fast Neutron Cross Sections for Deuterium, Beryllium, Carbon, Oxygen, Zirconium, Lead and Bismuth." G. A. 2156, May 15, 1961.

14. Goldstein, H., "Fast Neutron Data for Oxygen." NDA15C-15, November 1953.

15. Certaine, J and Aronson, R., "Distribution of Fission Neutrons in Water at the Indium Resonance Energy." NDA15C-40, June 15, 1954.

16. Hughes, D and Schwartz, R., Neutron Cross Sections. BNL 325, Second Ed., July 1, 1958.

17. Aronson, R., Certaine, J., Goldstein, H. and Preissen, S., "Penetrations of Neutrons from a Point Isotropic Fission Source in Water." NYO 6267, September 24, 1954.

18. Joanau, G. D., Goodjohn, A. J. and Wikner, N. F., "Moments Calculations of the Fermi Age in Moderators and Moderator-Metal Mixtures." Nuclear Sci. and Engineering: 13, 171-189, 1962.

REFERENCES (continued)

19. Trubey, D., Moran, H. and Weinberg, A., "Applied Nuclear Physics Division Annual Progress Report." ORNL-2389, pp 158-164, September 1, 1957.

20. Letter from M. Edward Anderson, Mound Laboratory, to H. B. Rosenthal, Martin Marietta Corporation, May 23, 1956.

21. Valente, Frank A., Editor, A Manual of Experiments in Reactor Physics. NYO 9077.

22. "Martin Critical Experiment Facility; Facility Report." Martin Company, MND-1110, 1957.

23. Letter from James A. Powers, Mound Laboratory, to Charles Fink, Martin Marietta Corporation, October 14, 1965.

24. Letter from Dr. F. D. Lonadier, Mound Laboratory, to James Powell, Martin Marietta Corporation, November 22, 1966.

25. Heath, R. L., "Scintillation Spectrometry-Gamma Ray Spectrum Catalog." IDO-16408, July 1957.

26. Goldstein, A., Fundamental Aspects of Reactor Shielding. Addison-Wesley Publishing Company., Inc., 1959.

27. Chandrasekhar, S., Radiative Transfer. Dover Publications, Inc., New York, N. Y., 1960.

APPENDIX A

STILBENE DATA REDUCTION PROGRAM

The stilbene data reduction program, obtained from Mound Laboratory and modified for IBM 7094 and IBM 360 systems, is presented in this section. A brief description of input, output, equations, a list of the source deck (FORTRAN IV) and input and output data from a typical problem are included. This program is used to compute the energy-dependent neutron spectrum from the light pulse count data obtained from the stilbene detection system.

1. Input

NCARDS = number of cards containing Hollerith information. Columns 2 through 72 of these cards may be used to include identifying information.

R = radius of stilbene crystal (cm)

T = thickness of stilbene crystal (cm)

HN = hydrogen atom density of stilbene (atoms/cm^3) (HN = 4.67×10^{22} atoms/cm)

EC = gamma calibration source Compton edge energy E_c (Mev)

A, B = constants associated with the proton-light response function. (A = 0.192, B = 1.342)

HC = channel number in which gamma Compton edge occurs (midpoint of measured Compton recoil edge)

HB = back bias, or channel number for which electron recoil energy function is zero. HB may be positive, zero or negative)

N = number of channels for which light response data are input

ID1 = (not used)

C(I) = count rate data for channels I = 1 to I = N

HLOW = lowest channel number of data to be analyzed by this run

HUP = highest channel number of data to be analyzed by this run

DH = channel width for data grouping (see Notes)

ID = if ID is zero, the data of this problem are to be re-analyzed using a new channel width, DH. If ID is not zero, a complete new set of data for the next case follows. (Constructive problems may be run by stacking data card sets one behind the other)

2. Output

JLOW1(I), JLOW2(I) = channel numbers representative of the Ith channel grouping

E(I) = midrange energy of the Ith channel grouping

DNE(I) = time integrated flux (n/cm^2-sec-Mev) of energy (E(I). Flux in units of (n/cm^2-sec-Mev) may be obtained by dividing this value by the total count time in seconds.

ERR(I) = the statistical error associated with the Ith flux value

TDE = is the total number of neutrons incident on the crystal (the integral of DNE over energy)

$Y1(I) = \frac{DNE(I)}{TDE}$

$Y2(I) = Y1(I) - \frac{ERR(I)}{TDE}$

$Y3(I) = Y1(I) + \frac{ERR(I)}{TDE}$

3. Program Notes

The notation in this section is similar to the FORTRAN program variable names.

Radiation from counter is entered without alteration. The total number of counts in any one channel must be in the range of 0 to 999,999.

Several of the consecutive raw data channels will be summed to form a group, i. At this point, unwanted data may be rejected by the choice of both the lower and upper levels which will bound the channels to be grouped together.

Let Cj be the number of raw data counts in Channel j. Let Ni be the number of counts in Group i. The number of raw data channels which will be grouped together is ΔH. The lowest and highest of the raw data channels to be summed are H_{LOW} and H_{UP}, respectively. Then

$$Ni = \sum_{j = H_{LOW} + (i-1)\Delta H}^{j = H_{LOW} + (i)\Delta H - 1} Cj$$

where

$i = 1, 2, 3, \cdots, H_{UP} - \frac{(H_{LOW} 1)}{\Delta H}$, and is always an integer.

The width of each group, in Mev-electron equivalent, ΔL, is computed from

$$\Delta L = \frac{C}{H_C - H_B} \Delta H$$

The height at the upper end of each group, i, in Mev-electron equivalent is

$$L_i = \left[\frac{H_{LOW} - H_B - 1/2 + i\Delta H}{H_C - H_B}\right] E_C$$

The neutron energy at the upper end of each group, i, is

$$E_i = \left[\frac{L_i}{a}\right]^{1/b}$$

Calculation of $\left(\frac{dL}{dE}\right)_i$ and $\left(\frac{d^2L}{dE^2}\right)_i$ (derivatives of the light pulse data)

$$\left(\frac{dL}{dE}\right)_i = \frac{bL_i}{E_i}$$

$$\left(\frac{d^2L}{dE^2}\right) = \frac{(b-1)bL_i}{E_i^2} = \frac{b-1}{E_i}\left(\frac{dL}{dE}\right)_i$$

Calculation of the hydrogen scattering cross section (cm^2)

$$\sigma(E_i) = \left\{\frac{3\pi}{(1.206\,E_i + (-1.860 + 0.0941491\,E_i + 0.000130658\,E_1^2))^2} + \frac{\pi}{(1.206\,E_i + (0.4223 + 0.1300\,E_i))^2}\right\} \times 10^{-24}$$

Calculation of the time integrated differential neutron flux

$$\left(\frac{dN_n}{dE_n}\right)_i = \frac{E_i}{\pi r^2 \tau N_n \sigma(E_i)}\left[\left(\frac{dL}{dE}\right)_i^2 \left(\frac{N_i - N_{i+1}}{(\Delta L)^2}\right) - \left(\frac{d^2L}{dE^2}\right)_i \frac{N_i}{\Delta L}\right]$$

where r, t and N_n are the crystal radius, thickness, and hydrogen atom density, respectively.

Calculation of the statistical error in $\left(\frac{dN_n}{dE_n}\right)_i$

$$\text{Error}\left(\frac{dN_n}{dE_n}\right)_i = \frac{E_i}{\pi r^2 \tau N_n \sigma(E_i)}\left[\left(\frac{dL}{dE}\right)_i^4 \left(\frac{N_i + N_{i+1}}{(\Delta L)^4}\right) + \left(\frac{d^2L}{dE^2}\right)_i^2 \frac{N_i}{(\Delta L)^2}\right]^{1/2}$$

$\sigma(0.068E_i)$ is calculated using equation of note g.

Compute $R_{max} = 1.524 \times 10^{-3} (E_i + 0.118)^{1.1815}$ (cm)

The correction for wall effect and double scattering (Ref. 8) is computed as

$$CF = 1 - \frac{0.78 R_{max}(E_i)}{\tau} + 0.090 N_n \tau \sigma (E_i) + 0.077 N_n \tau \sigma (0.068 E_i)$$

$\frac{dN_n}{dE_n}$ and error $\frac{dN_n}{dE_n}$ are corrected by dividing by CF of note i

Calculate ΔE_i from

$$\Delta E_i = E_{(i+1/2)} - E_{(i-1/2)} = \left[\frac{L_i + 1/2}{a}\right]^{1/b} - \left[\frac{L_i - 1/2}{a}\right]^{1/b}$$

and integrate over energy as $\sum_i \left(\frac{dN_n}{dE_n}\right)_i \Delta E_i$ to obtain the total number of neutrons incident on the crystal.

4. Stilbene Data Reduction Program--Source Deck List

```
C     CALCULATION NEUTRON FLUX USING STILBINE SPECTROMETER      -NLH    0031  10
C     ID=0 READ NEW DATA FOR CHANNELS NOT NEW TAPE                      0031  11
C     ID=1 READ NEW DATA AND NEW TAPE                                   0031  12
C                                                                       4-15-66
C      PROGRAM  MODIFIED  FOR  IBM 7094 , FORTRAN IV                    4-15-66
C      W.D.OWINGS                          APRIL 15,1966                4-15-66
C                                                                       4-15-66
      DIMENSION  C(500)  , E(400)  ,  DNE(400) , ERR(400) , AN(2)
     1            TABLE(500), JLOW1(400) , JLOW2(400)
     2           ,Y1(400), Y2(400), Y3(400)
      DIMENSION ICHAN(500) , SIGE(400) , SIGPF(400)
      COMMON   C  , TABLE
 1000 READ(5,850) NCARDS
  850 FORMAT(I6)
      WRITE(6,860)
      IF(NCARDS)760,760,750
  750 DO 751 J=1,NCARDS
      READ(5,851)
  751 WRITE(6,851)
  851 FORMAT(72H
     1
  760 CONTINUE
      READ(5,852) R,T,HN,EC,A,B,HC,HB,N,ID1
  852 FORMAT(6F12.5/2E12.5,2I12)
      READ(5,853) ( C(I),I=1,N)
  853 FORMAT(12F6.0)
      DO 2000 I=1,N
 2000   ICHAN(I) = I
```

```
      WRITE(6,860)
      WRITE(6,870)
  870 FORMAT(//22H  CHANNEL       COUNTS /)
      WRITE(6,871) (ICHAN(I),C(I),I=1,N)
  871 FORMAT(I6,1PE16.5)
   15 READ(5,855) HLOW,HUP,DH,ID
  855 FORMAT(3F12.5,I12)
      TDE=0.                                                    0031 155
      B1=1./B                                                   0031 160
      NG=(HUP-HLOW+1.)/DH                                       0031 170
      DL=EC*DH/(HC-HB)                                          0031 180
      JLOW=HLOW                                                 0031 181
      JHIGH=HLOW+DH-1.                                          0031 182
      AN(1)=0.                                                  0031 184
      DO 14 J=JLOW,JHIGH                                        0031 185
   14 AN(1)=AN(1)+C(J)                                          0031 186
      JLOW1(2)=JLOW                                             0031 195
      DO 10 I=2,NG                                              0031 200
      AI=I                                                      0031 210
      JLOW=HLOW+(AI-1.)*DH                                      0031 220
      JLOW2(I)=JLOW                                             0031 225
      JHIGH=HLOW+AI*DH-1.                                       0031 230
      JLOW2(I)=JHIGH                                            0031 235
      AN(2)=0.                                                  0031 240
      DO 8 J=JLOW,JHIGH                                         0031 260
    8 AN(2)=AN(2)+C(J)                                          0031 270
      AI=I-1                                                    0031 285
      AL=(HLOW-HB-.5+AI*DH)*EC/(HC-HB)                          0031 290
```

```
      E(I)=(AL/A)**B1                                                    0031 300
      DLE1=AL*B/E(I)                                                     0031 310
      DLE2=(B-1.)*DLE1/E(I)                                              0031 320
       X = E(I)
       AAA = 1.206 * X
       BBB = -1.86 + 0.0941491 * X + 0.000130658 * X * X
       BBB = BBB * BBB
       CCC = 0.4223 + 0.13 * X
       CCC = CCC * CCC
          DDD  = ( ( 9.42477 /(AAA + BBB)) +(3.14159 /(AAA + CCC)))
       SIGE(I) =   DDD   * 1.0E-24
       SIGA = SIGE(I)
 1002 KATY=0                                                             0031 344
      DNE(I)=(E(I)/(3.14159*R*R*T*HN*SIGA))*(DLE1*DLE1*(AN(1)-AN(2))/(DL
     1*DL)-DLE2*AN(1)/DL)                                                0031 360
      ERR(I)=(E(I)/(3.14159*R*R*T*HN*SIGA))*SQRT (DLE1**4*(AN(1)+AN(2))/
     1(DL**4)+DLE2*DLE2*AN(1)/(DL*DL))                                   0031 380
       X = 0.06R * E(I)
       AAA = 1.206 * X
       BBB = -1.86 + 0.0941491 * X + 0.000130658 * X * X
       BBB = BBB * BBB
       CCC = 0.4223 + 0.13 * X
       CCC = CCC * CCC
          DDD  = ( ( 9.42477 /(AAA + BBB)) +(3.14159 /(AAA + CCC)))
       SIGPE(I) =  DDD   * 1.0E-24
       SIGPA = SIGPE(I)
      RMAX=1.524E-03*(E(I)+.119)**1.815                                   0031 420
      CF=1.-.78*RMAX/T+.09*HN*T*SIGA+.077*HN*R*SIGPA
```

```
      DNE(I)=DNE(I)/CF                                                  0031 440
      ERR(I)=ERR(I)/CF                                                  0031 450
      AN(1)=AN(2)                                                       0031 455
      JLOW1(I+1)=JLOW                                                   0031 456
    9 AL1=(HLOW-HB-.5+(AI+.5)*DH)*EC/(HC-HB)                            0031 480
      AL2=(HLOW-HB-.5+(AI-.5)*DH)*EC/(HC-HB)                            0031 490
      TDE=TDE+DNE(I)*((AL1/A)**B1-(AL2/A)**B1)                          0030 500
   10 CONTINUE                                                          003H 510
      DO 903 I=2,NG
      IF(DNE(I))900,900,901
  900 Y1(I) = 0.0
      Y2(I) = 0.0
      Y3(I) = 0.0
      GO TO 903
  901 Y1(I) = DNE(I) / TDE
      Y2(I) = Y1(I) - (ERR(I) / TDE)
      IF(Y2(I))904,905,905
  904 Y2(I) = 0.0
  905 CONTINUE
      Y3(I) = Y1(I) + (ERR(I) / TDE)
  903 CONTINUE
      WRITE(6,860)
  860 FORMAT(50H1                          PROGRAM 0031                //)
      WRITE(6,861) R
      WRITE(6,862) T
      WRITE(6,863) HN
      WRITE(6,864) EC
      WRITE(6,865) A
```

```
      WRITE(6,866) B
      WRITE(6,867) HC
      WRITE(6,868) HB
      WRITE(6,869) N
  861 FORMAT(46H                          CRYSTAL  RADIUS        =   1PE12.5)
  862 FORMAT(46H                          CRYSTAL  DIAMETER      =   1PE12.5)
  863 FORMAT(46H                      HYDROGEN  DENSITY          =   1PE12.5)
  864 FORMAT(46H                GAMMA  CALIBRATION  ENERGY       =   1PE12.5)
  865 FORMAT(46H                             CONSTANT      A     =   1PE12.5)
  866 FORMAT(46H                             CONSTANT      B     =   1PE12.5)
  867 FORMAT(46H          GAMMA  CALIBRATION  CHANNEL             =   1PE12.5)
  868 FORMAT(46H                    BACK  BIAS                    =   1PE12.5)
  869 FORMAT(46H                    FULL  SCALE  CHANNELS         =   I8)
      WRITE(6,872)
  872 FORMAT(//30H    CHANNEL GROUPING                 /)
  873 FORMAT(30H                    LOWEST       =   1PE12.5)
  874 FORMAT(30H                    HIGHEST      =   1PE12.5)
  875 FORMAT(30H                     WIDTH       =   1PE12.5)
      WRITE(6,873) HLOW
      WRITE(6,874) HUP
      WRITE(6,875) DH
      WRITE(6,876)
  876 FORMAT (89H  CHANNELS      ENERGY            FLUX            ERROR
     1          Y1                Y2          ,7X,2HY3,7X,/)
      WRITE(6,877)(JLOW1(I),JLOW2(I),E(I),DNE(I),ERR(I),Y1(I),Y2(I),
     1                Y3(I),I=2,NG)
      WRITE(6,878) TDE
  877 FORMAT(2I4,1P6E16.5)

  878 FORMAT(//41H  TOTAL NEUTRONS INCIDENT ON CRYSTAL  =  1PE12.5)
   16 IF(ID)15,15,1000
      END                                                        0031 780
```

5. Input Data List--Typical Problem

The output of Section 6 is from this problem.

```
     6
RUN NO. 8     DECEMBER 14,1966
PU-BE SOURCE (M-740) IN WATER   SOURCE SURFACE TO DETECTOR CRYSTAL FACE
    SEPERATION DISTANCE IS 5.625 INCHES
    GROSS COUNT RATE = 2134 CPS        COUNTING TIME = 60 MINUTES
    SETTING  HV=1530(808.5)        FG = 0.8    CG=0.5   BL=20
    CS-137   HC=16.8  FOR  BL=20    ( ASSUME  HB = -6.0 )
        1.0           1.0       4.67+22        0.478        0.192        1.342
       16.8          -6.0           256
     0  3163122747317189311458264820230946207433191037173250158466144266
13418412557711985611413910880810429610088E 96785 95373 84374 85189 83095
80554 78161 75215 72608 70896 68315 66306 64280 62477 61605 60031 58080
56918 55165 54128 52039 51111 49374 48753 47446 47095 45626 44933 43394
42842 41598 41524 40909 40202 39060 38652 37447 37083 35365 34764 33896
34081 33276 32836 32466 31949 31225 30926 30483 29666 29310 28664 28147
27928 27466 26918 26196 25708 25269 24829 24784 24287 24101 24665 23678
23766 23759 23675 23373 23124 22440 21647 20296 18424 16705 15427 13765
12764 11872 11333 10769 10631 10281 10170  9860  9431  9426  9123  8838
 8582  8428  8021  7866  7725  7658  7319  6998  6796  6571  6431  6212
 5861  5724  5453  5193  5228  4852  4872  4540  4329  4290  4061  3915
 3826  3615  3499  3350  3226  3154  3002  2899  2771  2631  2575  2554
 2478  2476  2387  2346  2172  2071  1915  1804  1650  1466  1319  1314
 1179  1062  1003   924   897   850   749   769   737   643   652   582
  544   494   468   474   440   395   337   340   301   285   270   244
  209   221   219   192   192   194   173   157   140   139   148   143
  127   124   120   109   106    93    69    89    62    62    81    62
   48    42    59    48    36    38    43    33    30    22    27    10
   24    22    22    25     7    17    17    18     8    11    11    15
```

```
 14   14    5    5   10   12    4    9    8    3    3    2
  5    3    4    6    7    2    2    2    3    2    5    0
  1    0    3    1
      4.0       256.0        8.0        0
      4.0       256.0       10.0        0
      4.0       256.0       12.0        1
```

6. Output Data (see input of Section 5)

```
                          PROGRAM 0031

 RUN NO. 8     DECEMBER 14,1966
 PU-BE SOURCE (M-740) IN WATER   SOURCE SURFACE TO DETECTOR CRYSTAL FACE
    SEPERATION DISTANCE IS 5.625 INCHES
    GROSS COUNT RATE = 2134 CPS       COUNTING TIME = 60 MINUTES
    SETTING  HV=1530(808.5)        FG = 0.8   CG=0.5  BL=20
    CS-137   HC=16.8  FOR  BL=20   ( ASSUME  FB = -6.0 )
```

PROGRAM 0031

CHANNEL	COUNTS
1	0.
2	3.16300E 03
3	1.22747E 05
4	3.17189E 05
5	3.11458E 05
6	2.64820E 05
7	2.30946E 05
8	2.07433E 05
9	1.91037E 05
10	1.73250E 05
11	1.58466E 05
12	1.44266E 05
13	1.34184E 05
14	1.25577E 05
15	1.19856E 05
16	1.14139E 05
17	1.08898E 05
18	1.04296E 05
19	1.00885E 05
20	9.67850E 04
21	9.53730E 04
22	8.43740E 04
23	8.51890E 04
24	8.30950E 04
25	8.05540E 04
26	7.81610E 04
27	7.52150E 04
28	7.26080E 04
29	7.08960E 04
30	6.83150E 04
31	6.63060E 04
32	6.42800E 04
33	6.24770E 04
34	6.16050E 04
35	6.00310E 04
36	5.80800E 04
37	5.69180E 04
38	5.51650E 04
39	5.41280E 04
40	5.20390E 04
41	5.11110E 04
42	4.93740E 04
43	4.87530E 04
44	4.74460E 04
45	4.70950E 04
46	4.56260E 04
47	4.49330E 04
48	4.33940E 04
49	4.28420E 04
50	4.15980E 04
51	4.15240E 04
52	4.09090E 04
53	4.02020E 04
54	3.90600E 04
55	3.86520E 04
56	3.74470E 04
57	3.70830E 04
58	3.53650E 04
59	3.47640E 04
60	3.38960E 04
61	3.40810E 04
62	3.32760E 04
63	3.28360E 04
64	3.24660E 04
65	3.19490E 04
66	3.12250E 04
67	3.09260E 04
68	3.04830E 04
69	2.96660E 04
70	2.93100E 04
71	2.86640E 04
72	2.81470E 04
73	2.79280E 04
74	2.74660E 04
75	2.69180E 04
76	2.61960E 04
77	2.57080E 04
78	2.52690E 04
79	2.48290E 04
80	2.47840E 04
81	2.42870E 04
82	2.41010E 04
83	2.46650E 04
84	2.36780E 04
85	2.37660E 04
86	2.37590E 04
87	2.36750E 04
88	2.33730E 04
89	2.31240E 04
90	2.24400E 04
91	2.16470E 04
92	2.02960E 04
93	1.84240E 04
94	1.67060E 04
95	1.54270E 04
96	1.37650E 04
97	1.27640E 04
98	1.18720E 04
99	1.13330E 04
100	1.07690E 04
101	1.06310E 04
102	1.02810E 04
103	1.01700E 04
104	9.86000E 03
105	9.43100E 03
106	9.42600E 03
107	9.12300E 03
108	8.83800E 03
109	8.58200E 03
110	8.42800E 03
111	8.02100E 03
112	7.86600E 03
113	7.72500E 03
114	7.65800E 03
115	7.31900E 03
116	6.99800E 03
117	6.79600E 03
118	6.57100E 03
119	6.43100E 03
120	6.21200E 03
121	5.86100E 03
122	5.72400E 03
123	5.45300E 03
124	5.19300E 03
125	5.22800E 03
126	4.85200E 03
127	4.87200E 03
128	4.54000E 03
129	4.32900E 03
130	4.29000E 03
131	4.06100E 03
132	3.91500E 03
133	3.82600E 03
134	3.61500E 03
135	3.49900E 03
136	3.35000E 03
137	3.22600E 03
138	3.15400E 03
139	3.00200E 03
140	2.89900E 03
141	2.77100E 03
142	2.63100E 03
143	2.57500E 03
144	2.55400E 03
145	2.47800E 03
146	2.47600E 03
147	2.38700E 03
148	2.34600E 03
149	2.17200E 03
150	2.07100E 03
151	1.91500E 03
152	1.80400E 03
153	1.65000E 03
154	1.46600E 03
155	1.31900E 03
156	1.31400E 03
157	1.17900E 03
158	1.06200E 03
159	1.00300E 03
160	9.24000E 02
161	8.97000E 02
162	8.50000E 02
163	7.49000E 02
164	7.69000E 02
165	7.37000E 02
166	6.43000E 02
167	6.52000E 02
168	5.82000E 02

169	5.44000E 02
170	4.94000E 02
171	4.68000E 02
172	4.74000E 02
173	4.40000E 02
174	3.95000E 02
175	3.37000E 02
176	3.40000E 02
177	3.01000E 02
178	2.85000E 02
179	2.70000E 02
180	2.44000E 02
181	2.09000E 02
182	2.21000E 02
183	2.19000E 02
184	1.92000E 02
185	1.92000E 02
186	1.94000E 02
187	1.73000E 02
188	1.57000E 02
189	1.40000E 02
190	1.39000E 02
191	1.48000E 02
192	1.43000E 02
193	1.27000E 02
194	1.24000E 02
195	1.20000E 02
196	1.09000E 02
197	1.06000E 02
198	9.30000E 01
199	6.90000E 01
200	8.90000E 01
201	6.20000E 01
202	6.20000E 01
203	8.10000E 01
204	6.20000E 01
205	4.80000E 01
206	4.20000E 01
207	5.90000E 01
208	4.80000E 01
209	3.60000E 01
210	3.80000E 01
211	4.30000E 01
212	3.30000E 01
213	3.00000E 01
214	2.20000E 01
215	2.70000E 01
216	1.00000E 01
217	2.40000E 01
218	2.20000E 01
219	2.20000E 01
220	2.50000E 01
221	7.00000E 00
222	1.70000E 01
223	1.70000E 01
224	1.80000E 01
225	8.00000E 00
226	1.10000E 01
227	1.10000E 01
228	1.50000E 01
229	1.40000E 01
230	1.40000E 01
231	5.00000E 00
232	5.00000E 00
233	1.00000E 01
234	1.20000E 01
235	4.00000E 00
236	9.00000E 00
237	8.00000E 00
238	3.00000E 00
239	3.00000E 00
240	2.00000E 00
241	5.00000E 00
242	3.00000E 00
243	4.00000E 00
244	6.00000E 00
245	3.00000E 00
246	2.00000E 00
247	2.00000E 00
248	2.00000E 00
249	3.00000E 00
250	2.00000E 00
251	5.00000E 00
252	0.
253	1.00000E 00
254	0.
255	3.00000E 00
256	1.00000E 00

PROGRAM 0031

CRYSTAL RADIUS	=	1.00000E 00
CRYSTAL DIAMETER	=	1.00000E 00
HYDROGEN DENSITY	=	4.67000E 22
GAMMA CALIBRATION ENERGY	=	4.78000E-01
CONSTANT A	=	1.92000E-01
CONSTANT B	=	1.34200E 00
GAMMA CALIBRATION CHANNEL	=	1.68000E 01
BACK BIAS	=	-6.00000E 00
FULL SCALE CHANNELS	=	256

CHANNEL GROUPING

LOWEST	=	4.00000E 00
HIGHEST	=	2.56000E 02
WIDTH	=	8.00000E 00

CHANNELS	ENERGY	FLUX	ERROR	Y1	Y2	Y3
4 19	1.62017E 00	7.21368E 06	1.76845E 04	2.07731E-01	2.07222E-01	2.08241E-01
12 27	2.14484E 00	3.93187E 06	2.55055E 04	1.13226E-01	1.12491E-01	1.13960E-01
20 35	2.62845E 00	3.53586E 06	3.50329E 04	1.01822E-01	1.00813E-01	1.02831E-01
28 43	3.08320E 00	3.47398E 06	4.51760E 04	1.00040E-01	9.87388E-02	1.01341E-01
36 51	3.51600E 00	3.37997E 06	5.57375E 04	9.73325E-02	9.57274E-02	9.89375E-02
44 59	3.93125E 00	3.16135E 06	6.67866E 04	9.10370E-02	8.91138E-02	9.29603E-02
52 67	4.33198E 00	3.47044E 06	7.81076E 04	9.99379E-02	9.76886E-02	1.02187E-01
60 75	4.72040E 00	3.18152E 06	8.95944E 04	9.16179E-02	8.90379E-02	9.41979E-02
68 83	5.09816E 00	3.56048E 06	1.01232E 05	1.02531E-01	9.96154E-02	1.05446E-01
76 91	5.46658E 00	1.80487E 06	1.14046E 05	5.19746E-02	4.86904E-02	5.52588E-02
84 99	5.82669E 00	1.31332E 07	1.19128E 05	3.78195E-01	3.74765E-01	3.81626E-01
92 107	6.17934E 00	9.62154E 06	1.11663E 05	2.77070E-01	2.73855E-01	2.80286E-01
100 115	6.52523E 00	3.95701E 06	1.08691E 05	1.13949E-01	1.10819E-01	1.17079E-01
108 123	6.86496E 00	4.33519E 06	1.10215E 05	1.24840E-01	1.21666E-01	1.28014E-01
116 131	7.19903E 00	4.37499E 06	1.08767E 05	1.25986E-01	1.22854E-01	1.29118E-01
124 139	7.52788E 00	3.80723E 06	1.05200E 05	1.09636E-01	1.06607E-01	1.12666E-01
132 147	7.85188E 00	2.96042E 06	1.01260E 05	8.52508E-02	8.23349E-02	8.81668E-02
140 155	8.17138E 00	2.93930E 06	9.63025E 04	8.46425E-02	8.18693E-02	8.74158E-02
148 163	8.48665E 00	3.71343E 06	8.50862E 04	1.06935E-01	1.04485E-01	1.09385E-01
156 171	8.79797E 00	1.85827E 06	7.04296E 04	5.35124E-02	5.14843E-02	5.55406E-02
164 179	9.10557E 00	1.35438E 06	5.98191E 04	3.90020E-02	3.72794E-02	4.07246E-02
172 187	9.40965E 00	8.66708E 05	4.97549E 04	2.49585E-02	2.35257E-02	2.63913E-02
180 195	9.71041E 00	4.27438E 05	4.23379E 04	1.23089E-02	1.10897E-02	1.35281E-02
188 203	1.00080E 01	3.64897E 05	3.69036E 04	1.05079E-02	9.44517E-03	1.15706E-02
196 211	1.03026E 01	2.73917E 05	3.07259E 04	7.88795E-03	7.00314E-03	8.77276E-03
204 219	1.05944E 01	1.87049E 05	2.43878E 04	5.38643E-03	4.68414E-03	6.08872E-03
212 227	1.08834E 01	8.20075E 04	1.92494E 04	2.36156E-03	1.80724E-03	2.91588E-03
220 235	1.11698E 01	4.03441E 04	1.64828E 04	1.16178E-03	6.87132E-04	1.63644E-03
228 243	1.14538E 01	5.25936E 04	1.37049E 04	1.51453E-03	1.11987E-03	1.90919E-03
236 251	1.17353E 01	1.59333E 04	1.07253E 04	4.58828E-04	1.49973E-04	7.67684E-04

TOTAL NEUTRONS INCIDENT ON CRYSTAL = 3.47260E 07

PROGRAM 0031

CRYSTAL RADIUS	=	1.00000E 00
CRYSTAL DIAMETER	=	1.00000E 00
HYDROGEN DENSITY	=	4.67000E 22
GAMMA CALIBRATION ENERGY	=	4.78000E-01
CONSTANT A	=	1.92000E-01
CONSTANT B	=	1.34200E 00
GAMMA CALIBRATION CHANNEL	=	1.68000E 01
BACK BIAS	=	-6.00000E 00
FULL SCALE CHANNELS	=	256

CHANNEL GROUPING

LOWEST	=	4.00000E 00
HIGHEST	=	2.56000E 02
WIDTH	=	1.00000E 01

CHANNELS	ENERGY	FLUX	ERROR	Y1	Y2	Y3
4 23	1.75622E 00	6.61588E 06	1.44629E 04	1.92450E-01	1.92029E-01	1.92871E-01
14 33	2.39084E 00	3.66998E 06	2.17644E 04	1.06756E-01	1.06123E-01	1.07390E-01
24 43	2.97178E 00	3.48037E 06	3.06370E 04	1.01241E-01	1.00349E-01	1.02132E-01
34 53	3.51600E 00	3.36950E 06	4.00515E 04	9.80158E-02	9.68507E-02	9.91809E-02
44 63	4.03269E 00	3.38520E 06	4.98602E 04	9.84723E-02	9.70219E-02	9.99227E-02
54 73	4.52761E 00	3.15654E 06	6.00564E 04	9.18210E-02	9.00740E-02	9.35679E-02
64 83	5.00464E 00	3.48948E 06	7.04692E 04	1.01506E-01	9.94559E-02	1.03556E-01
74 93	5.46658E 00	2.68089E 06	8.13380E 04	7.79847E-02	7.56186E-02	8.03507E-02
84 103	5.91552E 00	1.35557E 07	8.44289E 04	3.94324E-01	3.91868E-01	3.96780E-01
94 113	6.35309E 00	5.74287E 06	7.86705E 04	1.67055E-01	1.64766E-01	1.69343E-01
104 123	6.78058E 00	4.12359E 06	7.88424E 04	1.19951E-01	1.17658E-01	1.22245E-01
114 133	7.19903E 00	4.38780E 06	7.81380E 04	1.27637E-01	1.25364E-01	1.29910E-01
124 143	7.60932E 00	3.68321E 06	7.48041E 04	1.07141E-01	1.04965E-01	1.09317E-01
134 153	8.01217E 00	2.59230E 06	7.12313E 04	7.54078E-02	7.33357E-02	7.74798E-02
144 163	8.40821E 00	3.78633E 06	6.36697E 04	1.10141E-01	1.08289E-01	1.11993E-01
154 173	8.79797E 00	1.90657E 06	5.11467E 04	5.54604E-02	5.39726E-02	5.69483E-02
164 183	9.18191E 00	1.29094E 06	4.13477E 04	3.75524E-02	3.63496E-02	3.87552E-02
174 193	9.56044E 00	5.84521E 05	3.30113E 04	1.70032E-02	1.60429E-02	1.79635E-02
184 203	9.93390E 00	3.68432E 05	2.76268E 04	1.07173E-02	9.91370E-03	1.15210E-02
194 213	1.03026E 01	2.82507E 05	2.23629E 04	8.21787E-03	7.56735E-03	8.86838E-03
204 223	1.06669E 01	1.61035E 05	1.68057E 04	4.68436E-03	4.19550E-03	5.17322E-03
214 233	1.10269E 01	5.85075E 04	1.27748E 04	1.70193E-03	1.33032E-03	2.07354E-03
224 243	1.13830E 01	4.54767E 04	1.02503E 04	1.32288E-03	1.02471E-03	1.62105E-03
234 253	1.17353E 01	2.30650E 04	7.74845E 03	6.70940E-04	4.45545E-04	8.96335E-04

TOTAL NEUTRONS INCIDENT ON CRYSTAL = 3.43772E 07

PROGRAM 0031

CRYSTAL RADIUS	=	1.00000E 00
CRYSTAL DIAMETER	=	1.00000E 00
HYDROGEN DENSITY	=	4.67000E 22
GAMMA CALIBRATION ENERGY	=	4.78000E-01
CONSTANT A	=	1.92000E-01
CONSTANT B	=	1.34200E 00
GAMMA CALIBRATION CHANNEL	=	1.68000E 01
BACK BIAS	=	-6.00000E 00
FULL SCALE CHANNELS	=	256

CHANNEL GROUPING

LOWEST	=	4.00000E 00
HIGHEST	=	2.56000E 02
WIDTH	=	1.20000E 01

CHANNELS	ENERGY	FLUX	ERROR	Y1	Y2	Y3
4 27	1.88876E 00	6.18018E 06	1.24489E 04	1.81186E-01	1.80821E-01	1.81551E-01
16 39	2.62845E 00	3.61423E 06	1.93585E 04	1.05959E-01	1.05392E-01	1.06527E-01
28 51	3.30202E 00	3.49457E 06	2.76578E 04	1.02451E-01	1.01640E-01	1.03262E-01
40 63	3.93125E 00	3.24143E 06	3.64881E 04	9.50297E-02	9.39599E-02	9.60994E-02
52 75	4.52761E 00	3.24853E 06	4.58114E 04	9.52377E-02	9.38947E-02	9.65808E-02
64 87	5.09816E 00	3.23737E 06	5.54250E 04	9.49105E-02	9.32856E-02	9.65355E-02
76 99	5.64762E 00	6.54282E 06	6.29860E 04	1.91817E-01	1.89970E-01	1.93664E-01
88 111	6.17934E 00	1.01446E 07	6.32035E 04	2.97410E-01	2.95557E-01	2.99263E-01
100 123	6.69583E 00	4.07415E 06	5.98736E 04	1.19443E-01	1.17687E-01	1.21198E-01
112 135	7.19903E 00	4.33098E 06	5.95974E 04	1.26972E-01	1.25225E-01	1.28719E-01
124 147	7.69046E 00	3.41017E 06	5.67754E 04	9.99767E-02	9.83122E-02	1.01641E-01
136 159	8.17138E 00	3.07380E 06	5.21940E 04	9.01153E-02	8.85851E-02	9.16454E-02
148 171	8.64279E 00	2.79961E 06	4.37452E 04	8.20767E-02	8.07943E-02	8.33592E-02
160 183	9.10557E 00	1.33970E 06	3.31857E 04	3.92763E-02	3.83034E-02	4.02492E-02
172 195	9.56044E 00	6.29079E 05	2.57502E 04	1.84428E-02	1.76879E-02	1.91977E-02
184 207	1.00086E 01	3.66138E 05	2.03799E 04	1.07341E-02	1.01367E-02	1.13316E-02
196 219	1.04488E 01	2.25609E 05	1.54277E 04	6.61422E-03	6.16192E-03	7.06651E-03
208 231	1.08834E 01	9.23364E 04	1.11573E 04	2.70704E-03	2.37994E-03	3.03414E-03
220 243	1.13121E 01	5.02047E 04	8.28423E 03	1.47186E-03	1.22899E-03	1.71473E-03
232 255	1.17353E 01	2.31050E 04	5.96255E 03	6.77374E-04	5.02569E-04	8.52179E-04

TOTAL NEUTRONS INCIDENT ON CRYSTAL = 3.41097E 07

APPENDIX B

MOMENTS SOLUTION FOR POINT ISOTOPIC NEUTRON SOURCE AND DETERMINATION OF THERMAL FLUX

The moments method, applicable to infinite homogeneous media, has been extensively employed for the solution of the neutron and gamma radiation transport equations. A summary of the method and results obtained are given by Goldstein (Ref. 26). A brief description of the method, with emphasis on the particular form of the equations used and flux reconstruction techniques, is presented in this appendix.

The transport equation for neutron radiation in terms of the number flux per unit lethargy interval is

$$\nabla . \Omega N + \Sigma_t N = \iint N(\underset{\sim}{r}, \mu', \Omega') \Sigma(\Omega' \rightarrow \Omega, E' \rightarrow E) E' d\mu' d\Omega' + S(\underset{\sim}{r}, \mu, \Omega) \qquad \text{(B-1)}$$

where

$N(\underset{\sim}{r}, \mu, \Omega)$ = neutron number flux per unit angle per unit lethargy.

Σ_t = macroscopic total cross section

$\mu = \ell n \left(\frac{E_o}{E}\right)$ = lethargy defined from an arbitrarily chosen reference energy, E.

and

$\Sigma(\Omega' \rightarrow \Omega, E' \rightarrow E)$ = cross section for scattering from Ω' into the element of solid angle $d\Omega$ about Ω and from E' to E in the range dE.

The source per unit lethargy, $S(\underset{\sim}{r}, \mu, r)$, is assumed continuous over a specified energy E_1 E_2) and is numerically equal to the product of the energy, E, and the source per unit energy $S(\underset{\sim}{r}, E, \Omega)$.

In spherical geometry, the angular flux depends on the magnitude r of $\underset{\sim}{r}$ and on the component $w = \frac{\Omega . \vec{r}}{r}$, which is the cosine of the angle between the neutron direction. For a point isotopic source, located at the origin, the source term becomes

$$S(\mu) \frac{\delta(r)}{4\pi r^2} \quad \frac{\delta(1-w)}{2\pi}$$

The first step in the derivation of the moments equation is the expansion of the angular flux as a Legendre polynomial series in w·

$$N(r, \mu, w) = \sum_{\ell=0}^{\infty} \frac{2\ell + 1}{4\pi} N_\ell(r, \mu) P_\ell(w) \qquad \text{(B-2)}$$

where the coefficients, N_ℓ, are, due to the orthogonality of the set $\{P_\ell\}$

$$N_\ell(r, \mu) = 2\pi \int_{-1}^{1} N(r, \mu, w) P_\ell(w) dw \qquad \text{(B-3)}$$

The coefficient number for which a solution is sought is readily identified as the scalar flux.

The spherical moments, $B^{(i)}_{n,\ell}$, where i is an index for a particular value of the lethargy U_i, are defined as

$$B^{(i)}_{n,\ell} = 2\pi \frac{\mu_0}{N^1}^{n+1} \int_0^\infty 4\pi r^2 \, dr \int_{-1}^{1} r^n \, P_\ell (w) \, N (r, \mu, w) \, dw \tag{B-4}$$

In terms of the angular expansion coefficient, the moments are

$$B^{(i)}_{n,\ell} = \frac{\mu_0}{n^1}^{n+1} \int_0^\infty r^n \, N_\ell^{(i)} (r, \mu) \; 4\pi r^2 \, d r \tag{B-5}$$

The dimensionless arbitrary constant μ_0 has been included to facilitate numerical solutions.

The procedure for obtaining a solution for the moments is:

(1) Obtain a set of integro-differential equations in N_ℓ by multiplying Eq. (B-1) by $P_\ell(w)$ and integrating overall solid angles utilizing the definition of N_ℓ and properties of the polynomials P_ℓ

(2) Multiplying the resultant set by $4\pi \, \mu_0^{N+1} \, r^{N+2}/N'$ and integrating over the spatial variable.

In Step (2), use is made of the assumption that N vanishes so rapidly at ∞ that $r^{N+\ell} \, N_\ell$ is zero at this limit. In this process, the scattering integral is approximated as a mechanical quadrature for numerical integration as

$$\sum_{j=1}^{i} M^{(\ell)}_{j_1 i} \; N^j_\ell (r) \tag{B-6}$$

where the coefficients $M^{(\ell)}_{j_1 i}$ represent the probability for scattering from lethargy j to the current value i with suitable integration weights. The resultant equation for the spherical moments is

$$B^{(i)}_{N,\ell} = \frac{1}{\Sigma_t - M^{(\ell)}_{i,i}} \left\{ \frac{\mu_0}{N} \; \frac{1}{2\ell + 1} \left[\ell \, (\ell + N + 1) \, B^{(i)}_{N-1,\, \ell-1} - (\ell + 1) \, (\ell - N) \, B^{(i)}_{N-1, \ell-1} \right] \right.$$

$$\left. + \sum_{j=1}^{i-1} M^{(\ell)}_{j,i} \; B^{(j)}_{N,\ell} + \mu_0 \, S^{(i)} \, \delta_{N,\,0} \, \delta_{N,\,0} \, \delta_{\ell,\,0} \right\} \tag{B-7}$$

This equation may be solved for all moments $B_{N,\,0}$ for which N = 0 or a positive even integer. Rigorous solution of the moments through $B_{p,\,0}$ requires a knowledge of

the scattering coefficients $M_{j,i}^{(\ell)}$ through order $\ell = P/2$. This solution for the moments is essentially exact. Small errors may only be introduced by the use of the mechanical quadrature and the numerical technique used to solve Eq. (B-7).

The final step in the solution is the reconstruction of the scalar flux N_0^i from a finite number of the moments for the scalar flux $B_{N,0}^{(i)}$. The first step is the selection of an analytical form for the flux. The coefficients of the assumed form are then solved for, utilizing the computed moments thus completing the solution. Traditionally, both exponential forms and polynomials with a preassigned exponential weight function have been employed. The representation of the flux as a sum of exponentials of the form

$$4\pi r^2 N_0^i(r) = \sum_{j=1}^{N} A_{j\,\ell}^{(i)} - \alpha_\gamma^{(i)} \mu_0 r \qquad \text{(B-8)}$$

is more appropriate for deep penetration due to the exponential nature of the observed flux. Two methods of reconstruction of the flux in exponential form are presented.

The first method of reconstruction is the unique determination of the 2N coefficients $A_j\ \alpha_{j\,j} = 1\ 2, \ldots, N$ from 2N even moments $B_{0,0}^{(i)}, B_{2,0}^{(i)}, \ldots, B_{2N-2,0}^{(i)}$

If the representation of Eq. (B-8) is substituted into Eq. (B-5) the following set of N nonlinear equations in N unknowns may be obtained. (For clarity the energy index superscript i is omitted. This set is obtained and must be solved for each energy point.)

$$\begin{aligned}
&\frac{A_1}{\alpha_1} + \frac{A_2}{\alpha_2} + \cdots + \frac{A_N}{\alpha_N} = B_{0,0} \\
&\frac{A_1}{\alpha_1^3} + \frac{A_2}{\alpha_2^3} + \cdots + \frac{A_N}{\alpha_N^3} = B_{2,0} \qquad \text{(B-9)} \\
&\frac{A_1}{\alpha_1^{4N-1}} + \frac{A_2}{\alpha_2^{4N-1}} + \cdots + \frac{A_N}{\alpha_N^{4N-1}} = B_{4N-2,\,0}
\end{aligned}$$

These equations may be solved by a method described by Chandrasekhar (Ref. 27) which introduces the constants m_0, m, m_{N-1} determined by the condition that

$$\begin{aligned}
&m_0 B_{0,0} + m_1 B_{2,0} + \cdots m_{N-1} B_{2N,0} + B_{2N+2,\,0} = 0 \\
&m_0 B_{2,0} + m_1 B_{4,0} + \cdots m_{N-1} B_{2N+2,\,0} + B_{2N+4,\,0} = 0 \qquad \text{(B-10)} \\
&m_0 B_{2N,0} + m_1, B_{2N-2,0} + \cdots m_{N-1} B_{4N-4,\,0} + B_{4N-2,\,0} = 0
\end{aligned}$$

It can be shown that Eqs. (B-10) are a necessary and sufficient condition that the α_j are the roots of the equation

$$m_0 + \frac{m_1}{\alpha^2} + \frac{m_2}{\alpha^4} + \cdots + \frac{m_{n-1}}{\alpha^{2N-2}} + \frac{1}{\alpha^{2N}} = 0 \qquad \text{(B-11)}$$

or

$$m_0 + m_1 \beta + M_2 \beta^2 + \cdots m_{N-1} \beta^{N-1} + \beta^N = 0 \qquad \text{(B-12)}$$

where

$$\beta_J = \frac{1}{\alpha_J^2}$$

The α_J are thus determined from the roots β_J, $J = 1, \ldots N$ of Eq. (B-12). Having determined the α_J, the A_J may be determined uniquely from any N equations of the set (B-9). Note that the roots of Eq. (B-12) must be real and positive, if not, the method fails.

The second method of reconstruction is the Gaussian iterative least squares technique.

An alternative method for reconstructing the flux in the exponential form (B-8) is an iterative method using an excess of moments. For simplicity the process will be illustrated for a single exponential $4\pi r^2 \, d(r) = A_\ell^{-\alpha \mu_0 r}$. This process is applicable for an arbitrary number of exponential terms N, provided at least 2N moments are available. Note first that, according to the definition of the moments

$$B_{2n,\,0} = \frac{A}{\alpha^{2N+1}} = F_n(A, \alpha) \qquad \text{(B-13)}$$

Given initial guesses or values obtained from the previous iterative i of α_1 and N moments where $N \geq 2$, the equations for ΔA and $\Delta\alpha$ are

$$\Delta A \left(\sum_{J=1}^{N} \frac{\alpha F}{\alpha A}\Big|_1 \right)^2 + \Delta\alpha \left(\sum_{J=1}^{N} \frac{\alpha F}{\alpha A}\Big|_1 \right) \left(\sum_{J=1}^{N} \frac{\alpha F}{\alpha 0}\Big|_1 \right) = \left(\sum_{J=1}^{N} \frac{\alpha F}{\alpha A}\Big|_1 \right)$$

$$\Delta A \left(\sum_{J=1}^{N} \frac{\alpha F}{\alpha A}\Big|_1 \right) \left(\sum_{J=1}^{N} \frac{\alpha F}{\alpha \delta}\Big|_1 \right) + \Delta\alpha \left(\sum_{J=1}^{N} \frac{\alpha F}{\alpha \delta}\Big|_1 \right)^2 = \left(\sum_{J=1}^{N} \Delta y_J \right) \left(\sum_{J=1}^{N} \frac{\alpha F}{\alpha \delta}\Big|_1 \right) \qquad \text{(B-14)}$$

where the notation $\big|_1$ means that the derivatives are to be evaluated with the current values A_1 and α_1

and

$$\Delta y_J = B_{2J,0} - F_J(A_1, \alpha_1)$$

The derivatives in the linear set (B-14) are

$$\frac{\partial F_n}{\partial A} = \frac{1}{\alpha^{2N+1,}} = \frac{\partial F}{\partial \alpha} = -\frac{(2N+1)\,A}{\alpha^{2N+2}}$$

Equations (B-14) are solved for ΔA_{i-1} and $\Delta\alpha_{i+1}$ and the new approximations for the next iterative are

$$A_{i=1} = A_i + h\Delta A$$

$$\alpha_{i=1} = \alpha_i + h\Delta\alpha$$

where h is an arbitrary constant less than or equal to unity. This procedure minimizes the value

$$E^2 = \sum_{J=1}^{N} (\Delta y_J)^2$$

and thus determine the coefficients A and α in the least squares sense. The solution is assumed converged when changes in E^2 between successive iteratives are less than some predetermined arbitrarily small number t.

A difficulty is that there is no guarantee of convergence. Normally, good initial guesses of A and α are required and obtaining a solution may be a trial and error process.

The exponential solution for the moments at epithermal energies may be utilized for determination of thermal (2200 m/sec) neutron flux (Ref. 10). Assuming that the epithermal absorption varies as 1/V and that the epithermal zeroth moment varies as 1/E in the energy region of importance for epithermal absorption, a solution may be written for the thermal flux in terms of spatial solution for an epithermal energy E_1. The zeroth moment and spatial dependence are written in terms of energy.

The redefined moment is

$$\psi^{L}_{0,0} = \frac{B^{1}_{0,0}}{\mu_0 E_1}$$

and the spatial dependence is

$$4\pi r^2 Q(E^1, r) = \sum_{J=1}^{N} M_J^{(1)} e^{-B_J^{(1)}}$$

where

$$M_J^{(1)} = \frac{A_J^{(1)}}{E_1}, \quad \beta_J^{(1)} = \mu_0 \alpha_J^{(1)}$$

Then the thermal flux $\phi(r)$ is given by

(B-15)

$$4\pi r^2 \phi(r) \cdot \frac{Lr}{2} e(E_0, E_1) \sum_{J=1}^{N} M_J^{(1)} \left\{ e^{r/L} E_1\left[\left(\beta_J + \frac{1}{L}\right)r\right] - e^{-r/L} E_1\left[\left(\beta_J - \frac{1}{L}\right)r\right]\right\}$$

where E_0 is the thermal range cutoff energy (taken as 0.625 ev)
$\sum_{\alpha}^{th}$ is the macroscopic thermal absorption cross section (2200 m/sec) and E_{th} is the thermal energy (0.025 ev).